AEC PROGRESS REPORT COO-3496-44

STUDIES OF NUCLEAR FISSION, LOW-ENERGY NUCLEAR REACTIONS AND TRANSURANIC NUCLEI

John R. Huizenga

Principal Investigator

June 1, 1973 - June 1, 1974

DISCLAIMER

University of Rochester

Department of Chemistry

AEC Progress Report COO-3496-44

June 1, 1973 - June 1, 1974

Studies of Nuclear Fission, Low-Energy Nuclear Reactions and Transuranic Nuclei

Supported by the U. S. Atomic Energy Commission

under Contract AT(11-1)3496

John R. Huizenga

Principal Investigator

TABLE OF CONTENTS

TABLE OF CONTENTS
(Continued)

TABLE OF CONTENTS
(Continued)

PAGE

I. INTRODUCTION

The research activity of the group supported under the United States Atomic Energy Commission contract AT(11-1)3496 is carried out in the Nuclear Structure Research Laboratory and in Hutchison Hall, the new Chemistry-Biology building of the University of Rochester. Our research program includes; 1) direct reaction studies on heavy targets including inelastic scattering and transfer reactions, 2) compound nucleus and statistical reactions including both experiment and theory, 3) nuclear fission studies, 4) heavy ion reactions with projectiles as heavy as ^{84}Kr and 5) the study of the effect of pressure on electron capture decay rates.

The major fraction of our experimental program is carried out with the Emperor tandem Van de Graaff in the Nuclear Structure Research Laboratory which is supported by a grant from the National Science Foundation. A collaborative program has been initiated during the past year to investigate very heavy-ion reaction mechanisms at the Berkeley Super-Hilac. This program requires extensive travel funds. In addition, our proposal entitled, "Negative Muon Induced Fission in the Actinide Elements" has been approved. In order to prepare for these experiments and gain experience with the muon channel of the LAMPF facility, one of our postdoctoral research associates, W.K. Hensley, has moved to Los Alamos.

We wish to acknowledge the direct support of our research programs by the U. S. Atomic Energy Commission. In addition,

we are grateful to the National Science Foundation for providing a large amount of indirect support through the use of the facilities at the Nuclear Structure Research Laboratory.

II. RESEARCH PROGRAM

27542

A. Direct Reactions

1. Levels of ^{233}Pa Excited in Helium-Induced Single-Proton Transfer Reactions -- Th. W. Elze* and J.R. Huizenga

Single-nucleon transfer reactions have been shown to be a sensitive means of studying heavy deformed nuclei. The distribution of strength among the levels of a rotational band depends[1] on the structure of the intrinsic state, and hence, the measured differential cross sections give direct and detailed information about the nuclear wave functions. Nuclear structure studies based on transfer reactions therefore often complement similar studies performed by investigating radioactive decay.

Measurements of the (^{3}He,d) reaction on ^{232}Th supplements our earlier work[2] of the (^{3}He,d) and (α,t) reactions exciting levels of ^{233}Pa. The experimental techniques and methods of data analysis are similar to those described previously[3]. The target was prepared by vacuum evaporation of Th metal onto a 20 $\mu g/cm^2$ carbon backing. The (^{3}He,d) experiment was performed with a 28.5 MeV ^{3}He beam while the (α,t) experiment was done with a 30 MeV ^{4}He beam.

The spectra of deuterons and tritons from the (^{3}He,d) and (α,t) reactions as recorded with an Enge split-pole magnetic spectrograph at 60° and 45°, respectively, are shown in Fig. 1. The excitation energies and absolute differential

---

*Institut für Kernphysik, Universität Frankfurt, Germany.

Fig. 1: Deuteron and triton spectra from the $^{232}Th(^{3}He,d)^{233}Pa$ and $^{232}Th(\alpha,t)^{233}Pa$ reactions, respectively. The individual peak numbers correspond to those in Table 1.

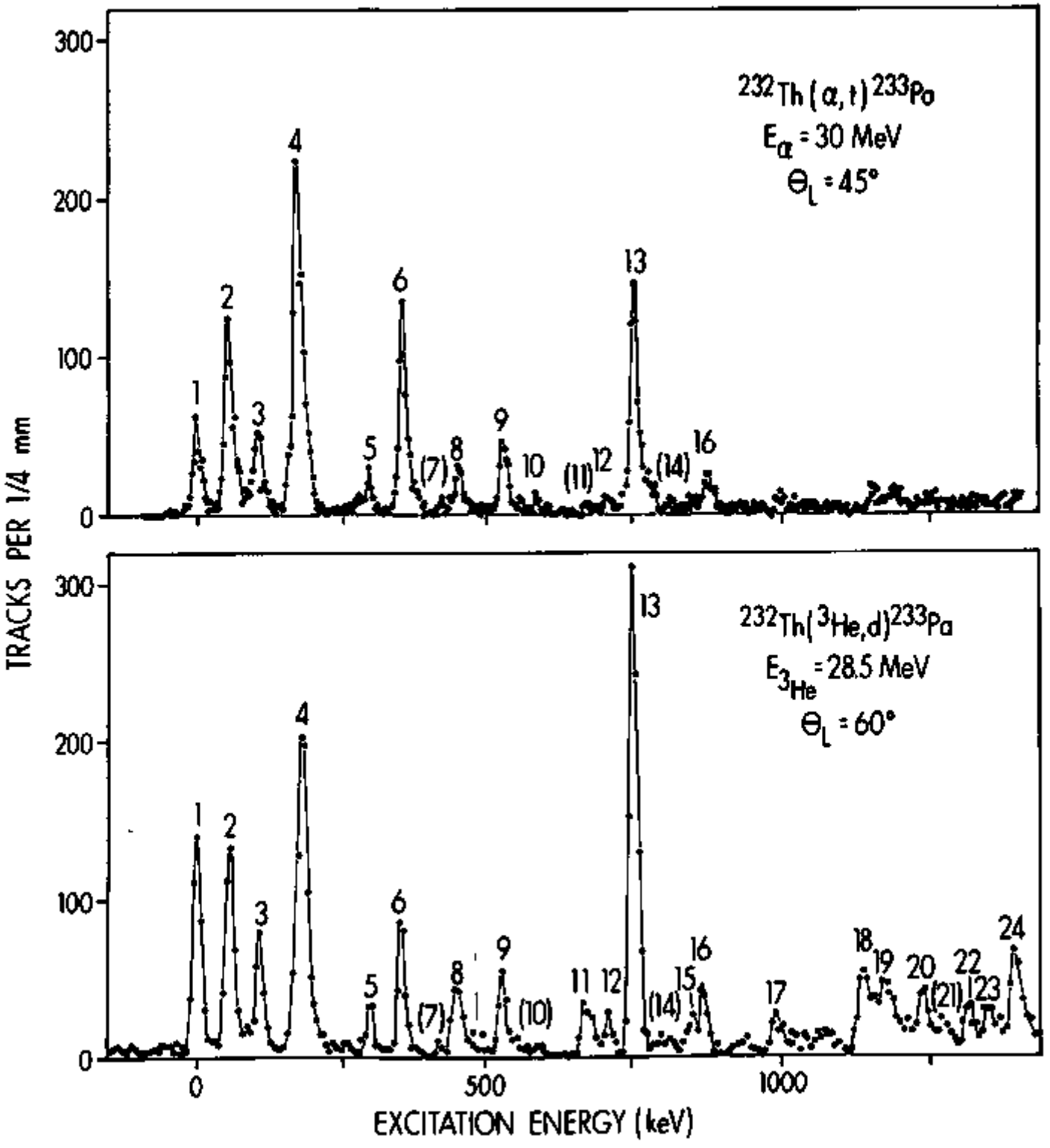
$^{232}Th(\alpha,t)^{233}Pa$
$E_\alpha = 30$ MeV
$\Theta_L = 45°$
$^{232}Th(^3He,d)^{233}Pa$
$E_{^3He} = 28.5$ MeV
$\Theta_L = 60°$
TRACKS PER 1/4 mm
EXCITATION ENERGY (keV)
0
100
200
300
500
1000

Figure 1

cross sections obtained for the various groups are listed in Table 1, along with the proposed assignments that resulted from the analysis described below. A partial level scheme of ^{233}Pa as deduced by combining our results with previously published data is shown in Fig. 2. Assigned levels observed in the present experiment are shown in Fig. 2 by the thicker lines, while the thinner lines indicate previously identified levels which are not measurably excited in our experiments.

The present reaction results are interpreted by distorted-wave Born-approximation (DWBA) analysis. The transferred angular momentum is determined for each transition from the cross section ratio, $R = d\sigma(\alpha,t)/d\sigma(^3He,d)$, which is a sensitive measure of the ℓ-value. For most of the assigned levels in ^{233}Pa, the ℓ-value was determined to within two units of ℓ.

Level assignments made here are based on a comparison of measured and calculated spectroscopic factors (see Table 2). The calculations were performed with Nilsson wave functions and included both Coriolis mixing and pairing effects. For the odd-parity bands, $1/2^-[530\uparrow]$, $3/2^-[521\uparrow]$ and $5/2^-[523\downarrow]$, the Coriolis mixing is found to be weak, and the calculated spectroscopic factors agree reasonably well with experiment. The spectroscopic factors of the even-parity levels (i.e. the $13/2^+$ states), however, deviate considerably from the experimental values.

In order to improve the agreement, we have performed Coriolis calculations which employed all of the even-parity levels known from radioactive decay, as well as the $13/2^+$

Table 1: Energy Levels of ^{233}Pa Excited by the ^{232}Th(^{3}He,d) and ^{232}Th(α,t) Reactions.

Line	Excitation energy (keV)	dσ/dΩ(μb/sr) (^{3}He,d)60°	dσ/dΩ(μb/sr) (α,t)45°	Assignment
1	0	9.0±0.9	10.0±2.5	$3/2^{-}[530\uparrow]$
2	57±1	8.6±0.9	24.0±2.0	$7/2^{-}[530\uparrow]$
3	107±2	4.7±0.6	10.8±1.9	$7/2^{+}+9/2^{+}[651\uparrow]$
4	173±1	16.6±1.2	53.0±6.0	$13/2^{+}[651\uparrow]$
5	298±3	1.6±0.4	4.2±0.7	$7/2^{+}[642\uparrow]+(7/2^{-}[523\downarrow]$
6	355±2	6.3±0.8	22.5±2.4	$(9/2^{-}[523\downarrow])$
(7)	421±4	(0.4±0.2)	(1.3±0.4)	$(11/2^{-}[523\downarrow])$
8	450±2	3.3±0.6	6.3±1.7	
9	529±2	3.6±0.6	9.1±0.7	$(13/2^{+}[660\uparrow])$
10	589±4	(0.4±0.2)	1.3±0.4	$(13/2^{+}[642\uparrow])$
11	670±3	2.6±0.5	(1.3±0.3)	$3/2^{-}[521\uparrow]$
12	704±3	1.5±0.4	2.6±0.4	$5/2^{-}[521\uparrow]$
13	749±1	21.7±1.5	29.2±2.4	$7/2^{-}[521\uparrow]$
(14)	803±4	(0.9±0.3	1.6±0.4	$9/2^{-}[521\uparrow]$
15	852±4	1.8±0.4		
16	871±2	3.0±0.4	6.5±1.1	$11/2^{-}[521\uparrow]$
17	990±4	1.8±0.4		
18	1143±3	4.4±0.6		
19	1179±3	4.1±0.6		
20	1240±3	2.7±0.5		
(21)	1274±5	(0.9±0.3)		
22	1318±4	1.5±0.4		
23	1358±4	1.2±0.3		
24	1403±3	3.5±0.6		

Fig. 2: Partial level scheme of ^{233}Pa. The thicker lines represent levels excited by the (^{3}He,d) and/or (α,t) reactions, while the thinner lines indicate previously identified levels which are not seen in the present work. All energies are rounded off to whole keV. The 104 and 109 keV states are not resolved in the present experiment. Their energies were adopted from radioactive-decay studies, as were the energies and assignments of all other previously known levels. Parentheses indicate uncertain assignments.

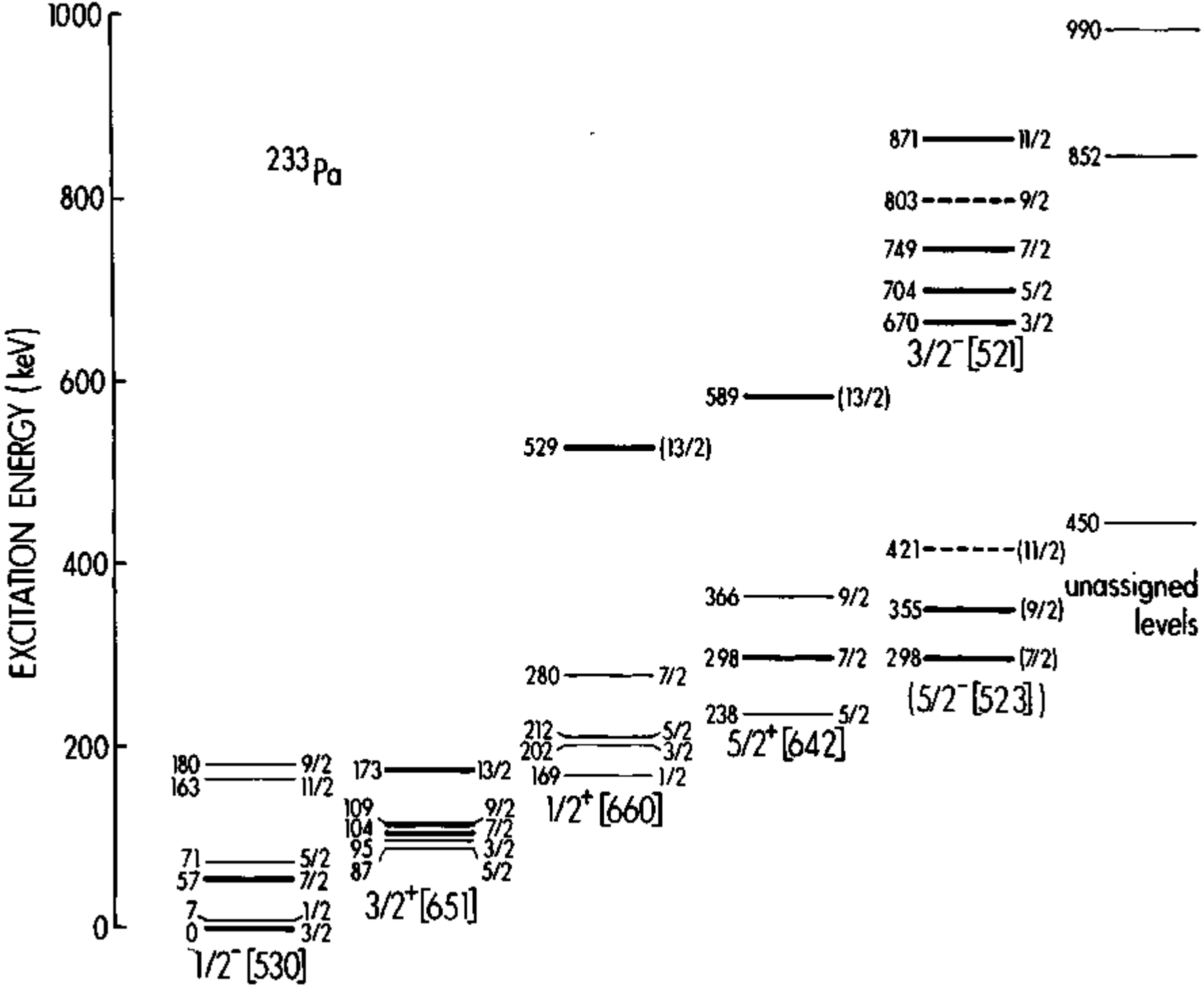
EXCITATION ENERGY (keV)
1000
800
600
400
200
0
233Pa
1/2⁻[530]
180 9/2
163 11/2
71 5/2
57 7/2
7 1/2
0 3/2
3/2⁺[651]
173 13/2
109 9/2
104 7/2
95 3/2
87 5/2
1/2⁺[660]
280 7/2
212 5/2
202 3/2
169 1/2
5/2⁺[642]
589 (13/2)
529 (13/2)
366 9/2
298 7/2
238 5/2
3/2⁻[521]
871 11/2
803 9/2
749 7/2
704 5/2
670 3/2
990
852
450
421 (11/2)
355 (9/2)
298 (7/2)
(5/2⁻[523])
unassigned levels

Figure 2

states. In these calculations, the Coriolis matrix elements, the band-head energies and the decoupling parameter of the $1/2^+[660\uparrow]$ band were treated as parameters and were determined from an energy fit to the known levels, while the rotational parameter $\hbar^2/2\mathcal{I}$ was held constant in each of the calculations. No satisfactory agreement between the experimental and calculated energies of the $13/2^+$ levels was obtained from this 3-band fit. From Table 2 it is seen that the measured spectroscopic factors are also at variance with the calculations.

These differences between experiment and calculation are not unexpected, however. The above-mentioned even-parity configurations all originate from the $i_{13/2}$ spherical state whose components are connected by large Coriolis matrix elements. The couplings to the $i_{13/2}$ components which are not included in the 3-band mixing calculation are therefore not negligible and must also be taken into account. In an attempt to estimate the spectroscopic factors we have diagonalized the complete Coriolis matrix for the $13/2^+$ levels of the $1/2^+[660\uparrow]$, $3/2^+[651\uparrow]$, $5/2^+[642\uparrow]$, $7/2^+[633\uparrow]$, $9/2^+[624\uparrow]$, $11/2^+[615\uparrow]$ and $13/2^+[606\uparrow]$ bands. In this calculation we used the Coriolis matrix elements between the $1/2^+[660\uparrow]$ and $3/2^+[651\uparrow]$ and between the $3/2^+[651\uparrow]$ and $5/2^+[642\uparrow]$ bands as determined from the 3-band fit, while the matrix elements connecting the remaining bands were calculated with Nilsson wave functions. The energy locations of the $7/2^+[633\uparrow]$, $9/2^+[624\uparrow]$, $11/2^+[615\uparrow]$ and $13/2^+[606\uparrow]$ configurations were determined by using the Nilsson eigenenergies for the unmixed

Table 2: Spectroscopic Factors*

State	U^2	S - factor			
		Calculated		Observed	
		pure config.	Coriolis mixed[a]	(^{3}He,d)	(α,t)
$1/2^-[530\uparrow]$	0.47	0.02	0.02		
$3/2^-$		0.15	0.16	0.42	0.26
$5/2^-$		00	0		
$7/2^-$		0.50	0.57	0.57	0.65
$9/2^-$		0.17	0.19	b)	b)
$11/2^-$		0.08	0.09	b)	b)
$5/2^-[523\downarrow]$	0.83	0.02	0.02		
$7/2^-$		0.05	0.04	0.10[c]	0.13[c]
$9/2^-$		1.55	1.57	1.47	1.80
$11/2^-$		0.03	0.03	(0.09)	(0.11)
$3/2^-[521\uparrow]$	0.90	0.07	0.07	0.09	0.05
$5/2^-$		0.02	0.02	0.08	0.09
$7/2^-$		1.40	1.34	1.15	1.08
$9/2^-$		0.18	0.15	0.19	0.14
$11/2^-$		0.09	0.08	0.62	0.59
$3/2^+[651\uparrow]$	0.43	0	0		
$5/2^+$		0	0.01		
$7/2^+$		0	0	0.35	0.28
$9/2^+$		0.06	0.13		
$11/2^+$		0.01	0.02		
$13/2^+$		0.78	2.31	4.96[d]	5.16[d]
$1/2^+[660\uparrow]$	0.25	0	0		
$3/2^+$		0	0		
$5/2^+$		0.01	0		
$7/2^+$		0	0		
$9/2^+$		0.05	0.03		

Table 2, cont'd

State	U^2	S - factor			
		Calculated		Observed	
		pure config.	Coriolis mixed[a]	(^{3}He,d)	(α,t)
$11/2^+$		0	0		
$13/2^+$		0.38	0.12	1.00	0.93
$5/2^+[642\uparrow]$	0.76	0	0		
$7/2^+$		0	0	0.12[c]	0.12[c]
$9/2^+$		0.05	0.01		
$11/2^+$		0.01	0		
$13/2^+$		1.45	0.18	0.11	0.14

*The S factor used in the table is related to the spectroscopic factor S defined by Satchler [ref. 1] by $S = S/(2J+1)$, where J is the spin of the rotational level excited by the stripping reaction.

a) Obtained from 3-band mixing calculations.

b) Obscured by the $13/2^+[651\uparrow]$ group.

c) Possible doublet $7/2^-[523\downarrow] + 7/2^+[642\uparrow]$. The entries in the table are calculated on the basis that the experimental strength is due only to one level.

d) May contain admixtures from the $9/2^-$ and $11/2^-[530\uparrow]$ levels.

single-proton levels with an appropriate correction for pairing effects. No further adjustments were made. The spectroscopic factors obtained from this 7-band calculation for the $13/2^+[642\uparrow]$, $13/2^+[660\uparrow]$ and $13/2^+[651\uparrow]$ levels are 0.31, 1.08 and 3.14, respectively. The corresponding values from the 3-band fit are 0.18, 0.12 and 2.31, whereas the experimental values are 0.13, 0.97 and 5.06. On the whole, the agreement with experiment is improved when the additional bands are taken into account. It is important to mention, however, that the spectroscopic factors are very sensitive to changes both in the energies of the levels which are included in the mixing calculation and in the values of the matrix elements which connect the various levels. Hence, the S-factors resulting from the present calculation are only approximative. More exact Coriolis calculations will become feasible to make when additional components of the $i_{13/2}$ shell are identified by experiment.

1) G.R. Satchler, Ann. Phys. (N.Y.) 3, 275(1958).

2) Th. W. Elze and J.R. Huizenga, in: Contributions, International Conference on Properties of Nuclear States, Montreal (1969) p.253.

3) Th. W. Elze and J.R. Huizenga, Phys. Rev. C1, 328(1970), and Nucl. Phys. A149, 585(1970).

2. Collective Levels Populated by the ^{230}Th(d,d'), ^{240}Pu(d,d') and ^{244}Pu(d,d') Reactions -- R.C. Thompson, J.R. Huizenga, Th. W. Elze* and J.P. Unik**

Inelastic scattering of deuterons strongly populates states of collective nature in heavy nuclei. In particular the low-lying octupole bands in the actinide nuclei are amenable to study with the (d,d') reaction. Earlier work[1,2] has shown that the octupole bands observed with this reaction exhibit a rather stable, characteristic signature pattern in the actinide region.

Isotope separated targets of ^{230}Th, ^{240}Pu and ^{244}Pu have been bombarded with 16 MeV deuterons. The scattered particles were detected at two angles, 90° and 125°, and were analyzed by an Enge split-pole magnetic spectrograph. The deuterons were detected by photographic plates in the focal plane of the spectrograph.

The 125° spectra of the ^{230}Th(d,d')^{230}Th, ^{240}Pu(d,d')^{240}Pu and ^{244}Pu(d,d')^{244}Pu reactions are shown in Figures 3, 4 and 5, respectively. In addition to the excitation energies of the levels in each reaction, the absolute cross sections of each level were measured at the above two angles. The energies and cross sections of the low-lying levels of ^{230}Th, ^{240}Pu and ^{244}Pu are summarized in Tables 3, 4 and 5, respectively.

In the ^{230}Th(d,d')^{230}Th reaction we have populated the ground state band up to the 8^+ level and have seen the 0^+ beta

---

*Institut für Kernphysik, Universität Frankfurt, Germany.
**Argonne National Laboratory, Argonne, Illinois 60439.

Fig. 3: Levels of ^{230}Th excited by inelastic scattering of 16 MeV deuterons.

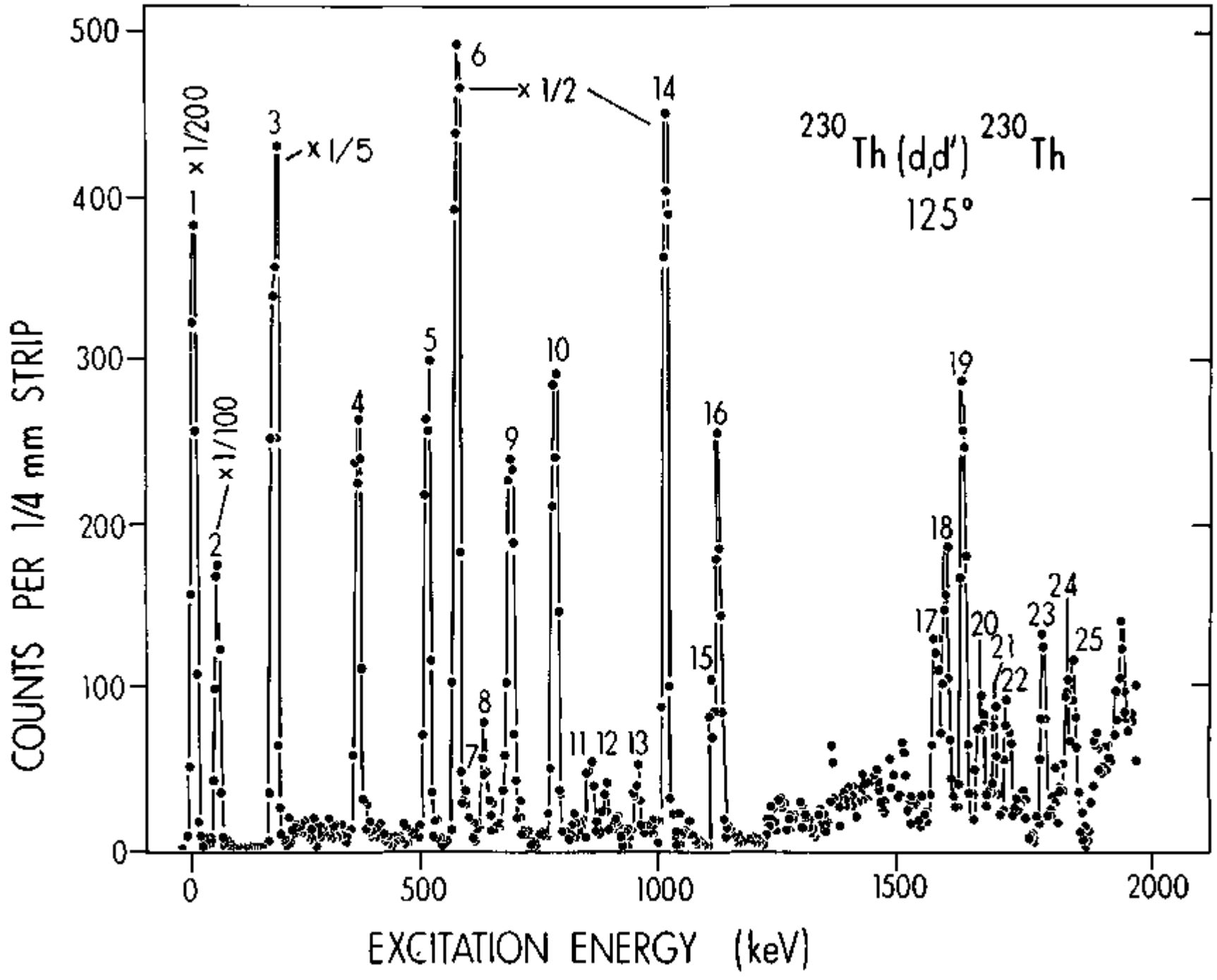
COUNTS PER 1/4 mm STRIP
EXCITATION ENERGY (keV)
^{230}Th (d,d') ^{230}Th
125°
× 1/200
× 1/100
× 1/5
× 1/2
0
100
200
300
400
500
0
500
1000
1500
2000
1
2
3
4
5
6
7
8
9
10
11
12
13
14
15
16
17
18
19
20
21
22
23
24
25

Figure 3

Fig. 4: Levels of ^{240}Pu excited by inelastic scattering of 16 MeV deuterons.

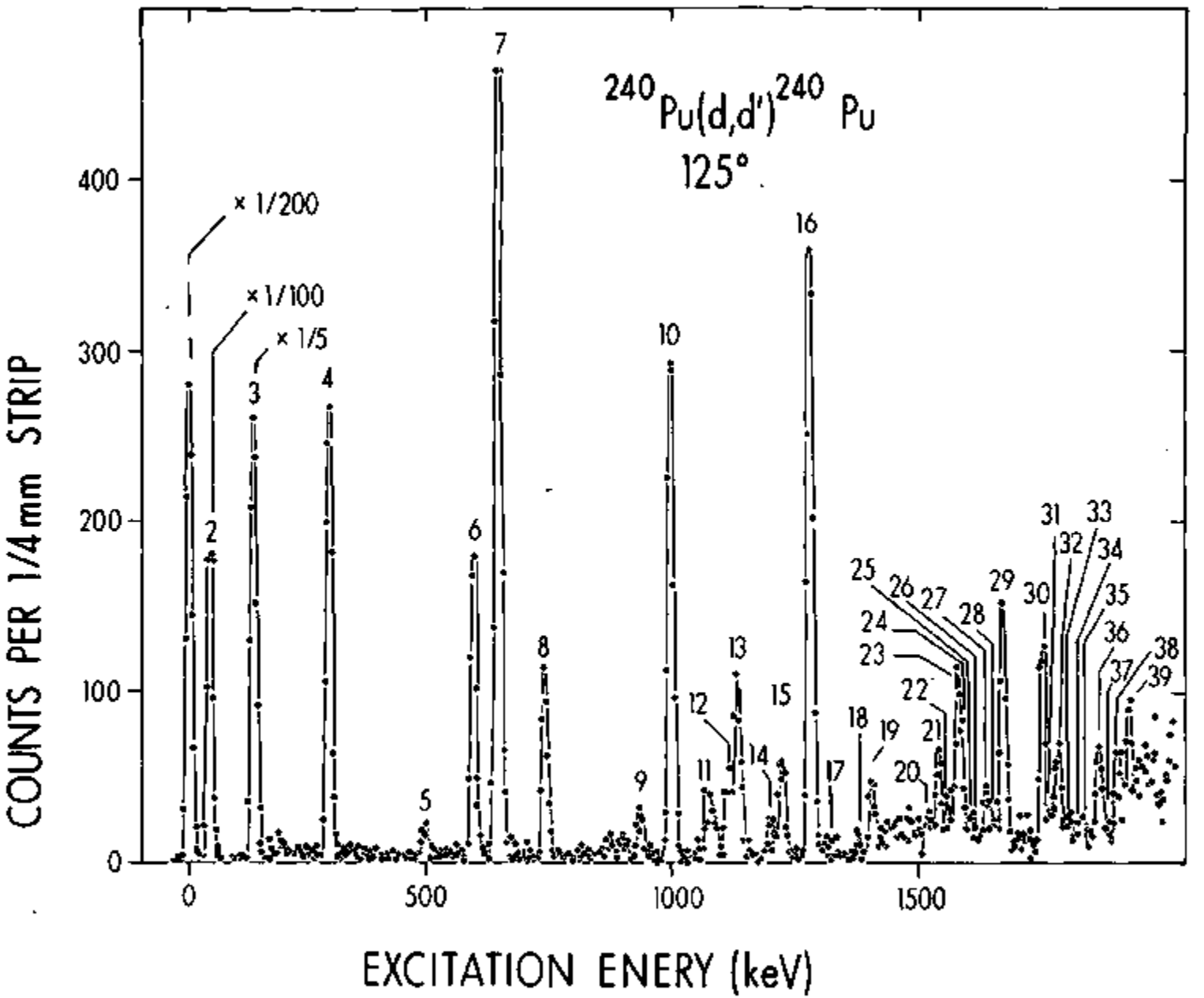
^{240}Pu(d,d')^{240} Pu
125°
× 1/200
× 1/100
× 1/5
COUNTS PER 1/4mm STRIP
EXCITATION ENERY (keV)
0
100
200
300
400
0
500
1000
1500
1
2
3
4
5
6
7
8
9
10
11
12
13
14
15
16
17
18
19
20
21
22
23
24
25
26
27
28
29
30
31
32
33
34
35
36
37
38
39

Figure 4

Fig. 5: Levels of ^{244}Pu excited by inelastic scattering of 16 MeV deuterons.

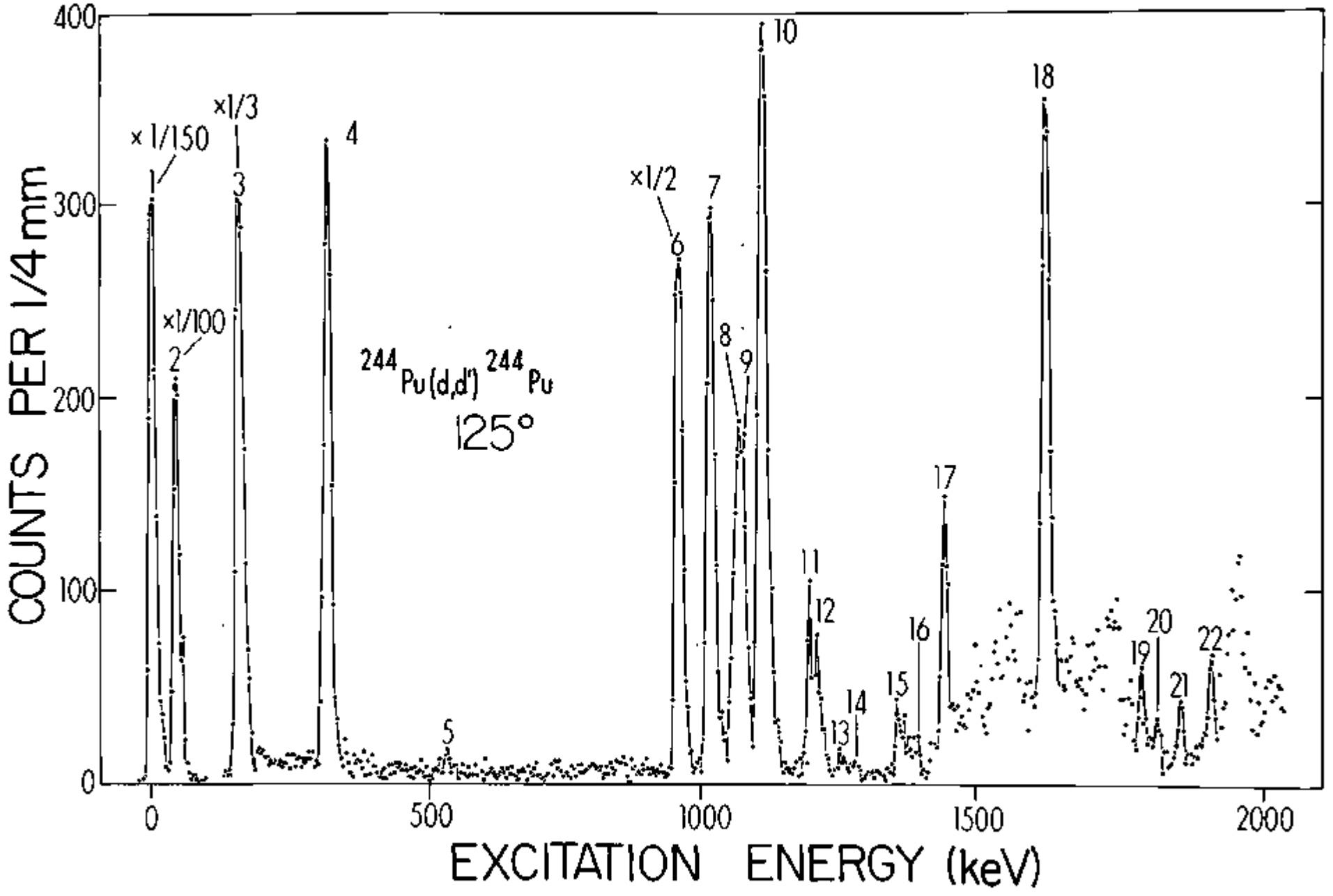
400
300
200
100
0
COUNTS PER 1/4 mm
0
500
1000
1500
2000
EXCITATION ENERGY (keV)
x 1/150
x1/3
x1/100
x1/2
1
2
3
4
5
6
7
8
9
10
11
12
13
14
15
16
17
18
19
20
21
22
^{244}Pu(d,d')^{244}Pu
125°

Figure 5

Table 3. Cross sections and energies of levels in ^{230}Th excited by the (d,d') reaction.

Line	Energy keV(±keV)	$\frac{d\sigma}{d\omega}(90°)$ [a] μb/sr	$\frac{d\sigma}{d\omega}(125°)$ μb/sr	$R=\frac{d\sigma(90°)}{d\sigma(125°)}$	Assignment [b] K, J^π
1	0	39300	8290	4.74	$0,0^+$
2	54(2)	5012	2140	2.34	$0,2^+$
3	173(2)	541	259	2.09	$0,4^+$
4	357(2)	29.0	35.2	.82	$0,6^+$
5	506(2)	32.5	37.7	.86	$0,1^-$
6	570(2)	246.	126.	1.95	$0,3^-$
7	592(4)	--	10.3	--	$0,8^+$
8	632(3)	8.4	9.4	.89	$0,0^+$
9	682(2)	39.7	35.3	1.12	$0,5^+$
10	781(2)	83.5	38.9	2.14	$2,2^+$
11	852(4)	--	7.8	--	$(0,7^-)$
12	881(4)	12.4	6.0	2.07	$(2,4^+)$
13	951(3)	12.1	7.3	1.66	$1,1^-$
14	1011(2)	175.	108.	1.62	$1,3^-$
15	1110(4)	23.1	12.1	1.91	$(2,3^-)$
16	1125(3)	28.2	23.9	1.18	$(1,5^-)$
17	1571(3)	36.8	19.2	1.92	
18	1591(3)	38.2	24.1	1.59	
19	1628(2)	65.3	38.5	1.70	
20	1663(3)	23.1	13.5	1.71	
21	1695(4)	20.0	9.9	2.02	
22	1718(3)	18.6	12.1	1.54	
23	1791(3)	32.9	15.9	2.07	
24	1842(4)	26.4	12.6	2.10	
25	1858(4)	37.1	12.6	2.94	

a) The absolute values of the 90° cross sections for levels 4 through 25 were not experimentally determined. The normalization was adjusted so that the $K,J^\pi=0,3^-$ level has the same 90°/125° cross section ratio as the average of the ratios of the $0,3^-$ levels in ^{234}U, ^{236}U, ^{238}U, ^{240}Pu, and ^{242}Pu.

b) Assignments in parentheses are uncertain.

Table 4. Cross sections and energies of levels in ^{240}Pu excited by the (d,d') reaction.

Line	Energy keV(±keV)	$\frac{d\sigma}{d\omega}(90°)$ μb/sr	$\frac{d\sigma}{d\omega}(125°)$ μb/sr	$R=\frac{d\sigma(90°)}{d\sigma(125°)}$	Assignment K, J^π
1	0	50000	10400	4.81	$0,0^+$
2	45(1)	8280	3760	2.20	$0,2^+$
3	142	541	370	1.46	$0,4^+$
4	292(1)	53.6	73.2	.73	$0,6^+$
5	497(2)	8.0	7.6	1.05	$0,8^+$
6	596(2)	28.0	47.5	.59	$0,1^-$
7	649(1)	289	128	2.26	$0,3^-$
8	742(1)	21.1	30.4	.69	$0,5^-$
9	939(3)	9.4	11.3	.83	$2,2^+$
10	1001(1)	146	80.5	1.81	$2,3^-$(a)
11	1077(4)	21.9	16.8	1.30	
12	1118(2)	13.9	15.3	.91	
13	1135(2)	66.1	30.8	2.15	
14	1199(2)	11.8	7.2	1.64	
15	1224(3)	28.5	22.0	1.30	
16	1282(2)	162	95.7	1.69	3^-(a)
17	1313(3)	28.4	6.4	4.44	
18	1379(4)	--	5.8	--	
19	1407(3)	--	18.6	--	
20	1519(4)	--	8.2	--	
21	1538(3)	--	17.4	--	
22	1558(4)	--	10.0	--	
23	1574(2)	33.4	20.9	1.60	
24	1586(4)	29.0	17.4	1.67	
25	1609(6)	21.8	7.7	2.83	
26	1625(6)	15.9	6.0	2.65	
27	1641(5)	16.1	12.3	1.31	
28	1658(5)	15.0	6.6	2.27	
29	1675(2)	69.8	37.3	1.87	
30	1752(3)	47.2	35.2	1.34	

continued

Table 4. (Continued)

Line	Energy keV(±keV)	$\frac{d\sigma}{d\omega}(90°)$ μb/sr	$\frac{d\sigma}{d\omega}(125°)$ μb/sr	$R=\frac{d\sigma(90°)}{d\sigma(125°)}$	Assignment K, J^{π}
31	1771(4)	17.0	7.4	2.30	
32	1784(3)	19.9	17.4	1.14	
33	1804(6)	--	7.9	--	
34	1824(6)	--	5.7	--	
35	1837(4)	17.0	7.2	2.36	
36	1861(3)	24.8	19.3	1.28	
37	1880(6)	--	7.6	--	
38	1902(3)	36.5	19.3	1.89	
39	1923(3)	45.0	34.0	1.32	

[a] K value uncertain.

Table 5. Cross sections and energies of levels in ^{244}Pu excited by the (d,d') reaction.

Line	Energy keV(±keV)	$\frac{d\sigma}{d\omega}(90°)$ μb/sr	$\frac{d\sigma}{d\omega}(125°)$	$R=\frac{d\sigma(90°)}{d\sigma(125°)}$	Assignment K, J^π
1	0	50300	10400	4.84	$0,0^+$
2	46(2)	10400	4592.	2.26	$0,2^+$
3	154(2)	615.	262.	2.35	$0,4^+$
4	315(2)	89.8	81.2	1.11	$0,6^+$
5	537(4)	13.7	--		$0,8^+$
6	957(2)	367.	147.	2.50	$2,3^-$
7	1015(2)	278.	81.7	3.40	
8	1061(4)	26.7	37.7	.71	
9	1075(4)	47.0	37.0	1.27	
10	1108(2)	368.	125.	2.94	3^-(c)
11	1194(3)	19.4	20.9	.93	
12	1210(3)	31.7	15.7	2.02	
13	1251(4)	---a)	3.9		
14	1278(4)	---a)	5.4		
15	1353(4)	---a)	11.1		
16	1378(3)	100b)	21.4		
17	1434(3)	150b)	35.7		
18	1613(3)	270b)	105.		3^-(c)
19	1783(3)	40b)	19.3		
20	1805(3)	30b)	9.8		
21	1847(3)	---a)	10.1		
22	1896(3)	70b)	21.7		

a) Obscured in 90° spectrum. It is possible that these levels are not ^{244}Pu states.

b) There are very large errors associated with these cross sections.

c) K assignment uncertain.

band head at 632 keV. The 2^+ level of the γ-vibrational band has been observed at 781 keV. The $K^\pi=0^-$, $I^\pi=1^-$ band is observed at 506 keV along with the 3^-, 5^- and 7^- rotational members. The level at 1011 keV is strongly excited and is clearly a 3^- level. A level at this energy has been previously assigned a tentative spin-parity of 2^+. The 1011 keV level is probably a member of the K=1 octupole band with the band head at 951 keV (line 13).

In the ^{240}Pu(d,d')^{240}Pu and ^{244}Pu(d,d')^{244}Pu reactions we have also observed the ground state rotational members up to the 8^+ states. Of the four possible octupole bands we assign the $K^\pi=0^-$ band and the 3^- levels of two additional bands in ^{240}Pu. One of the striking differences between ^{244}Pu and the lighter actinide nuclei is that the $K^\pi=0^-$ band is no longer the lowest octupole band. In the case of ^{244}Pu, the lowest energy octupole band is the $K^\pi=2^-$ band. From Fig. 5, one observes that the very intense 3^- level (line 6) is the first line excited above the ground state band.

The relative values of the $B(E\lambda;0^+\rightarrow\lambda^\pi)$ have been extracted from the cross sections for the identified 2^+ and 3^- levels of each nucleus. The relative values of the B(E3) reduced matrix elements for ^{230}Th are in fairly good agreement with the microscopic calculations of Neergard and Vogel[3]. In this case, two octupole bands are strongly excited. For the isotopes ^{240}Pu and ^{244}Pu, all four octupole bands are rather strongly excited and the strength is about evenly distributed over the four band for ^{244}Pu.

1) Th. W. Elze and J.R. Huizenga, Nucl. Phys. A187, 545(1972).

2) J.S. Boyno, J.R. Huizenga, Th. W. Elze and C.E. Bemis, Nucl. Phys. A209, 125(1973).

3) K. Neergard and P. Vogel, Nucl. Phys. A149, 217(1970).

3. Collective Levels in ^{233}U and ^{239}Pu Excited by Inelastic Deuteron Scattering -- R.C. Thompson, J.R. Huizenga, Th. W. Elze* and J.P. Unik**

Inelastic scattering of 16 MeV deuterons has been used to excite the collective levels of the odd-A nuclei ^{233}U and ^{239}Pu. The scattered deuterons were analyzed with an Enge Split-pole magnetic spectrograph and detected with photographic plates. Spectra were taken at 90° and 125° for each nucleus. The resulting plates are in the process of being scanned.

---

*Institut für Kernphysik, Universität Frankfurt, Germany.

**Argonne National Laboratory, Argonne, Illinois 60439.

27544

4. Study of the ^{192}Os(p,t)^{190}Os, ^{190}Os(p,t)^{188}Os and ^{188}Os(p,t)^{186}Os Reactions -- R.C. Thompson, J.R. Huizenga, D.G. Burke*, Th. W. Elze** and J.S. Boyno***

As a result of shape isomerism being observed in the Sm[1] and Gd[2] nuclei by the (p,t) reaction, there has been some interest in applying this method to the transition region between the rare-earth and lead regions. We have looked at the (p,t) reaction with targets of ^{192}Os, ^{190}Os, and ^{188}Os.

The targets were made by evaporating isotopically enriched samples of osmium metal onto carbon backings. These were then bombarded with 18-MeV protons and the exiting tritons were analyzed by an Enge split-pole spectrograph and detected by photographic plates. The disparity in the (p,t) strengths of the ground states and the excited states made it necessary to make two separate exposures for each spectrum. The short exposure provided information on the ground state and first $J^{\pi} = 2^{+}$ level, and the long exposure showed the excited states. The ground state band 2^{+} level was seen in both the long and short runs and enabled us to extract absolute cross sections for all states.

For the reactions on all three targets, complete angular distributions from 10° to 65° in 5° steps were made for the short runs. In the ^{192}Os(p,t)^{190}Os and ^{188}Os(p,t)^{186}Os

---

*Physics Department, McMaster University, Hamilton, Ontario.
**Institut für Kernphysik, Universität Frankfurt, Germany.
***Cyclotron Laboratory, Michigan State University, East Lansing, Michigan 48824.

reactions the same complete angular distributions were taken for the long runs. In the ^{190}Os(p,t)^{188}Os reaction, however, only four long exposure spectra were taken: 10°, 25°, 40°, and 55°. The very stable and characteristic angular distributions of the $\ell = 0$ transfer enabled us to make $J^{\pi} = 0^{+}$ assignments in ^{188}Os with as much confidence as in the ^{190}Os and ^{186}Os nuclei.

A (p,t) run was also made on a target of natural osmium. From this we have been able to determine the ground state Q-values of the ^{192}Os(p,t), ^{190}Os(p,t), ^{189}Os(p,t), ^{188}Os(p,t) and ^{187}Os(p,t) reactions. These are given in Table 6.

In Table 7 are listed the low-lying excited states observed in the ^{192}Os(p,t)^{190}Os and ^{190}Os(p,t)^{188}Os reactions and the cross sections for the 25° spectra. The spectra of the ^{188}Os(p,t)^{186}Os reaction are in the process of being analyzed.

One of the crucial criteria for the observance of shape isomerism in a (p,t) reaction is the population of an excited 0^{+} state with an appreciable fraction of the ground state strength. As an example, in the Gd nuclei there are states with approximately 15% of the ground state cross section[2]. Table 8 shows the strengths of the excited 0^{+} states of ^{188}Os and ^{190}Os relative to their ground states. All of the states have small cross sections. From this one can conclude that the ground states of ^{192}Os, ^{190}Os, and ^{188}Os are similar in character.

Table 6

Q-values for (p,t) Reactions on Osmium

Target Mass	Ground State Q-value (keV)	S_{2n} from present results (keV)
187	-6074±4	14556±4
188	-5803±4	14285±4
189	-5432±4	13914±4
190	-5237±4	13719±4
192	-4837±4	13319±4

Table 7

Levels populated in the $^{192}Os(p,t)^{190}Os$ and $^{190}Os(p,t)^{188}Os$ reactions.

$^{192}Os(p,t)^{190}Os$				$^{190}Os(p,t)^{188}Os$			
line number	Excitation (keV)	Cross section[a] (μb/sr)	Assignment (J^π)	line number	Excitation (keV)	Cross section[a] (μb/sr)	Assignment (J^π)
1	0	823	0^+	1	0	815	0^+
2	187	79		2	155	79	
3	548	8.2		3	477	15	
4	558	20		4	632	17	
5	911	23	0^+	5	965	{5.4}	
6	954	5.7		6	976		
7	966	1.1		7	1086	24	0^+
8	1055	1.6		8	1279	2.1	
9	1113	1.8		9	1304	5.0	
10	1162	1.0		10	1413	10	
11	1384	{13}		11	1458	1.5	
12	1396			12	1477	16	0^+
13	1434	2.7		13	1566	3.1	
14	1540	8.8	0^+	14	1617	{5.0}	
15	1613	1.0		15	1626		
16	1680	3.4		16	1666	2.9	
17	1706	2.0		17	1702	6.2	0^+
18	1717	1.3		18	1732	1.3	
19	1731	23	0^+	19	1747	1.8	
				20	1763	1.5	
				21	1769	≤ 0.4	
				22	1808	3.0	
				23	1821	3.5	0^+

[a] Cross section for 25°.

Table 8

Relative strengths of the $J^{\pi} = 0^{+}$ levels populated in the $^{192}Os(p,t)^{190}Os$ and $^{190}Os(p,t)^{188}Os$ reactions.

$^{192}Os(p,t)^{190}Os$		$^{190}Os(p,t)^{188}Os$	
Excitation (keV)	% of ground state[a]	Excitation (keV)	% of ground state[a]
911	5.55	1086	5.97
1540	1.82	1477	3.40
1731	7.19	1702	1.30
		1821	1.05

a) The total cross section of the states are taken to be the sum of the differential cross sections of the 10°, 25°, 40°, and 55° spectra.

It is possible that the nonobservance of shape isomers in osmium results from the fact that the (p,t) reaction looks at the ground state change with the addition of two neutrons. In the osmium region deformation changes fairly slowly with neutron number but quite rapidly with proton number. The reverse is true in the Gd-Sm transition region. In addition to shape isomers caused by abrupt deformation change, there has been some question as to whether there might be observable effects caused by the change in γ-stability of the osmium which has been indicated by a microscopic calculation of Kumar and Baranger[3]. There seems to be no obvious effect on the (p,t) cross sections.

1) J.R. Maxwell, G.M. Reynolds and N.M. Hintz, Phys. Rev. 151, 1000(1966).

2) Th. W. Elze, J.S. Boyno, and J.R. Huizenga, Nucl. Phys. A187, 473(1972).

3) K. Kumar and M. Baranger, Nucl. Phys. A122, 273(1968).

27545

B. Compound Nucleus and Statistical Reactions

1. Level Densities for Spherical Nuclei -- J.R. Huizenga, A.N. Behkami[†], J.S. Sventek[††] and R.W. Atcher

The nuclear level spacings determined from neutron resonance experiments for nuclei with $20 \lesssim A \lesssim 148$ and $181 \lesssim A \lesssim 209$ have been compared with spacings calculated for spherical nuclei with a microscopic theory which includes the nuclear pairing interaction. The level density of a spherical nucleus for a particular value of the angular momentum I is given by

$$\rho(E,I) = \omega(E,M=I) - \omega(E,M=I+1) \qquad (1)$$

where M is the projection of I on a space-fixed axis and $\omega(E,M)$ is the density of states of a particular projection M. Since many independent degrees of freedom contribute to M, the density of states $\omega(E,M)$ is expected to approach a normal distribution,

$$\omega(E,M) = [\omega(E)/(2\pi\sigma^2(E))^{1/2}] \exp[-M^2/2\sigma^2(E)] \qquad (2)$$

where $\omega(E)$ is the total state density and $\sigma^2(E)$ is defined as a spin cutoff factor. From eqs. (1) and (2), one obtains to a good approximation the spin dependent level density,

$$\rho(E,I) = [(2I+1)/(8\pi)^{1/2}\sigma^3(E)]\omega(E)\exp[-I(I+1)/2\sigma^2(E)]. \qquad (3)$$

The state density $\omega(E)$ is calculated with realistic sets of single particle levels[1,2] by the grand partition

---

[†]Department of Physics, Pahlavi University, Shiraz, Iran.

[††]Lawrence Berkeley Laboratory, University of California, Berkeley, California 94720.

function method for a system of interacting Fermions. The Hamiltonian describing a system of paired Fermions is approximately diagonalized by means of a transformation where the quasi-particle excitations are considered to be independent Fermions with energy[3]

$$E_k = [(\varepsilon_k - \lambda)^2 + \Delta^2]^{1/2} \qquad (4)$$

where λ is the chemical potential, ε_k the single particle energy and Δ the gap parameter which gives a measure of the pairing correlation. The spin cutoff factor $\sigma^2(E)$ is calculated also with the microscopic theory.

The theoretical to experimental level spacings from neutron capture resonance data are plotted in Fig. 6. The solid points are based on the single particle levels of Seeger, et al.[1] and the open points are based on the single particle levels of Nilsson, et al.[2]. The gross features of the experimental data due to nuclear shells are reproduced with the microscopic theory. In addition, the absolute agreement between experiment and theory is reasonable (67% of the 151 cases examined agree to within a factor of 2) in view of uncertainties in the experimental data, the theoretical single particle levels and the pairing strength.

In Table 9 a comparison is made for several nuclei for single particle levels of Seeger, et al. and Nilsson, et al. The overall agreement, for all nuclei between experiment and theory for each set of single particle levels is comparable. However, the single particle levels of Nilsson, et al. give a

Fig. 6: The ratio of the theoretical level spacing to the experimental level spacing as a function of mass number. The different symbols refer to the different types of nuclei. Closed symbols refer to theoretical spacings calculated with single particle levels of Seeger and Perisho[1] and the open symbols refer to theoretical spacings calculated with single particle levels of Nilsson, et al.[2]. The ratios $D_{theo.}/D_{exp.}$ plotted in this figure are calculated with the most favorable value of $D_{exp.}$

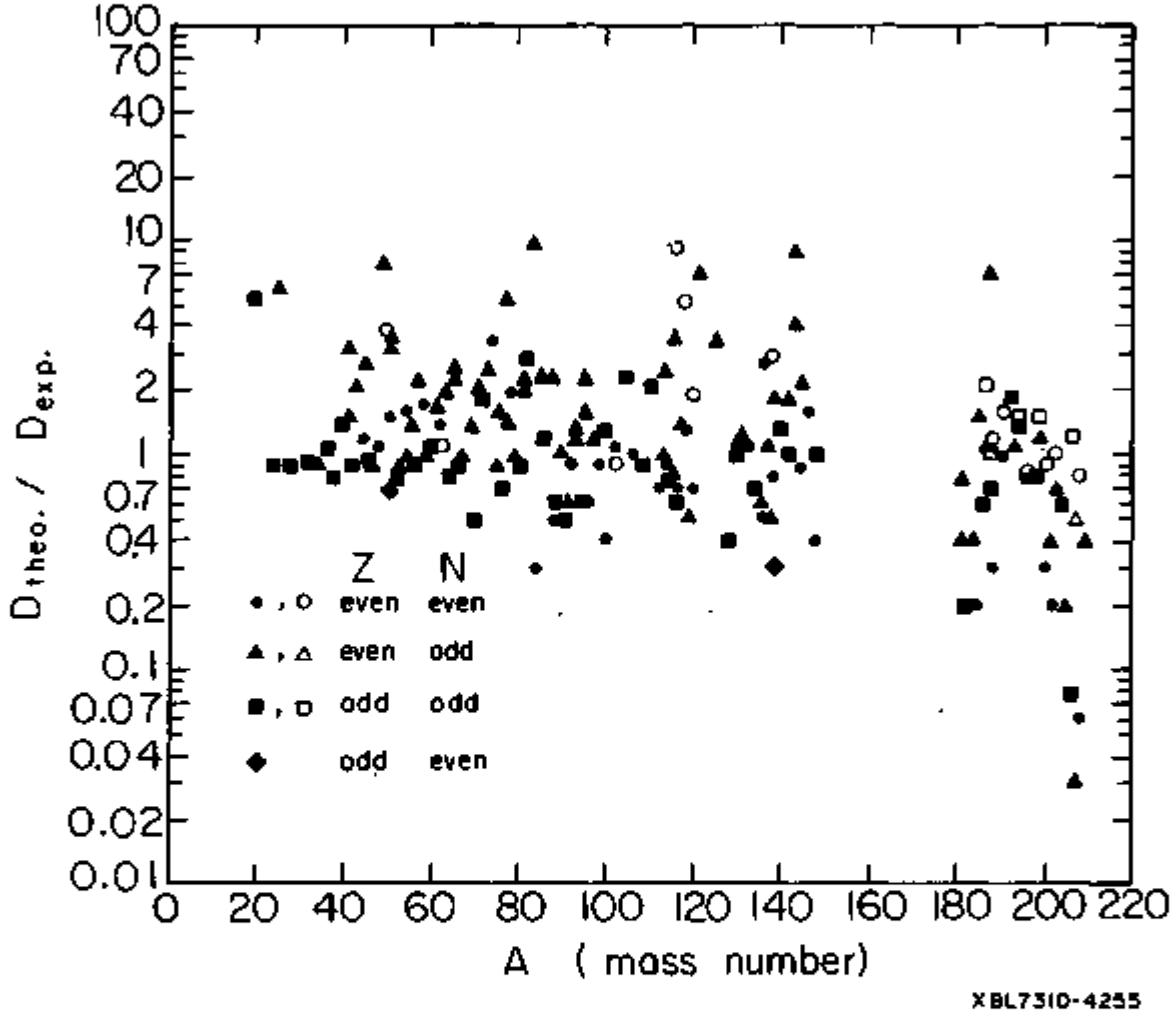
100
70
40
20
10
7
4
2
1
0.7
0.4
0.2
0.1
0.07
0.04
0.02
0.01
D theo. / D exp.
Z N
•, ○ even even
▲, △ even odd
■, □ odd odd
◆ odd even
0 20 40 60 80 100 120 140 160 180 200 220
A (mass number)
XBL7310-4255

Figure 6

Table 9. Comparison of theoretical level spacings calculated with spherical single particle levels of Seeger and Perisho[1] and Nilsson, et al.[2].

Target	I_o, π	Compound Nucleus	$I_o \pm \frac{1}{2}, \pi$	E^* MeV	D_{exp} in eV (a)	(b)	(c)	D_{Theo} in eV (d)	(e)
^{49}Ti	$\frac{7}{2}-$	^{50}Ti	3-,4-	11.67		3600	6000	9100	23,000
^{61}Ni	$\frac{3}{2}-$	^{62}Ni	1-,2-	10.63		2300	1400	3300	2600
^{101}Ru	$\frac{5}{2}+$	^{102}Ru	2+,3+	9.22	16	15	18	20	13
^{115}Sn	$\frac{1}{2}+$	^{116}Sn	0+,1+	9.57	50	50		36	470
^{117}Sn	$\frac{1}{2}+$	^{118}Sn	0+,1+	9.33	25	65	45	33	350
^{119}Sn	$\frac{1}{2}+$	^{120}Sn	0+,1+	9.10	30	62	70	20	130
^{137}Ba	$\frac{3}{2}+$	^{138}Ba	1+,2+	8.61	200	460	230	160	460
^{185}Re	$\frac{5}{2}+$	^{186}Re	2+,3+	6.18	3.8	3.2	3.3	2	8
^{187}Re	$\frac{5}{2}+$	^{188}Re	2+,3+	5.87	4.5	6.4	3.8	3	7
^{187}Os	$\frac{1}{2}-$	^{188}Os	0-,1-	7.99		14	9.1	3	10
^{189}Os	$\frac{3}{2}-$	^{190}Os	1-,2-	7.79		5	4.3	5	8
^{193}Ir	$\frac{3}{2}+$	^{194}Ir	1+,2+	6.07	8.2	8.5	8.0	12	12

(continued)

Table 9. (continued)

Target	I_o, π	Compound Nucleus	$I_o \pm \frac{1}{2}, \pi$	E^* MeV	D_{exp} in eV (a)	(b)	(c)	D_{Theo} in eV (d)	(e)
^{195}Pt	$\frac{1}{2}$ -	^{196}Pt	0-,1-	7.92	18	19	12	15	15
^{197}Au	$\frac{3}{2}$ +	^{198}Au	1+,2+	6.51	17	16	16	12	25
^{199}Hg	$\frac{1}{2}$ -	^{200}Hg	0-,1-	8.03	70	84	75	24	60
^{201}Hg	$\frac{3}{2}$ -	^{202}Hg	1-,2-	7.76	100	110	90	20	100
^{205}Tl	$\frac{1}{2}$ +	^{206}Tl	0+,1+	6.54	10,000	19,000	4000	300	5000
^{206}Pb	0+	^{207}Pb	$\frac{1}{2}$ +	7.11		24,000	50,000	800	11,400
^{207}Pb	$\frac{1}{2}$ -	^{208}Pb	0-,1-	7.67	8000	22,000	60,000	500	6700

a) Data compiled by Lynn, The Theory of Neutron Resonance Reactions (1968), Clarendon, Press, Oxford.

b) Data compiled by Baba, Nucl. Phys. A159(1970)625.

c) Data compiled by Vonach, et al., Nucl. Phys. A217(1973)269.

d) Calculated with spherical single particle levels of Seeger and Perisho[1].

e) Calculated with spherical single particle levels of Nilsson, et al.[2].

much better agreement with experiment for nuclei very near ^{208}Pb. This is associated with the 82 proton and 126 neutron shell gaps being smaller for the Seeger single particle levels than the Nilsson, et al. single particle levels.

The theoretical values of the level spacings which are reported here were calculated with single particle levels for spherical nuclei. Although the well known statically deformed nuclei in the lanthanide and actinide regions of the periodic table are not included in this survey, some nuclei are included which may have small deformations and others which are in transition regions between spherical and deformed nuclei. This subject of the effect of deformation on the level density is discussed in the following report. For the nuclei included here, no enhancement in the level density due to either rotational or vibrational levels is assumed. The general agreement between the experimental and theoretical spacings for the included nuclei as a function of A may be interpreted to mean that no enhancement due to collective excitation is justified. This conclusion is, however, not warranted since uncertainties in the pairing energy and single particle density mentioned earlier allow for the possibliity of some contribution to the level density due to collective excitations. If such an enhancement exists, the present results indicate that it is rather independent of A.

Values of the spin cutoff parameter $\sigma^2(E)$, calculated with the microscopic theory, are plotted for several even-even

nuclei in Fig. 7. The excitation energy for all nuclei is 7 MeV. The values of $\sigma^2(E)$ do not increase smoothly with A as expected on the basis of the macroscopic theory with a rigid-body moment of inertia. Instead the values of $\sigma^2(E)$ show structure reflecting the angular momenta of the shell model orbitals near the Fermi energy. The total magnitude of $\sigma^2(E)$ is made up of a sum of a neutron and proton component. The trends in the values of $\sigma^2(E)$ with A calculated with the microscopic theory are in general agreement with experimental information.

In summary, the values of the level spacings and spin cutoff factors calculated with the microscopic theory including nuclear pairing for realistic sets of single particle levels are in good agreement with experiment. In particular, gross features of the experimental data due to nuclear shells are reproduced.

1) P.S. Seeger and R.C. Perisho, Los Alamos Scientific Laboratory Report, LA-3751 (1957).

2) S.G. Nilsson, et al., Nucl. Phys. A131(1969)1.

3) N.N. Bogoliubov, Nuovo Cimento 1(1958)794.

Fig. 7: The spin cutoff parameter, σ^2, for an excitation energy of 7 MeV is plotted as a function of the mass number A for even-even spherical nuclei.

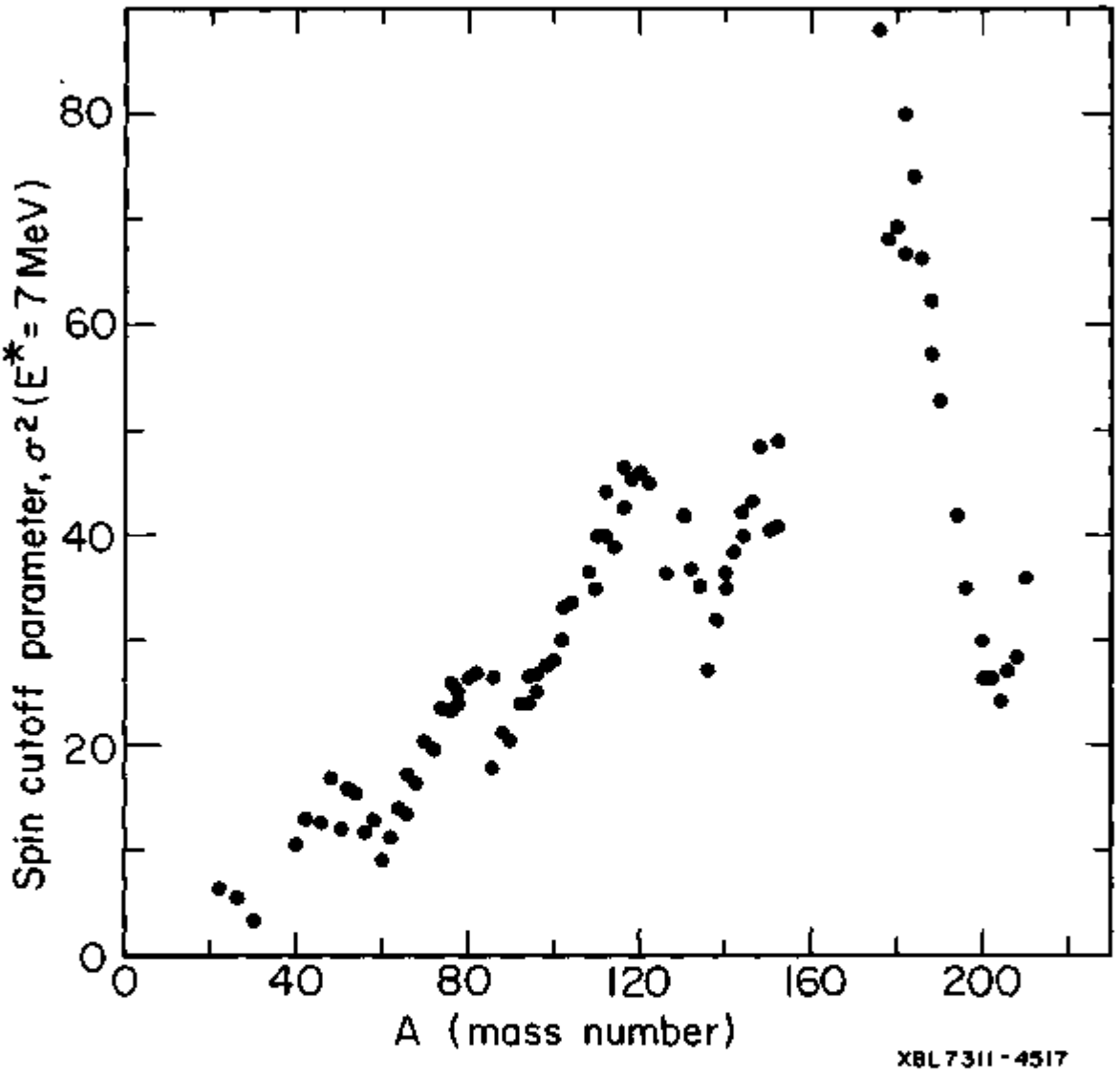
Spin cutoff parameter, σ^2 (E^* = 7 MeV)
0
20
40
60
80
0
40
80
120
160
200
A (mass number)
XBL 7311-4517

Figure 7

27546

2. Level Densities for Nuclei with Static Deformation --

J.R. Huizenga, A.N. Behkami†, R.W. Atcher, J.S. Sventek††, H.C. Britt††† and H. Freiesleben††††

A level density formula including low-energy rotational levels for nuclei with axially symmetric deformation has been tested with neutron resonance data for lanthanide and actinide nuclei. With the inclusion of rotational levels, the spin dependent level density is given by,

$$\rho(E,I) = [1/(8\pi)^{1/2}\sigma_{||}(E)]\omega_{intr}(E) \sum_{K=-I}^{K=+I} \exp - \frac{K^2}{2\sigma_{||}^2(E)} \cdot \frac{I(I+1)-K^2}{2\sigma_{\perp}^2(E)} \quad (1)$$

where $\omega_{intr}(E)$ is the particle state density and $\sigma_{||}^2$ and $\sigma_{\perp}^2$ are spin cutoff parameters defined paralled and perpendicular to the nuclear symmetry axis. The quantity $\sigma_{||}^2$ is related to the total projection of the particle angular momentum on the nuclear symmetry axis and is calculated with the microscopic theory whereas $\sigma_{\perp}^2$ is estimated with a macroscopic theory. The energy dependence of the level density is contained in $\omega_{intr}(E)$ which is calculated with a microscopic theory including nuclear pairing. It is rather easy to show that the particle state density is related to the total state density which includes particle and collective rotational states by,

$$\omega(E) \approx \omega_{intr}(E)\ \sigma^2(E). \quad (2)$$

†Department of Physics, Pahlavi University, Shiraz, Iran.
††Lawrence Berkeley Laboratory, University of California, Berkeley, California 94720.
†††Los Alamos Scientific Laboratory, Los Alamos, New Mexico.
††††Fachbereich Physik, Universität Marburg, Germany.

The calculations are performed with deformed single particle levels of Nilsson, et al.[1].

The theoretical to experimental level spacings from neutron capture resonance data are plotted in Fig. 8. The solid points represent deformed nuclei where deformed single particle levels are used and collective rotational levels are added in the theoretical calculations. The open points represent spherical nuclei where spherical single particle levels are used and only particle excitations are included in the theoretical calculations.

The question of the sensitivity of $D_{theo.}$ to a particular set of single particle levels was investigated by performing calculations with single particle levels calculated by Nix, et al.[2] and with single particle levels calculated with the deformations and parameters of Tsang, et al.[3]. The results are compared in Table 10 and are quite similar.

In the present formulation, any enhancement in the level density due to vibrations has been neglected. For the case of an axially symmetric nucleus, the enhancement in the level density due to vibrations is calculable with the same type of formalism as that discussed for rotations and is given approximately by[4] $[1-\exp(-\hbar\omega/T]^{-g}$. The exponential factor is for a vibrational mode with g-fold degeneracy. The predicted enhancement in the level density depends on the ratio of $\hbar\omega/T$ and g. For heavy nuclei, $\hbar\omega/T$ is of the order of 1 to 2. Hence, the enhancements in the level density for heavy nuclei due to vibrational excitations is expected to be an order of magnitude less than that due to rotations.

Fig. 8: The ratios of the theoretical spacings to the experimental spacings are plotted as a function of mass number. The points represented by solid symbols are for calculations of $D_{theo.}$ based on single particle levels calculated for deformed nuclei with the deformations and parameters of Nilsson, et al.[1]. The open symbols are the same except for spherical nuclei where $D_{theo.}$ is calculated with the equations for spherical nuclei in the previous report.

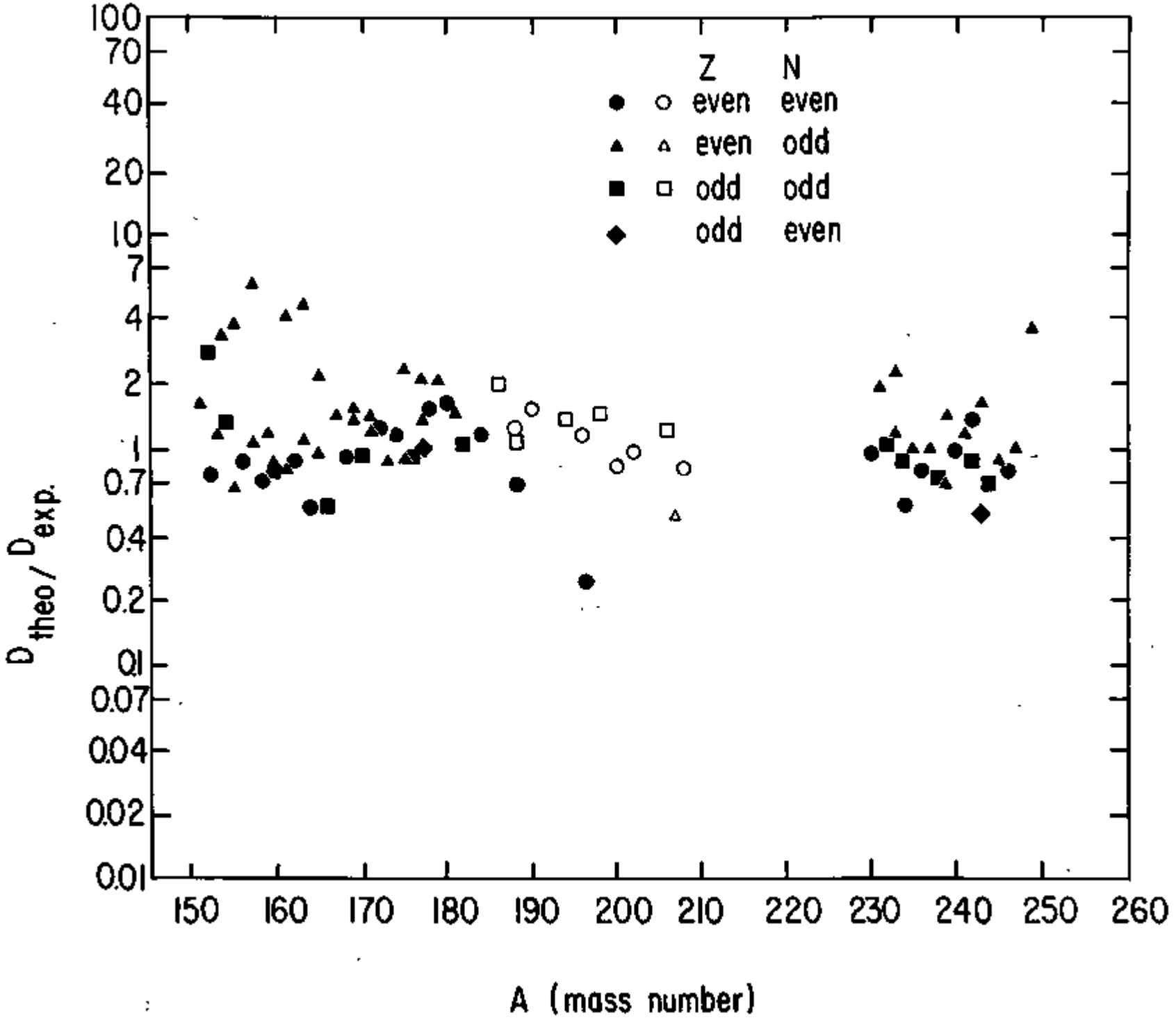
100
70
40
20
10
7
4
2
1
0.7
0.4
0.2
0.1
0.07
0.04
0.02
0.01
Z N
even even
even odd
odd odd
odd even
D theo / D exp.
150 160 170 180 190 200 210 220 230 240 250 260
A (mass number)

Figure 8

Table 10. Comparison of experimental and theoretical level spacings for three sets of single particle levels.

Target	I_o,π	Compound Nucleus	$I_o \pm \frac{1}{2},\pi$	E^* MeV	D_{exp} in eV (a)	(b)	D_{Theo} in eV (c)	(d)	(e)
^{167}Er	$\frac{7}{2}+$	^{168}Er	3+,4+	7.77	4	4.1	3.8		4.4
^{172}Yb	$\frac{1}{2}-$	^{172}Yb	0-,1-	8.02	7.2	6.5	9.5		8.2
^{229}Th	$\frac{5}{2}+$	^{230}Th	2+,3+	6.79	0.58	0.60	0.56	0.55	
^{235}U	$\frac{7}{2}-$	^{236}U	3-,4-	6.55	0.67	0.53	0.43	1.0	
^{241}Pu	$\frac{5}{2}+$	^{242}Pu	2+,3+	6.30	1.2		1.7	1.8	2.4
^{245}Cm	$\frac{7}{2}+$	^{246}Cm	3+,4+	6.45		1.5	1.2	1.0	

[a]Data compiled by Baba, Nucl. Phys. A159, 625(1970).

[b]Data compiled by Vonach, et al., Nucl. Phys. A217, 269(1973).

[c]Calculated with deformed single particle levels of Nilsson, et al.[1].

[d]Calculated with deformed single particle levels of Tsang, et al.[3].

[e]Calculated with deformed single particle levels of Nix, et al.[2].

In adding the collective rotational levels to the intrinsic or particle level density, one is concerned about the redundance in the two types of degrees of freedom. One knows that at low excitation energy, each intrinsic level has built upon it a rotational band. At these low energies, the nucleus has a well-defined deformation and one can clearly separate the particle and collective motion. However, as the temperature and excitation energy increase, it is probably no longer a good approximation to assume that the particle and collective degrees of freedom are independent of each other. In the limit where the temperature is very large and the particle and collective degrees of freedom are thoroughly mixed, then $\omega_{intr}(E)$ contains all of the available states and there is no enhancement in the level density due to collective rotations.

The question remains as to whether the level density will be enhanced for deformed lanthanide and actinide nuclei at excitation energies corresponding to the neutron binding energy where the temperature is about 0.5 MeV. It has been estimated[4] that at a nuclear temperature of the order of $40A^{-1/3}$ δ MeV (where δ is the deformation) the fluctuations in the nuclear orientation becomes so large that it is not meaningful to speak of a separation of the rotational and intrinsic motion. For the actinide nuclei this estimate of 1.6 MeV for this nuclear temperature is well in excess of the actual temperature of 0.5 MeV at the neutron binding energy. The good agreement between the experimental spacings and the theoretical

spacings for the actinide and lanthanide nuclei supports the general validity of the formalism described in this paper where collective rotations are added to the level density for axially deformed nuclei. In the limit where no enhancement in the level density due to collective rotations is included, the experimental spacings of the actinide and lanthanide nuclei are not even reproduced when the pairing gap parameters are reduced to zero. The elimination of pairing gives a larger effective excitation energy and results in a larger level density. Although the absolute value of $D_{theo.}$ is altered slightly by varying the gap parameters, the complete elimination of pairing is not justified. Hence, for the deformed nuclei it is necessary to add the collective excitations in order to obtain a fit to the experimental data.

1) S.G. Nilsson, et al., Nucl. Phys. A131, 1(1969).

2) J.R. Nix, et al., Private Communication (1973); We wish to thank Dr. Nix for supplying us with these single particle levels.

3) C.F. Tsang, et al., Private Communication (1973).

4) S. Bjørnholm, A. Bohr and B.R. Mottelson, Third International Conference on the Physics and Chemistry of Fission, University of Rochester, Paper IAEA-174/205 (1973).

3. Angular Momentum Dependent Level Density --

A.N. Behkami* and J.R. Huizenga

Level density calculations are in progress which take explicit account of the angular momentum. These calculations make use of realistic sets of single particle levels (see sections B1 and B2). However, in the present calculations the space fixed projection of the angular momentum is introduced as an additional constant of motion by means of an appropriate Lagrange multiplier. In addition to the angular momentum projection M the other constants of motion are, as in the previous calculations, the particle number N and the total energy E,

$$M = \sum_k m_k \left[\frac{1}{1+\exp\beta(E_k-\gamma m_k)} - \frac{1}{1+\exp\beta(E_k+\gamma m_k)}\right] \quad (1)$$

$$N = \sum_k \left\{1-\frac{\epsilon_k-\lambda}{2E_k}\left[\tanh\tfrac{1}{2}\beta(E_k-\gamma m_k)+\tanh\tfrac{1}{2}\beta(E_k+\gamma m_k)\right]\right\} \quad (2)$$

$$E = \sum_k \epsilon_k\left\{1-\frac{\epsilon_k-\lambda}{2E_k}\left[\tanh\tfrac{1}{2}\beta(E_k-\gamma m_k)+\tanh\tfrac{1}{2}\beta(E_k+\gamma m_k)\right]\right\} - \frac{\Delta^2}{G} \quad (3)$$

The quantities ϵ_k and m_k are the single particle energies and spin projections, respectively; β, λ and γ are the Lagrange multipliers; E_k is the quasiparticle energy given by $E_k = [(\epsilon_k-\lambda)^2 + \Delta^2]^{1/2}$; G is the pairing strength and Δ is the gap parameter.

*Department of Physics, Pahlavi University, Shiraz, Iran.

The logarithm of the grand partition function for one type of fermion is,

$$\ell n\ Z(\beta,\lambda,\gamma) = -\beta \sum_k (\epsilon_k - \lambda - E_k) + \sum_k \ell n\{1+\exp[-\beta(E_k-\gamma m_k)]$$

$$+ \sum_k \ell n\{1+\exp[-\beta(E_k+\gamma m_k)] - \beta\Delta^2/G \qquad (4)$$

where in all the above equations the summations are over doubly degenerate orbitals designated by k. This equation is valid only if the quantities Δ, λ, β and γ satisfy the gap equation,

$$\frac{2}{G} = \sum_k \frac{1}{2E_k} \{\tanh\tfrac{1}{2}\beta(E_k-\gamma m_k) + \tanh\tfrac{1}{2}\beta(E_k+\gamma m_k)\} \qquad (5)$$

The entropy and level density are now calculated as a function of angular momentum and excitation energy.

One of the new features of such calculations[1] is the dependence of the pairing gap parameter Δ on both the nuclear temperature ($1/\beta$) and the angular momentum I. The transition from the paired to the unpaired region can be made either by increasing the temperature at constant angular momentum or by increasing the angular momentum at a constant temperature. The relation between Δ, T and I are illustrated for neutrons and protons separately for the nucleus ^{124}Te in Fig. 9. One interesting feature shown in this figure is the double-valued nature of the critical temperature for values of the angular

Fig. 9: Relation between the pairing gap Δ (MeV), nuclear temperature T (MeV), and angular momentum I (in units of $\hbar$) for ^{124}Te. Single particle levels of Seeger and Perisho[3] were used in the calculations. (a) Neutrons, $\Delta_n(T=0, M=0) = 1.36$ MeV (b) Protons, $\Delta_p(T=0, M=0) = 1.34$ MeV. Note the double-values nature of the critical temperature for values of the angular momentum near the critical angular momentum.

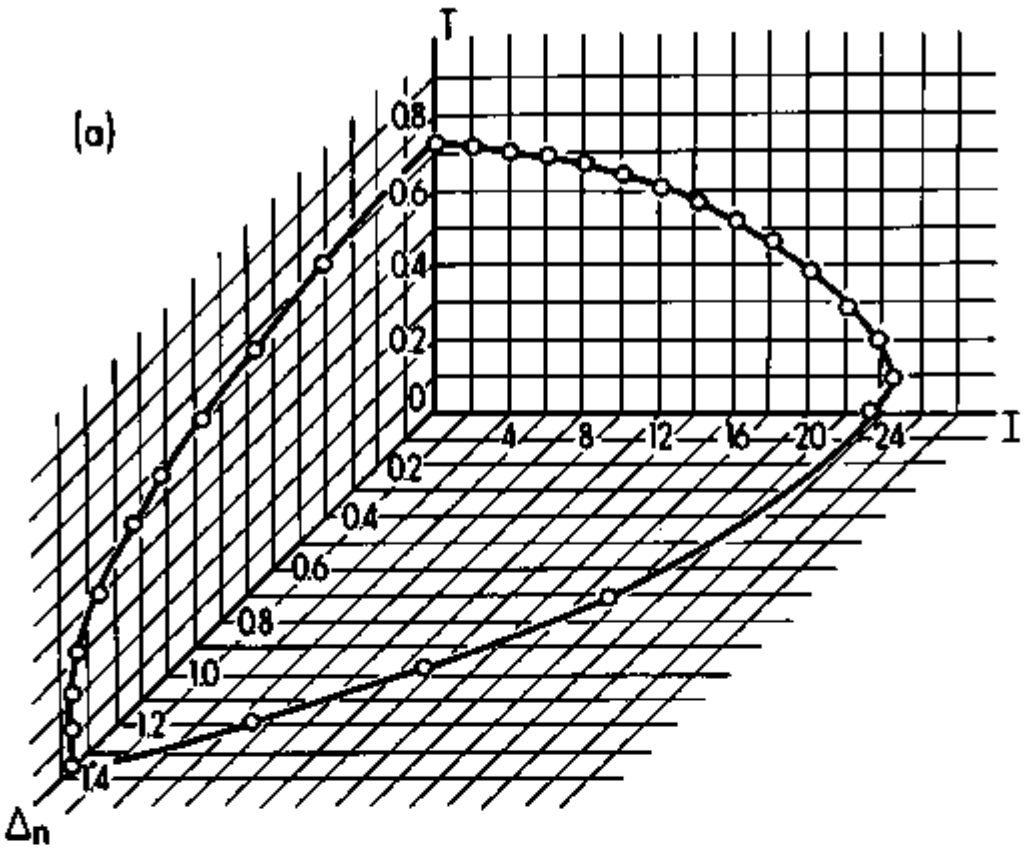
(a)
T
0.8
0.6
0.4
0.2
0
4
8
12
16
20
24
I
0.2
0.4
0.6
0.8
1.0
1.2
1.4
Δn

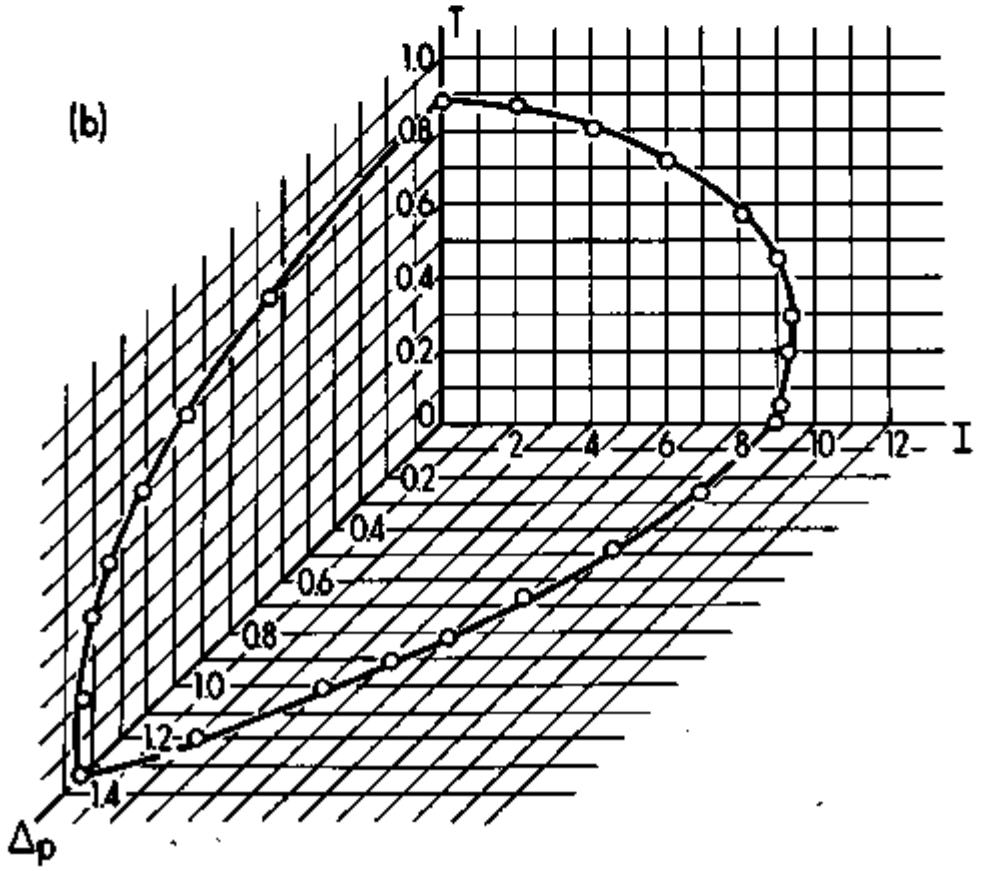
(b)
T
1.0
0.8
0.6
0.4
0.2
0
2
4
6
8
10
12
I
0.2
0.4
0.6
0.8
1.0
1.2
1.4
Δp

Figure 9

momentum near the critical angular momentum. This effect has been explained[2] in terms of blocking. At large I and for T = 0 the effect of blocking is a maximum because all the quasiparticles are tightly packed around the Fermi surface. An initial increase of the temperature spreads out the quasiparticles (instead of breaking pairs) and thus diminishes the effect of blocking. A similar behavior has been observed for several other nuclei including ^{68}Zn, ^{96}Mo, ^{136}Ba, ^{192}Pt, and ^{200}Hg.

1) L.G. Moretto, Nucl. Phys. A216, 1(1973).

2) L.G. Moretto, Nucl. Phys. A185, 145(1972).

3) P.A. Seeger and R.C. Perisho, Los Alamos Scientific Laboratory Report, LA-3751 (1957).

4. Elastic Scattering of α-Particles from ^{238}U --

H. Freiesleben* and J.R. Huizenga

Angular distributions of elastically scattered alpha particles from ^{238}U were measured with surface barrier detectors at 16, 19, 23 and 27 MeV in the angle range 30° - 170° and, in addition, at intermediate energies at 4 angles. Since the resolution in the elastic scattering measurement is insufficient to resolve low-lying inelastic excited states, the measured scattering cross section represents the sum of these cross sections. Angular distributions of scattered α-particles from ^{238}U at two energies are shown in Fig. 10 along with optical model fits.

Firstly, the optical model code JIB III[1)] was used. The potential parameters for the ^{238}U + α reaction were obtained by fitting simultaneously the elastic scattering and total reaction cross section data at several energies. As pointed out above, the elastic scattering data include unresolved inelastic states which are mainly excited via Coulomb excitation in our energy range. Since Coulomb excitation is not included in the optical model code JIB III, the cross sections of the first and second excited states have to be treated as part of the elastic scattering cross section. Due to our small incident energies which are near the Coulomb barrier, the angular distributions of the elastically scattered particles are nearly structureless. Hence, the optical model potential was restricted to a four

---

*Fachbereich Physik, Universität Marburg, Germany.

Fig. 10: Angular distributions of scattered α particles from ^{238}U at 23 and 27 MeV. The solid lines refer to a coupled channel calculation and the dashed lines to a spherical optical model fit.

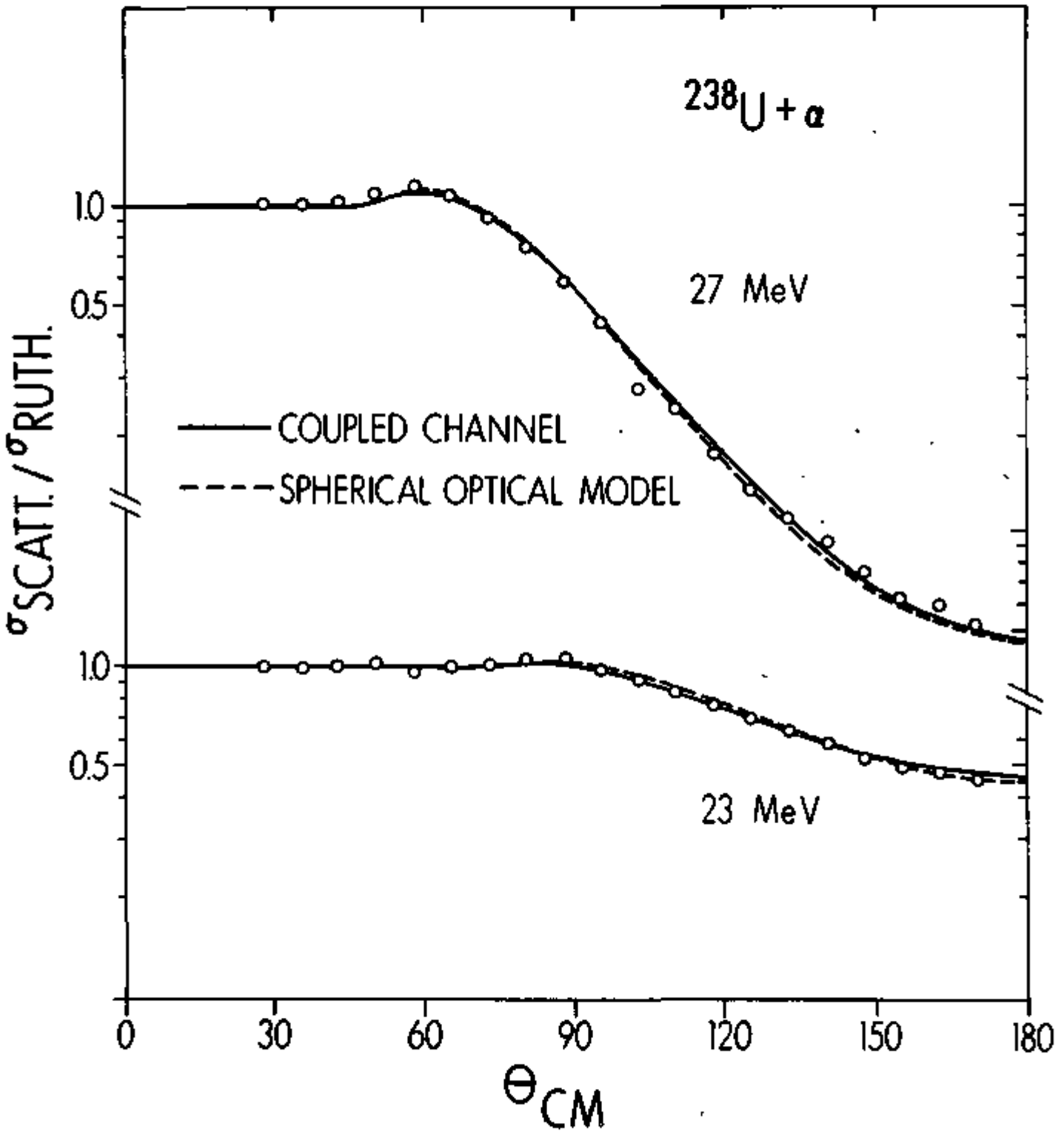
$^{238}U + \alpha$
27 MeV
23 MeV
COUPLED CHANNEL
SPHERICAL OPTICAL MODEL
$\sigma_{SCATT.}/\sigma_{RUTH.}$
1.0
0.5
1.0
0.5
0
30
60
90
120
150
180
Θ_{CM}

Figure 10

parameter Saxon-Woods potential with volume absorption. One of the optimum sets of parameters which were derived for this spherical potential is given in Table 11. These parameters are very similar to those used by Aponick, et al.[2] for α scattering on rare earth nuclei. As indicated in Table 11, a slight improvement in the agreement between theory and experiment was obtained by assuming a slight energy dependence for W_D above E = 19 MeV.

Secondly, in order to investigate the influence to target deformation, coupled channel calculations were performed with the JUPITOR 1 code of Tamura[3]. A complex form factor was used and inelastic scattering to the first 2^+ and 4^+ states was included in the calculation. Target deformation parameters of $\beta_2 = 0.22$ and $\beta_4 = 0.05$ were chosen. Again in this calculation no Coulomb excitation was included in order to be consistent with the spherical potential optical model calculations. A four parameter Saxon-Woods potential with volume absorption was used. One of our sets of parameters which gave the best description of both the scattering and the total reaction cross section data is given in Table 11. Since the unresolved inelastically scattered particles (due to the Coulomb and nuclear interactions) are included in the experimental elastic scattering cross section, we have treated the theoretical scattering and reaction cross sections in a similar way. The small contribution (always less than 5%) of the inelastic nuclear scattering cross section to the 2^+ and 4^+ states has been added to the

Table 11. Potential parameters obtained by fitting ^{238}U + α angular distributions using a spherical optical model and a coupled channel calculation.

	Spherical optical pot. model parameters		Coupled channel pot. parameters	
E (MeV)	27.00	23.00	27.00	23.00
V_0 (MeV)	111.45		95.0	
W_D (MeV)	20.40	15.84	15.0	10.44
r (fm)	1.41		1.37	
a (fm)	0.565		0.635	
r_{oc} (fm)	1.45		1.45	
β_2	0.00		0.22	
β_4	0.00		0.05	

theoretical elastic scattering cross section and makes a negligible change in the elastic scattering cross section.

Both of the above theoretical calculations describe the experimental data quite well. Hence, the quality of the theoretical fits to the data does not provide an argument for choosing one of the models over the other. A similar result was obtained by Aponick, et al.[2] in their study of α-scattering on deformed rare earth nuclei.

1) F.G. Perey, JIB Local Optical Potential Program with Automatic Parameter Search, 1965.

2) A.A. Aponick, C.M. Clusterfield, D.A. Bromley and N.K. Glendenning, Nucl. Phys. A159, 267(1970).

3) T. Tamura, Rev. Mod. Phys. 37, 679(1965) and JUPITOR 1, ORNL-4152, 1967.

5. Total Reaction Cross Sections of Deformed Nuclei: A Study of the $^{233,238}U$ + α Systems -- H. Freiesleben* and J.R. Huizenga

The question whether total reaction cross sections depend on static target deformation, as suggested by Rasmussen, et al.[1], has been studied with the $^{233,238}U$ + α reactions. These reactions were chosen in order to assure a simple experimental situation where a) the projectile is spherical and b) direct processes such as break up and transfer are negligible. For these fissionable systems, the fission cross sections are very nearly equal to the total reaction cross sections.

The fission cross sections were measured by detecting fission fragments in two 300 mm^2 surface barrier detectors placed at distances of 60 and 90 mm from the target and at angles of 90° and 150° to the beam, respectively. The fission cross sections of the $^{233}U(\alpha,f)$ and $^{238}U(\alpha,f)$ reactions have been studied previously[2]; however, the lowest bombarding energy was 18.4 MeV, and this energy was obtained by degrading a 43 MeV α-beam from a cyclotron. The range straggling introduces considerable uncertainty in the energy in a region where the cross section is changing rapidly with energy. For an accurate evaluation of the cross section in this energy region where the effects of deformation are expected to be most pronounced, we felt that it was necessary both to repeat the previous measurements with a variable energy tandem beam and to extend the measurements to even lower energies.

---

*Fachbereich Physik, Universität Marburg, Germany.

The measured total fission cross section for $^{233,238}U$ targets are listed in Table 12 and displayed in Fig. 11. The error bars on the data are mainly due to the counting statistics and the uncertainty in the solid angle. The data were compared with various theoretical calculations for the total reaction cross section in order to investigate the effect of static target deformation. The reaction cross sections calculated on the basis of a model which assumes a parabolic approximation to the barrier of a spherical or deformed potential are not reliable since this model itself is not applicable at energies near and below the barrier where the deformation effect is expected to be a maximum. This shortcoming of the model is overcome with more sophisticated models. In a spherical optical model, potential parameters can be found which describe the scattering and the total reaction cross section (curve I in Fig. 11) very well over the energy range investigated. Using a quite different optical potential in a coupled channel calculation, where the target deformation is explicitly accounted for, fits to be scattering and reaction cross section (curve II in Fig. 11) can also be obtained (see also the report on elastic scattering of α-particles from $^{233,238}U$).

Hence, it is not possible to verify that the inclusion of static target deformation is essential in order to describe experimental reaction cross section data for this deformed target nucleus. However, this does not mean that static target deformation does not influence the total reaction cross section.

Table 12. Total fission cross sections for the $^{233}U + \alpha$ and $^{238}U + \alpha$ reactions as a function of energy.

E_α(lab energy in MeV)	σ_f(mb)	
	$^{233}U(\alpha,f)$	$^{238}U(\alpha,f)$
15	0.0018±0.0015	0.0009±0.0007
16	0.0051±0.0029	0.0030±0.0009
17	0.039±0.016	0.0253±0.0031
18	0.279±0.086	0.205±0.023
19	1.73±0.50	1.43±0.14
20	7.81±1.17	6.54±0.52
21	27.5±1.9	24.5±1.7
22	68.0±4.8	61.0±4.3
23	138.0±9.7	133.8±9.4
24		216.0±15.1
25	332.9±20.0	360.3±21.6
26	569.0±34.2	532.4±31.9
27	618.0±30.9	639.6±32.0

Fig. 11: Experimental fission cross sections as a function of energy for α induced fission of ^{233}U and ^{238}U. Calculated reaction cross sections are shown for a spherical optical model (curve I) and a coupled channel calculation (curve II).

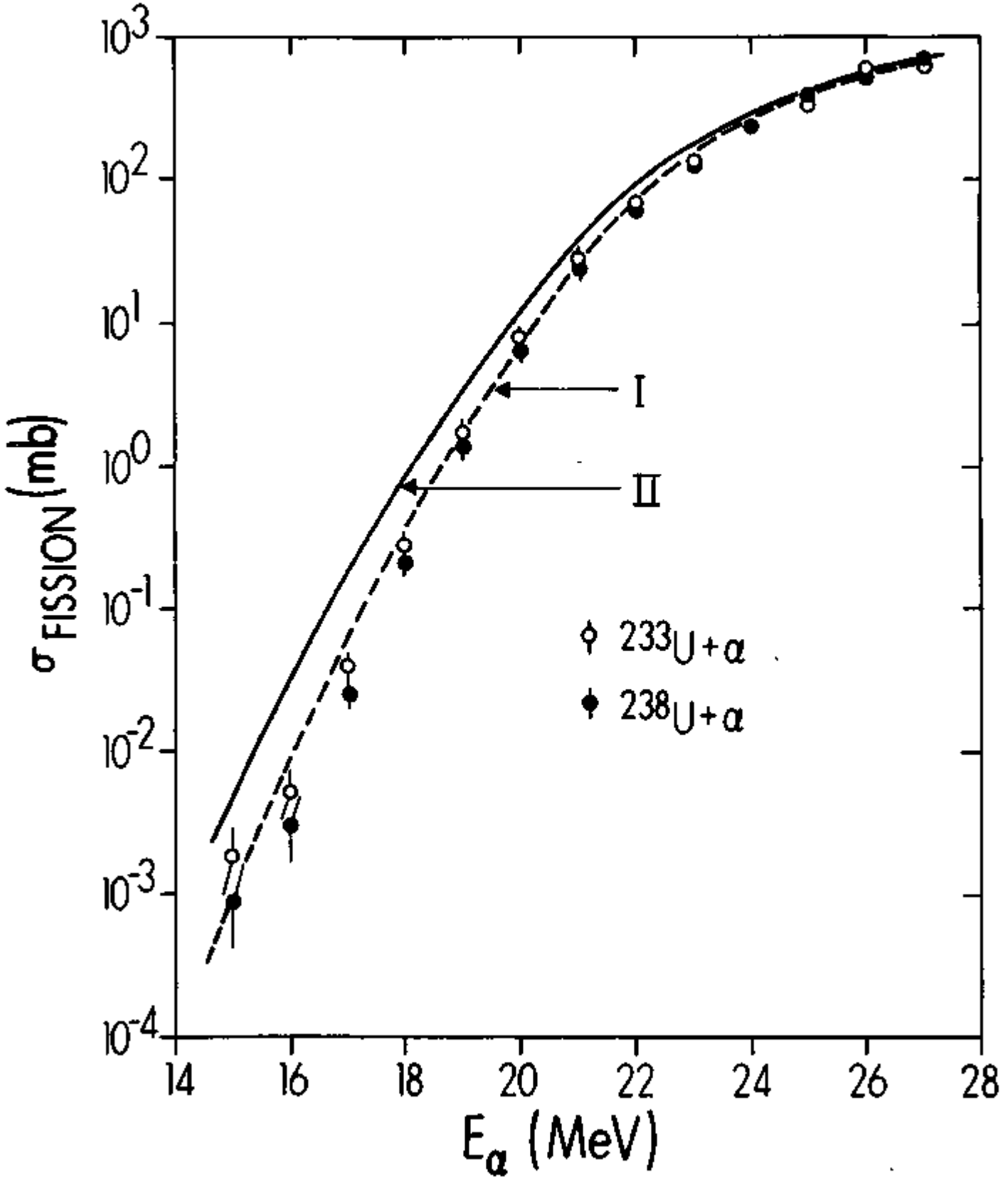
10^3
10^2
10^1
10^0
10^{-1}
10^{-2}
10^{-3}
10^{-4}
$\sigma_{FISSION}$ (mb)
I
II
$^{233}U+\alpha$
$^{238}U+\alpha$
14
16
18
20
22
24
26
28
E_α (MeV)

Figure 11

Since we cannot establish a model predicted effect of static target deformation on the reaction cross section, we have chosen to compare experimental cross sections for reactions on spherical and deformed nuclei. Recently total cross sections for α-induced reactions on ^{208}Pb and ^{209}Bi have been measured by Lilley, et al.[3]. These results, along with our results for ^{233}U, are included in the left part of Fig. 12. The experimental cross sections for the different reactions in Fig. 12 show an almost parallel rise. From the right-hand side of Fig. 12, this fact is even more obvious. In this part of the figure, the incident α-energy is divided by the respective interaction barrier height E_B for each of the three systems in the laboratory frame. It is evident that all three reaction cross sections have the same energy dependence. Hence, the static target deformation of the ^{233}U target does not enhance the reaction cross section in the vicinity of and well below the interaction barrier when compared to reaction cross sections of spherical target nuclei like ^{208}Pb and ^{209}Bi.

Closely connected with the reaction cross section for systems involving statically deformed targets is the interaction barrier of such a system. If one defines the interaction barrier by the condition $T_{\ell=0} = 0.5$, the interaction barrier is in principle dependent on the model used to calculate the transmission coefficients T_ℓ when fitting the experimental data. Surprisingly, the interaction barriers we extracted from our experimental data using six

Fig. 12: Comparison of the experimental reaction cross sections for the $^{208}Pb + \alpha$, $^{209}Bi + \alpha$ and $^{233}U + \alpha$ systems. The results for the spherical nuclei ^{208}Pb and ^{209}Bi are from Lilley, et al.[3]. Left, the reaction cross sections are plotted versus the incident energies E_α in the laboratory frame. Right, the reaction cross sections are plotted versus the ratios E_α/E_B where E_B is the respective interaction barrier in the laboratory frame for each of the three systems.

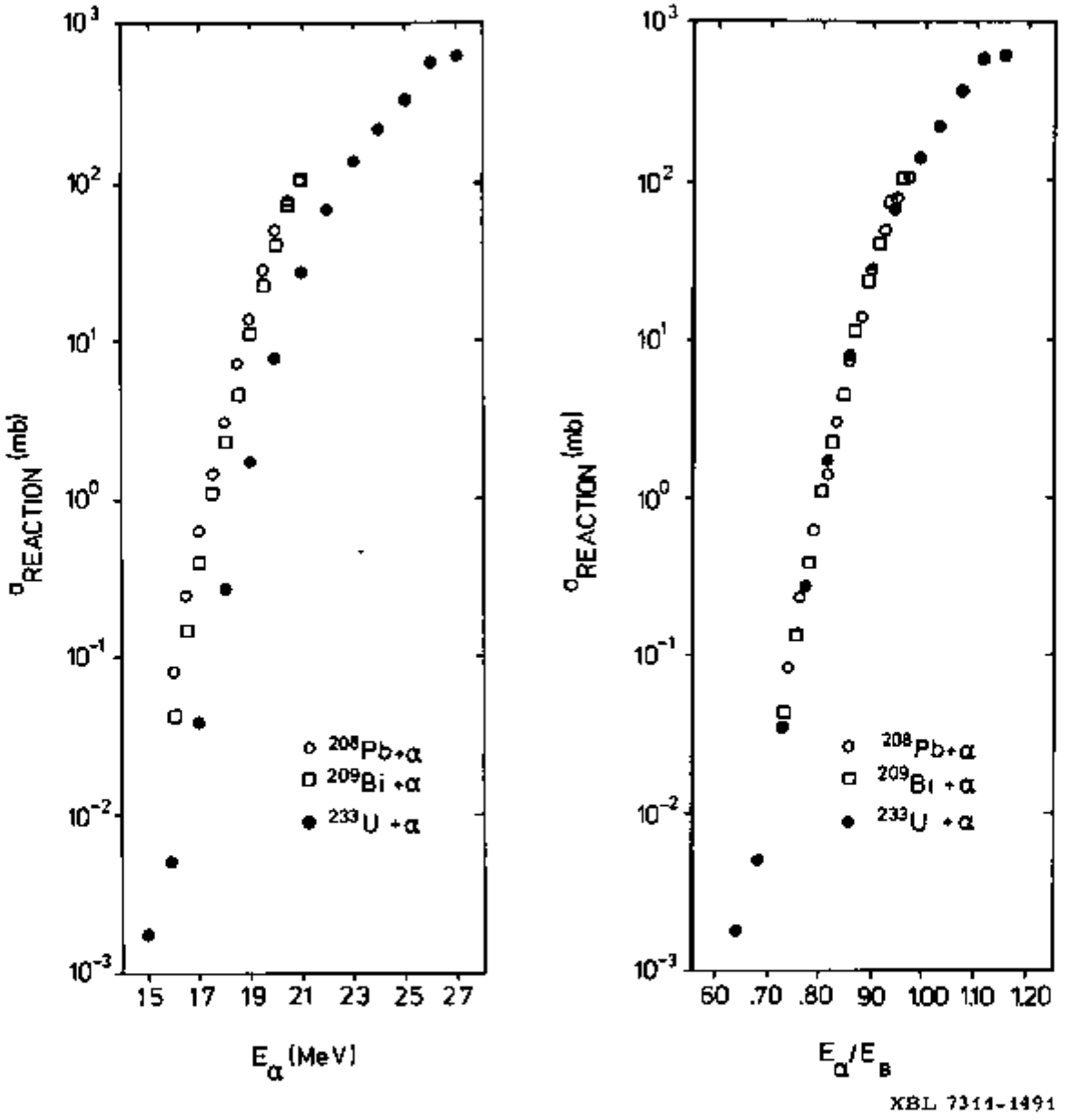
10^3
10^2
10^1
10^0
10^{-1}
10^{-2}
10^{-3}
$\sigma_{REACTION}$ (mb)
15 17 19 21 23 25 27
E_α (MeV)
○ $^{208}Pb+\alpha$
□ $^{209}Bi+\alpha$
● $^{233}U+\alpha$
60 .70 .80 90 100 110 120
E_α/E_B
XBL 7311-1491

Figure 12

different methods are equal to within 2-3%, giving a best value of 22.34 MeV for the $^{238}U + \alpha$ system. This value agrees with the result derived from a simple theoretical formula[4].

1) J.O. Rasmussen and K. Sugwara-Tanabe, Nucl. Phys. A171 497(1971).

2) J.R. Huizenga, R. Vandenbosch and H. Warhanek, Phys. Rev. 124, 1964(1961).

3) J.S. Lilley and M. Franey, Bull. Am. Phys. Soc. 18, 605 (1973) and A.R. Barnett and J.S. Lilley, to be published.

4) H.J. Krappe and J.R. Nix, Proceedings of the Third IAEA Symposium on the Chemistry and Physics of Fission, Rochester, N.Y. 1973.

6. Level Widths of T=0 and T=1 Isospin States of ^{30}P at an Excitation Energy of 19.6 MeV -- M. Kildir and J.R. Huizenga

In order to determine the level widths of the T=0 and T=1 isospin states of the ^{30}P composite nucleus, excitation functions for the $^{29}Si(p,\alpha_0)$, $^{29}Si(p,\alpha_1)$ and $^{29}Si(p,\alpha_2)$ reactions were measured with good energy resolution. The average level widths of the different isospin states of ^{30}P are obtained from a statistical analysis of these excitation functions. The determined level widths are then used to calculate relative level densities of the T=0 and T=1 isospin states in the highly excited composite system.

The excitation functions were measured in the proton energy interval from 13.50 to 15.50 MeV in 25-keV energy steps. These excitation functions show a decrease in average cross section with increasing energy. This energy dependence of the average cross section is attributed to the opening of more reaction channels with increasing energy. The energy dependence is removed from each excitation function before the fluctuation analysis is done. A Hauser-Feshbach calculation was performed to estimate this energy dependence. Two typical examples of the excitation functions are shown in the figure 13. The level widths are determined from the half widths of Lorentzian curves fitted to the experimental auto-correlation functions. The values of the level widths are shown in Table 13A. These values contain a small correction for the finite energy interval of the experimental data.

Fig. 13: Excitation functions of the $^{29}Si(p,\alpha_0)^{26}Al$ reaction at 110° and 130°.

The emission of alpha particles from the composite nucleus, ^{30}P, leads to the residual nucleus of ^{26}Al. The first three levels in the ^{26}Al nucleus (ground state, first excited and second excited states) have total isospin values of T=0, T=1 and T=0, respectively. If isospin is a good quantum number, then the average level width determined from the (p,α_0) and (p,α_2) reaction channels is that of T=0 isospin states in the composite nucleus ^{30}P. The fluctuation analysis of the (p,α_1) channel gives the level width of T=1 isospin states in the composite system. From these fluctuation analyses the level widths of T=0 and T=1 isospin states of ^{30}P at an excitation energy of 19.6 MeV are 81±17 keV and 104±35 keV, respectively.

The level widths of the above two isospin states are used to calculate the relative level densities of these states. In Table 13B the ratios of level densities of the two isospins are given for different sets of level density parameters of the residual nuclei. This ratio depends only very weakly on the level density parameters. Calculations of the relative densities of levels of different isospin with a more realistic model are in progress. The preliminary results of these calculations are in good agreement with the experimental values of the relative level densities.

Table 13B. The relative level densities of the $T_<$ and $T_>$ isospin states for the composite nucleus, ^{30}P, at an excitation energy of 19.6 MeV.

a	$\Delta(^{29}Si)$	$\Delta(^{29}P)$	$\Delta(^{26}Al)$	$\Delta(^{28}Si)$	$\frac{\rho(U_c, J=0, T=1)}{\rho(U_c, J=0, T=0)}$
A/9	0.0	0.0	-1.0	3.0	0.85
A/9	1.0	1.0	-1.0	3.0	0.86
A/9	0.0	0.0	0.0	3.0	0.84
A/8	0.0	0.0	-1.0	3.0	0.87
A/10	2.0	2.0	0.0	4.0	0.88

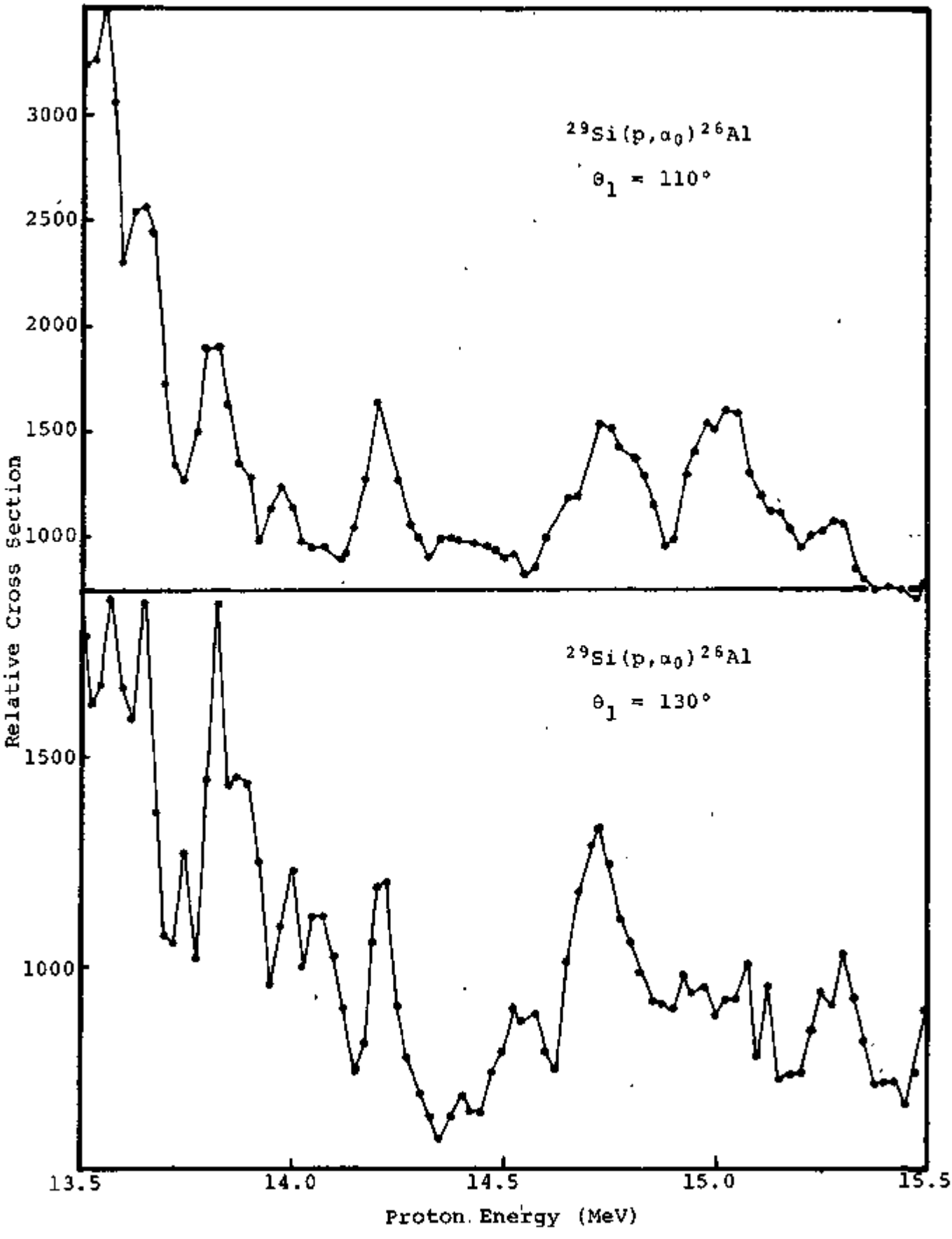
$^{29}Si(p,\alpha_0)^{26}Al$
$\theta_1 = 110°$
$^{29}Si(p,\alpha_0)^{26}Al$
$\theta_1 = 130°$
Relative Cross Section
3000
2500
2000
1500
1000
1500
1000
13.5
14.0
14.5
15.0
15.5
Proton Energy (MeV)

Figure 13

Table 13A. The experimental level widths for the composite nucleus of ^{30}P at an excitation energy of 19.6 MeV.

Reaction	Angle, θ (lab.) (deg.)	Sample Size	Coherence Width Γ (keV)	Average Coherence Width† <Γ> (keV)
$^{29}Si(p,\alpha_0)^{26}Al$	90	9	76	
$^{29}Si(p,\alpha_2)^{26}Al$	90	9	73	
$^{29}Si(p,\alpha_0)^{26}Al$	110	9	87	
$^{29}Si(p,\alpha_2)^{26}Al$	110	9	84	
$^{29}Si(p,\alpha_0)^{26}Al$	130	9	68	81±17
$^{29}Si(p,\alpha_2)^{26}Al$	130	9	60	
$^{29}Si(p,\alpha_0)^{26}Al$	165	9	116	
$^{29}Si(p,\alpha_1)^{26}Al$	110	8	121	
$^{29}Si(p,\alpha_1)^{26}Al$	130	8	56	104±35
$^{29}Si(p,\alpha_1)^{26}Al$	165	8	136	

†The error on the average level width is based on the mean square deviation of the individual Γ values from <Γ>.

C. Nuclear Fission

1. Energy Dependence of Γ_f/Γ_n for the Nucleus ^{216}Rn -- H. Freiesleben*, H.C. Britt** and J.R. Huizenga

A study of the competition between fission and neutron emission for the nucleus ^{216}Rn has been performed[1]. The ^{209}Bi + ^{7}Li reaction was used to produce the compound nucleus ^{216}Rn at excitation energies corresponding to bombarding energies in the range of 24-34 MeV.

The cross section for the (^{7}Li,f) reaction was measured by detecting coincident fission fragment pairs with surface barrier detectors in a large geometry arrangement. It was advantageous to detect fission fragment pairs during the measurement of the very small fission cross section in the presence of the intense elastic line. If the compound nucleus does not fission, multiple neutron emission leads to residual Rn isotopes. Since all of these nuclei are α-emitters, their formation cross sections are easily determined by measurement of their α-activities. The identification of these α-groups is unique based on their known α-energies and half-lives which range from about 100 μs to minutes. Using a pulsed Li-beam to produce the Rn-isotopes, we measured the α-activities between beam pulses with standard surface barrier detectors, essentially free of background due to prompt α-groups (Fig. 14). The cross sections for the (^{7}Li,2n), (^{7}Li,3n), (^{7}Li,4n) and (^{7}Li,f) reactions are listed in Table 14

---

*Fachbereich Physik, Universität Marburg, Germany

**Los Alamos Scientific Laboratory, Los Alamos, New Mexico.

Fig. 14: Alpha particle spectra observed at various bombarding energies for the $^{209}Bi + ^{7}Li$ reaction.

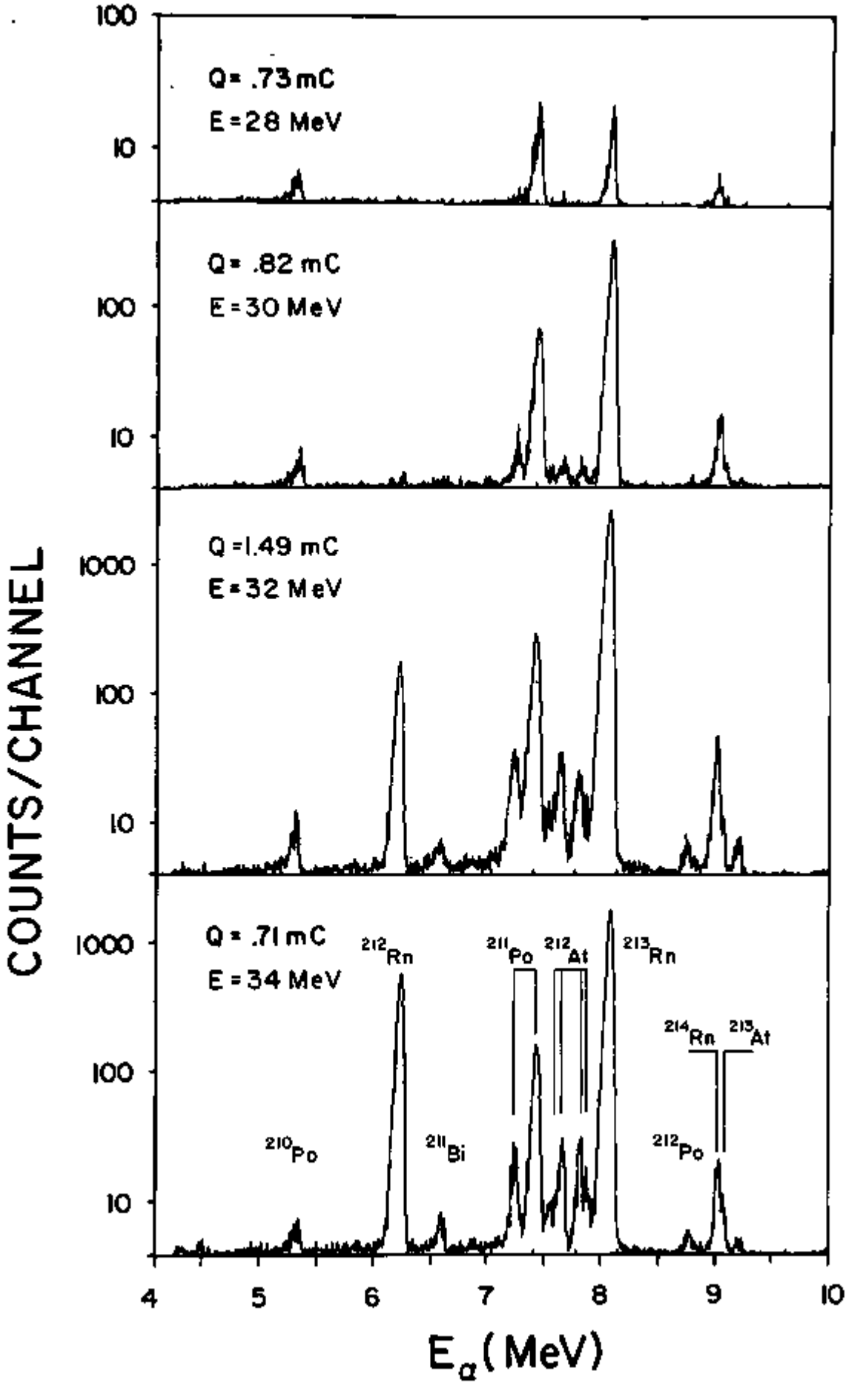
Q= .73mC
E=28 MeV
Q= .82 mC
E=30 MeV
Q=1.49 mC
E=32 MeV
Q= .71mC
E=34 MeV
212Rn
211Po
212At
213Rn
214Rn
213At
210Po
211Bi
212Po
COUNTS/CHANNEL
Eα(MeV)

Figure 14

Table 14. Measured cross sections in millibarns for various compound nucleus reactions

Laboratory Energy (MeV)	$\sigma(^7Li,2n)$	$\sigma(^7Li,3n)$	$\sigma(^7Li,4n)$	$\sigma(^7Li,f)$	$\sigma(^6Li,2n)$	$\sigma(^6Li,3n)$	$\sigma(^6Li,f)$
34	4.6±1.6	187±19	77±15	1.77±0.03			2.25±0.05
33	4.7±1.6	189±19	51±15	1.05±0.05			1.34±0.04
32	4.1±0.9	134±13	11±3	0.58±0.03			0.75±0.02
31	4.4±0.6	89±10	1.4±0.7	0.24±0.01			0.29±0.01
30	3.3±0.7	41±4		0.086±0.008	1.9±0.4	43±4	0.12±0.006
29	2.0±0.4	16±2		0.020±0.002			0.32±0.002
28	1.1±0.3	4.7±0.5		0.0064±0.0008	1.0±0.2	5.8±0.6	0.0094±0.0010
27	0.5±0.11	1.0±0.1		0.0014±0.0009			0.0015±0.0003
26	0.3±0.07	0.14±0.04					
25	0.4±0.013	0.026±0.013					

as a function of bombarding energy. The data for ^{6}Li induced fission have been used to correct the ^{7}Li data for contributions due to second chance fission. An effect of less than 6% was obtained at our highest incident energy of ^{7}Li of 34 MeV.

The experimental ratios of Γ_f/Γ_n are plotted in Fig.15 as a function of the compound nucleus excitation energy. The ratio of Γ_f/Γ_n varies slowly with excitation energy since the excitation energies are well above the fission barrier even though the bombarding energies are below the Coulomb barrier. The solid curve in Fig. 15 represents an absolute calculation of Γ_f/Γ_n with a statistical model making use of the theoretical fission barrier[2] of 14.8 MeV. The level densities of the residual nucleus and the saddle point nucleus are calculated with a microscopic model. The appropriate energies of the single particle levels were obtained from calculations of Möller and Nix[2]. The level density of the spherical residual nucleus was calculated with the formalism described in section B1. The level density of the highly deformed saddle point nucleus was calculated with the formalism described in section B2 and includes an enhancement due to collective rotations[3]. Since the above theoretical calculation contains no free parameters, the agreement between experiment and theory is surprisingly good. However, the agreement between theory and experiment could be improved by reducing the rotational enhancement in the saddle point level density at the higher energies. This is the expected result

Fig. 15: Fission-to-neutron competition for the compound nucleus ^{216}Rn. The points represent experimental data and the solid line is a theoretical fit to the data using the theoretical fission barrier and no adjustable parameters.

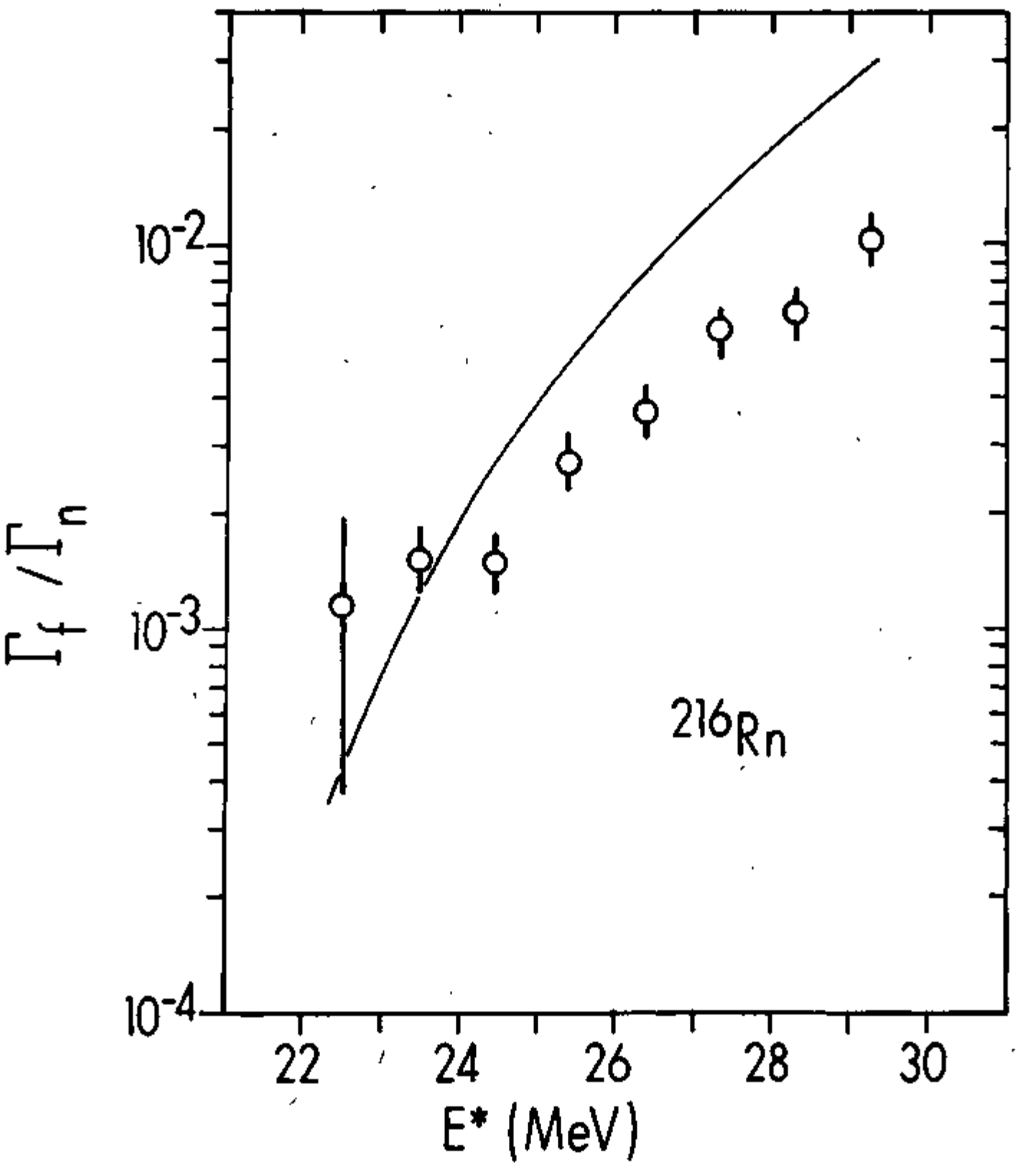

Figure 15

with increasing temperature. In the limit where the temperature is very large and the particle and collective degrees of freedom are thoroughly mixed, then $\omega_{intr}(E)$ contains all of the available states and there is no enhancement in the level density due to collective rotations.

If one introduces a normalization constant and an adjustable fission barrier into the theoretical calculation and requires a best fit to the experimental data, one obtains a fission barrier height of E_f = 13.8±0.7 MeV and a normalization constant of 0.05.

1) Paper presented at the Third International Symposium on the Physics and Chemistry of Fission, Rochester, N.Y. (1973), paper IAEA/SM - 174/56.

2) P. Möller and J.R. Nix, above conference, paper IAEA/SM-174/202 and private communication.

3) T. Ericson, Nucl. Phys. 6, 62(1958); S. Björnholm, A. Bohr and B.R. Mottelson, above conference, paper IAEA/SM - 174/205; J.R. Huizenga, A. Behkami, R.W. Atcher, J.S. Sventek, H.C. Britt and H. Freiesleben, Nucl. Phys., to be published.

2. ^{6,7}Li Induced Fission of ^{232}Th and ^{238}U --

H. Freiesleben* and J.R. Huizenga

Relatively large cross sections have been measured for lithium-ion induced transfer reactions on ^{209}Bi at energies below the Coulomb barrier (see section D1). In lithium-ion incuded reactions on heavy targets like ^{232}Th and ^{238}U one also expects direct processes to occur, namely, nucleon-transfer or projectile break-up followed by capture of one of the projectile fragments. However, for these heavy actinide targets the fission barriers are so small that these direct reaction processes are expected to be followed by fission with a relatively large probability, at least in the case of ^{238}U. The contribution to the total fission cross section of fission following direct reaction is expected to be important only at energies where the compound nucleus formation cross sections are small, that is at low incident energies where the Coulomb barrier is the controlling factor.

Therefore, in order to search for differences in the direct reaction cross sections of ^{6}Li and ^{7}Li we have repeated our fission cross section measurements[1] at very low lithium-ion energies. This was done very carefully by detecting fission fragment pairs in coincidence rather than single fragments in order to eliminate the possibility of misinterpreting the single events. However, no differences in the fission cross section data were obtained when using the coincidence and single spectra of two independent experiments.

---

*Fachbereich Physik, Universität Marburg, Germany.

We checked the ^{6}Li and ^{7}Li induced fission cross sections repeatedly by switching back and forth between the two Li-beams on both targets at various energies. The results for ^{6}Li induced fission are in very good agreement with our earlier data, while the new ^{7}Li data show a steeper rise of the excitation function than in the case of ^{6}Li (see Figs. 16 and 17).

We assume that this characteristic difference is due to incomplete momentum transfer processes followed by fission. For example, the Coulomb break-up cross sections for the two Li-isotopes may be different (the α-d threshold is 1.47 MeV and the α-t threshold is 2.47 MeV). The break-up process not only follows an excitation to an unbound state (2-state process) but also occurs as a one step disintegration, the inverse of a radiative capture reaction. Thus, the ^{6}Li break-up is expected to be favored due to its lower threshold. It follows that if the probabilities for absorbing deuterons and tritons by a ^{238}U nucleus are similar, one expects the ^{6}Li induced fission cross section to be larger than that of ^{7}Li induced fission at low energies.

Unfortunately, a fission fragment correlation angle measurement is not suitable for determining the contribution of direct reaction processes proceeding by incomplete momentum transfer. The α-particles from lithium break-up as well as those from subcoulomb-transfer reactions are mainly scattered backwards. Hence, the recoiling fissioning nucleus may get

Fig. 16: ^{6}Li and ^{7}Li induced fission cross sections of ^{232}Th as a function of bombarding energy.

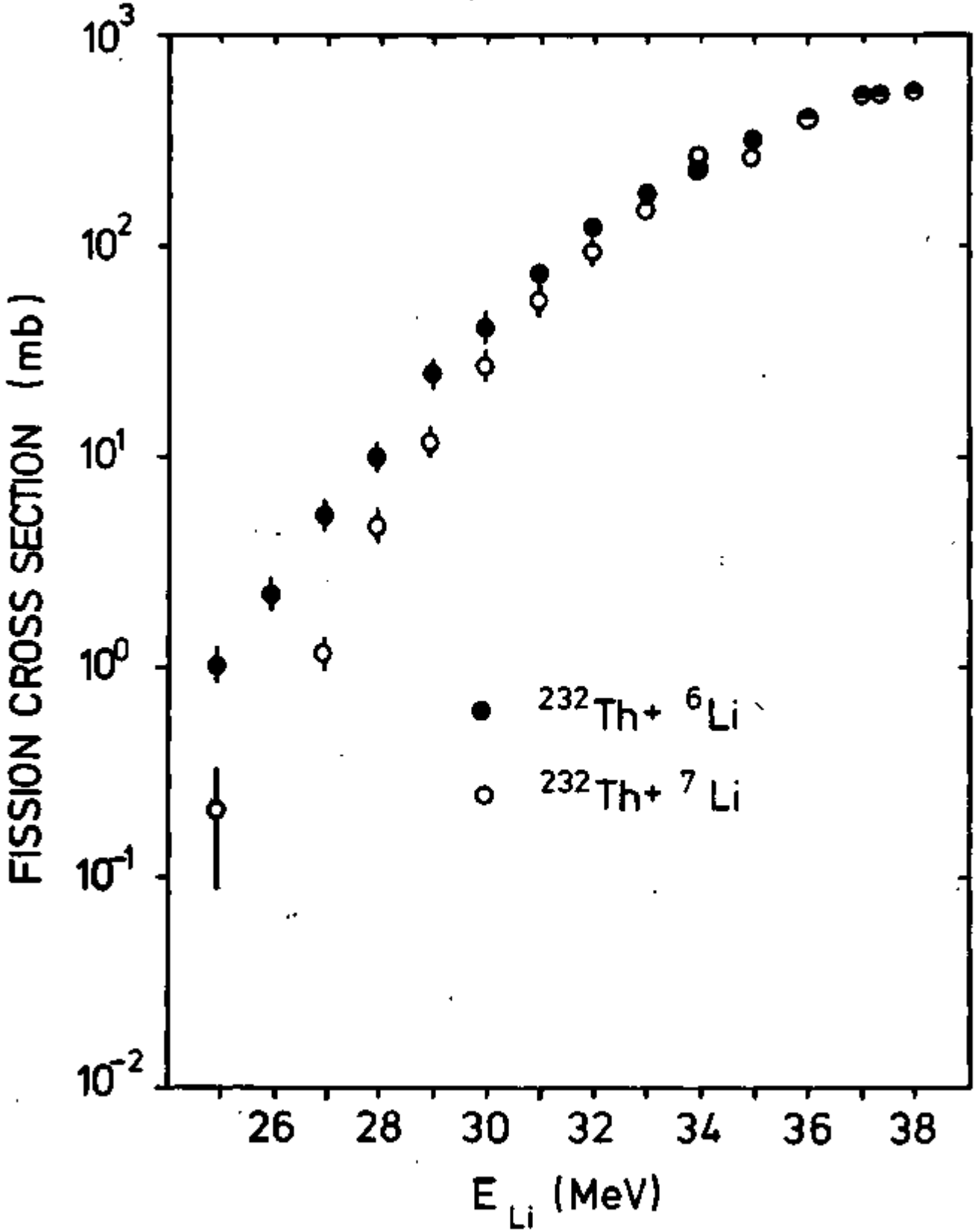
FISSION CROSS SECTION (mb)
10^3
10^2
10^1
10^0
10^{-1}
10^{-2}
^{232}Th+ ^{6}Li
^{232}Th+ ^{7}Li
26
28
30
32
34
36
38
E_{Li} (MeV)

Figure 16

Fig. 17: ^{6}Li and ^{7}Li induced fission cross sections of ^{238}U as a function of bombarding energy.

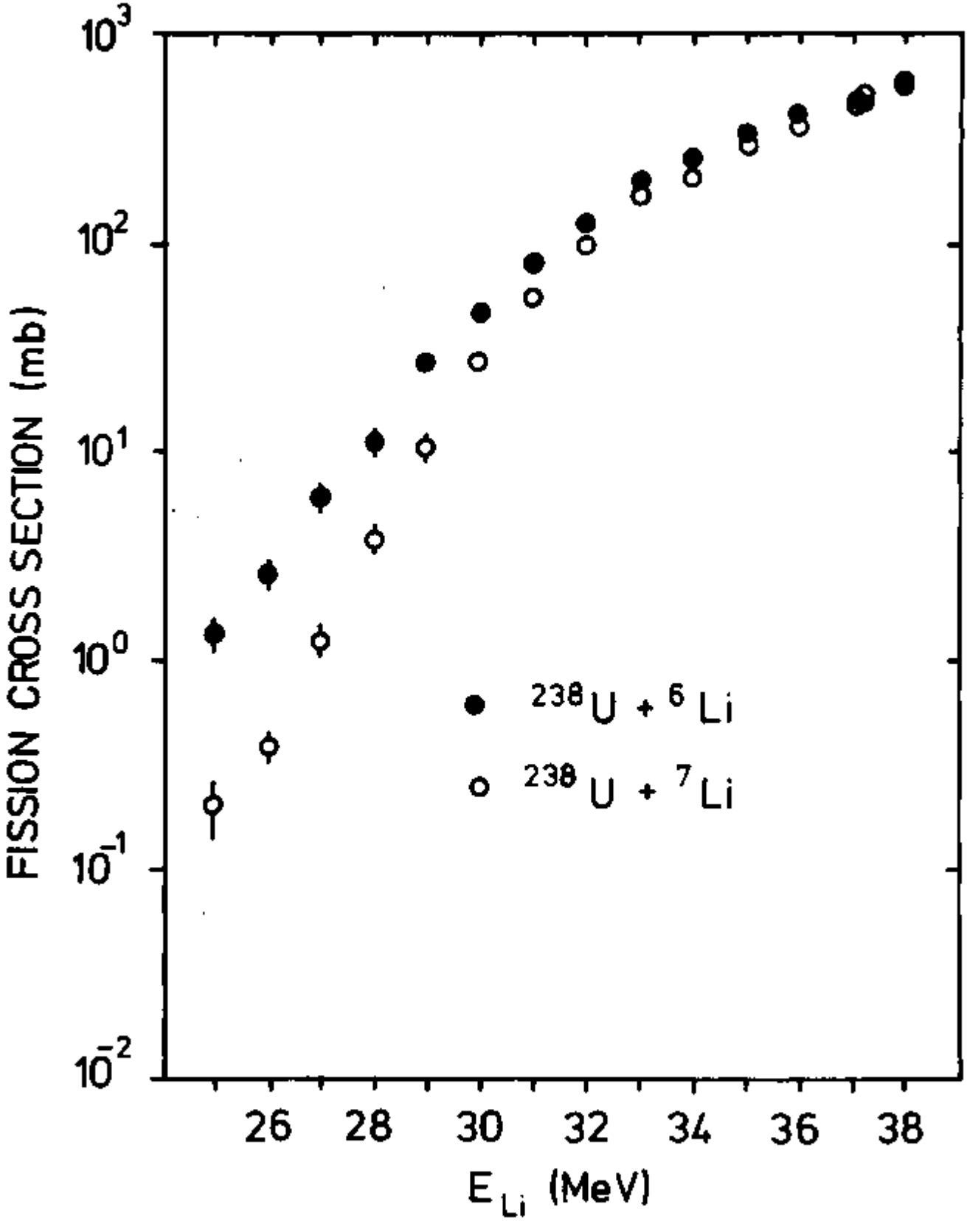
FISSION CROSS SECTION (mb)
10^3
10^2
10^1
10^0
10^{-1}
10^{-2}
$^{238}U + ^{6}Li$
$^{238}U + ^{7}Li$
26
28
30
32
34
36
38
E_{Li} (MeV)

Figure 17

more than the full incident momentum. Thus, a measurement of the correlation angle distribution for fission fragments does not show the characteristic asymmetric shape[1] for reactions proceeding by both complete and incomplete momentum transfer and does not allow for a discrimination between the different processes inducing fission. At present our above explanation for the differences in the ^{6}Li and ^{7}Li induced fission cross sections seems plausible, however, this explanation needs verification.

1) AEC Progress Report COO-3496-29 (1973).

3. Reevaluation of Experimental Estimates of the Pairing Gap at the Fission Saddle Point -- H.C. Britt* and J.R. Huizenga

Several years ago it was shown[1-6] that measurements of fission-fragment angular distributions at energies near the fission threshold could be used to estimate the magnitude of the pairing gap for even-even nuclei at the highly deformed fission saddle point. In particular, angular-distribution measurements from (d,pf) and (t,pf) reactions[2,3], (n,f) reactions[4,5], and (α,f) reactions[6] showed discontinuities in K_o^2 at energies corresponding to the onset of two-quasiparticle excitations at the fission saddle point. The pairing gap at the saddle point, $2\Delta_s$, could then be approximately equated to the difference between the energy for the onset of two-quasiparticle excitations, E^*_{2qp}, and the height of the fission barrier, E_f. However, at the time of these experiments it was not realized that the fission barriers for actinide nuclei are double peaked and that fission threshold properties are strongly influenced by shell effects at both the ground-state and saddle-point deformation.

Recent analyses[7,8] of fission results, taking into account the two-peaked nature of the fission barrier and allowing for the effects of shells on Γ_f/Γ_n, have led to new values for the heights of the fission barriers for ^{236}U and ^{240}Pu. These new barrier estimates lead to revised values for

---

*Los Alamos Scientific Laboratory, Los Alamos, New Mexico.

$2\Delta_s$ for these nuclei as indicated in Table 15. Most evidence now suggests[9,10] that the angular distribution of the fragments is determined at the deformation of the second peak for ^{236}U and ^{240}Pu and, therefore, the estimate of the pairing gap is assumed to correspond to that deformation for these nuclei.

For ^{236}U and ^{240}Pu the new values for $2\Delta_s$ are not significantly different from typical values, $2\Delta_{g.s.} \approx 1.4$ MeV, for actinide nuclei at their ground-state deformations. Since the relative values of Δ at the saddle and ground-state deformations are influenced both by the relative pairing strengths G_s and $G_{g.s.}$ and the relative densities of single-particle states near the Fermi surface, it is not possible to conclude from these experimental results alone whether or nor the pairing strength G varies with deformation.

Large values of the pairing gap, $2\Delta_s \approx 4$ MeV for ^{210}Po and $2\Delta_s \approx 2.7$ MeV for ^{227}Ra have also been reported[5,6]. For ^{210}Po the $2\Delta_s \approx 4$ MeV estimate is based on $E_f = 20$ MeV. Reanalysis of this data taking into account shell effects at the ground state, but not at the saddle point, have led to a new estimate[11] of the fission barrier, $E_f = 21 \pm 1$ MeV. More recent attempts[12] to realistically include shell effects at the saddle point have shown that with various assumptions about the saddle point level densities the data may be consistent with values of the barrier in the range $E_f = 19$ to 22 MeV. Therefore, at present the estimate of E_f for ^{210}Po must be considered very uncertain and the angular-distribution data

Table 15. Estimates of saddle-point pairing gaps $2\Delta_s$ from previous measurements of the energies for the onset of two-quasiparticle excitations E^*_{2qp} and estimates for the height of second peak in the fission barrier E_B.

Nucleus	E^*_{2qp} (MeV)	E_B (MeV)	$2\Delta_s$ (MeV)
^{236}U	7.4±0.2[a]	5.7±0.2[b]	1.7±0.3
^{240}Pu	7.0±0.2[c]	5.4±0.2[d]	1.6±0.3

a) Reference 3.

b) Reference 8.

c) Average of values 6.9 MeV from Ref. 3 and 7.1 MeV from Ref. 4.

d) Average of values 5.35 MeV from Ref. 7 and 5.45 MeV from Ref. 8.

consistent with a value $2\Delta_s$ in the range 2-5 MeV. Therefore, these results also do not at present give conclusive evidence that the pairing strength is a strong function of deformation.

For ^{227}Ra the data near threshold[5] show a rather sharp structure which is suggestive of a subbarrier resonance. Current theoretical fission-barrier calculations[13] do not predict subbarrier resonance structures near threshold for Ra isotopes but they also fail to predict observed subbarrier resonance structures for Th isotopes[8]. Therefore, in this case we cannot completely rule out the possibility that a subbarrier resonance has led to an underestimate of E_f and a subsequent overestimate of $2\Delta_s$.

In summary, we conclude that because of uncertainties in fission-barrier heights current experimental estimates of $2\Delta_s$ do not provide an unambiguous answer to the question of whether the pairing strength depends on the nuclear surface area.

1) J.J. Griffin, Phys. Rev. 132, 2204(1963).

2) H.C. Britt, R.H. Stokes, W.R. Gibbs, and J.J. Griffin, Phys. Rev. Lett. 11, 343(1963); Phys. Rev. 139, B354(1965).

3) H.C. Britt, F.A. Rickey, Jr., and W.S. Hall, Phys. Rev. 175, 1525(1968).

4) J.R. Huizenga, A.N. Behkami, J.W. Meadows, Jr., and E.D. Klema, Phys. Rev. 174, 1539(1968).

5) V.T. Ippolitov, Yu. A. Nemilov, Yu. A. Selitskii, and V.B. Funshtein, Uad. Fiz. 14, 939(1971)[transl.:Sov. J. Nucl. Phys. 14, 526(1972)].

6) L.G. Moretto, R.C. Gatti, S.G. Thompson, J.R. Huizenga and J.O. Rasmussen, Phys. Rev. 178, 1845(1969).

7) H.C. Britt, M. Bolsterli, J.R. Nix, and J.L. Norton, Phys. Rev. C7, 801(1973).

8) B.B. Back, Ole Hansen, H.C. Britt, and J.D. Garrett, in Proceedings of the Third International Conference on the Physics and Chemistry of Fission, Rochester, 1973 (International Atomic Energy Agency, Vienna, to be published), paper No. 27.

9) S. Bjørnholm and V.M. Strutinsky, Nucl. Phys. A136, 1 (1969).

10) J.R. Huizenga and H.C. Britt, in Proceedings of the International Conference on Photonuclear Reactions, 2, 833(1973).

11) L.G. Moretto, S.G. Thompson, J. Routti, and R.C. Gatti, Phys. Lett. 38B, 471(1972).

12) H. Freiesleben, H.C. Britt, and J.R. Huizenga in Proceedings of the Third International Conference on the Physics and Chemistry of Fission, Rochester, 1973 (see Ref. 8), paper No. 56.

13) See for example, P. Möller and J.R. Nix, in Proceedings of the Third International Conference on the Physics and Chemistry of Fission, Rochester, 1973 (see Ref. 8), paper No. 202.

D. Heavy Ion Reactions

1. Lithium Ion Induced Reactions on ^{209}Bi --

H. Freiesleben*, H.C. Britt**, J.R. Birkelund and J.R. Huizenga

There have been a variety of previous experiments[1-8] performed to investigate the interactions of ^{6}Li and ^{7}Li projectiles with targets in the gold through bismuth region and in one case[8] with actinide targets. In most cases these measurements study direct reactions by observing the emission of α, d or t particles. Hence, it is difficult to differentiate between reactions involving the breakup in the Coulomb field of $^{6}Li(^{7}Li)$ into α + d (t) where both particles are emitted with high energy and those two-body reactions where only one particle is emitted and the residual piece of the projectile is captured. However, a recent experiment[7] where both alpha particles and tritons were observed from the ^{7}Li + ^{208}Pb reaction at 30 MeV showed a very much larger cross section for alpha than for triton production. These results suggest that most of the alpha particles come from reactions where an excited ^{211}Bi nucleus was formed. A reaction of this type could proceed by either a direct stripping reaction or by a two step reaction where the ^{7}Li first breaks up into α + t and then the triton is captured. Experimentally it is very difficult to tell the difference between these two processes and in this report

*Fachbereich Physik, Universität Marburg, Germany.
**Los Alamos Scientific Laboratory, Los Alamos, New Mexico.

we will refer to a two-body reaction such as $^{7}Li + ^{208}Pb \rightarrow \alpha + ^{211}Bi$ as a "transfer" reaction even though we cannot rule out the possibility that there may be some contributions from two-step pricesses, i.e. breakup + capture. At energies near the Coulomb barrier for Sn isotopes, recent measurements[6] indicate that direct alpha particle emission cross sections are much larger for ^{6}Li than for ^{7}Li projectiles at the same bombarding energy. This result might indicate that the Coulomb breakup mechanism is more important for ^{6}Li than for ^{7}Li which would be consistent with the binding energy differences for the two projectiles.

In this report we present experimental results on the cross sections for producing various isotopes of Rn, At, Po and Bi following the bombardment of ^{209}Bi by ^{6}Li or ^{7}Li projectiles in the laboratory energy range of 25-34 MeV. In addition, fission cross sections were measured and the branching ratios Γ_f/Γ_n were obtained[9] (section C1).

Because of their proximity to the N = 126 and Z = 82 closed shells most of the residual nuclei formed in $^{6,7}Li + ^{209}Bi$ reactions are short-lived alpha particle emitters. The alpha decay characteristics for nuclei which can be formed following various ^{7}Li reactions are shown in Fig. 18. Cross sections for the formation of nuclei with $N \geq 127$ and for ^{212}Rn were obtained by bombarding a ^{209}Bi target with pulsed $^{6,7}Li$ beams and observing the alpha particle decays between beam pulses. Absolute cross sections were obtained by measuring the rate of alpha particle emission relative to elastic scattering in the same semiconductor detector.

Fig. 18: Diagram of nuclei populated by various reactions for the $^{7}Li + ^{209}Bi$ system. Entries in each box give mass number, decay energy of major alpha decay groups (MeV), alpha decay halflife and reaction by which a particular residual product can be formed.

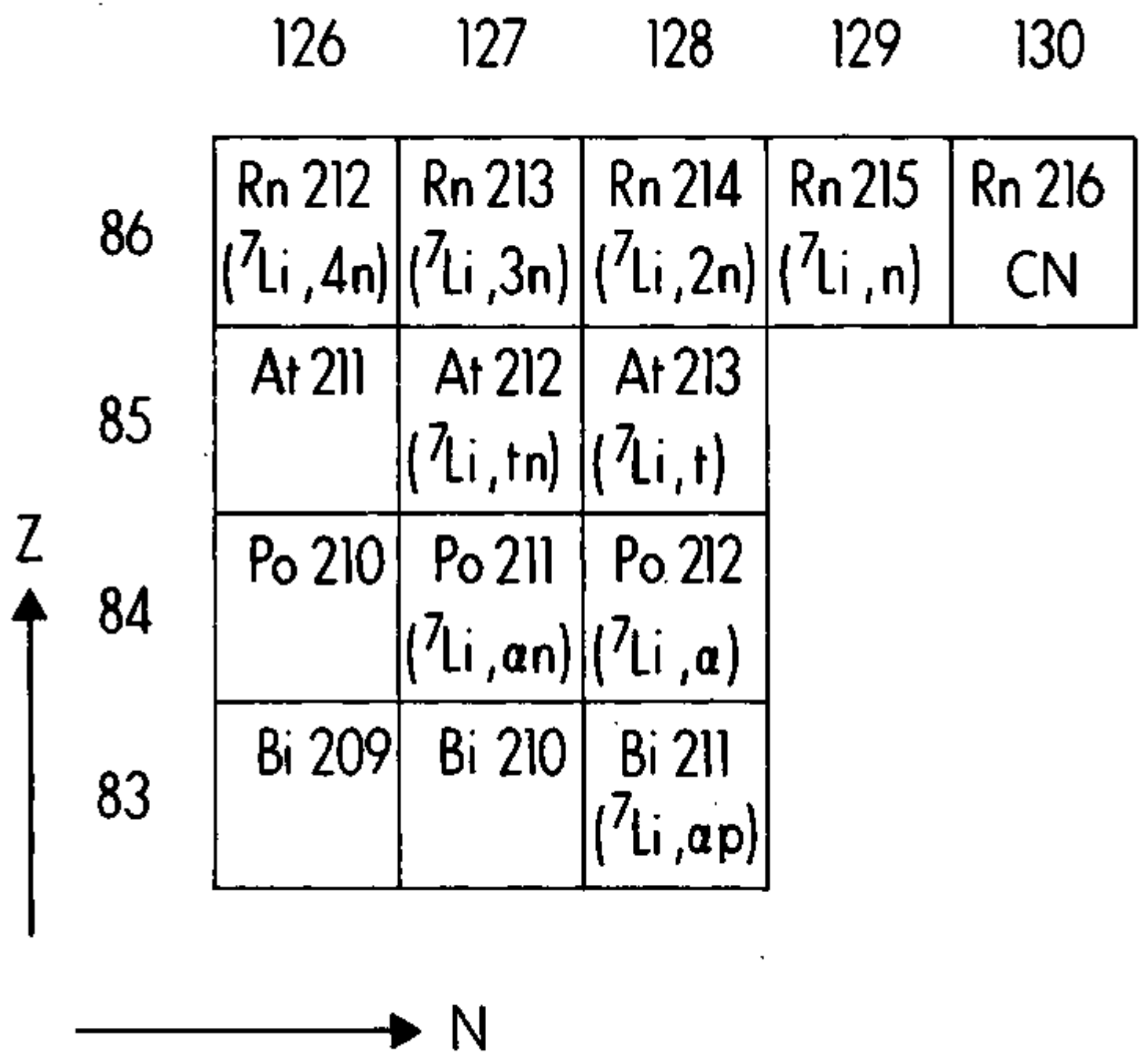
126
127
128
129
130
86
85
84
83
Rn 212 (7Li ,4n)
Rn 213 (7Li ,3n)
Rn 214 (7Li ,2n)
Rn 215 (7Li ,n)
Rn 216 CN
At 211
At 212 (7Li ,tn)
At 213 (7Li ,t)
Po 210
Po 211 (7Li ,αn)
Po 212 (7Li ,α)
Bi 209
Bi 210
Bi 211 (7Li ,αp)
Z
N

Figure 18

At ^{7}Li energies of 30 and 32 MeV the cross section for forming ^{210}Po was also measured by bombarding a target for several hours with a dc beam and then counting the 5.31 MeV decay alpha particles off line in known geometry. Again measurements were made relative to an absolute elastic scattering cross section at 90°.

Targets were produced by vacuum evaporation of deposits of ∿200 μg/cm^2 on carbon backings of thickness 20 μg/cm^2 and 100 μg/cm^2. The targets with 20 μg/cm^2 gave the best energy resolution for the alpha particle observation so that weak peaks and close doublets could be resolved but not all of the recoil nuclei were stopped in the target plus backing so that a correction was necessary for nuclei which recoiled out of the target. This correction was determined from the observation of the large cross section group using targets with 100 μg/cm^2 backings.

The excitation functions for the various reactions are shown in Fig. 19 and the actual cross sections obtained are listed in Tables 14 and 16. In Figs. 18 and 19 the excitation of particular final nuclides have been labelled with particular reactions that could lead to these nuclides. In some cases these reactions are not unique and for example ^{210}Po could be populated either by the (^{7}Li,α2n) or (^{7}Li,^{6}He) reactions.

The most remarkable features of these results are the large cross sections associated with transfer reactions relative to the fusion reactions and the much steeper slope for the fusion excitation function. For example, at 32 MeV

Fig. 19: Measured excitation functions for various reactions from $^{6,7}Li$ bombardment of ^{209}Bi. The excitation function labelled by 9.22 MeV is that of an unidentified isomer. We do not know the halflife of this transition and in converting to total cross sections we assumed that it was of the order or longer than our pulse repetition time (400 ns). If the lifetime of this decay were less than 100 ns then the cross section estimate would be significantly low.

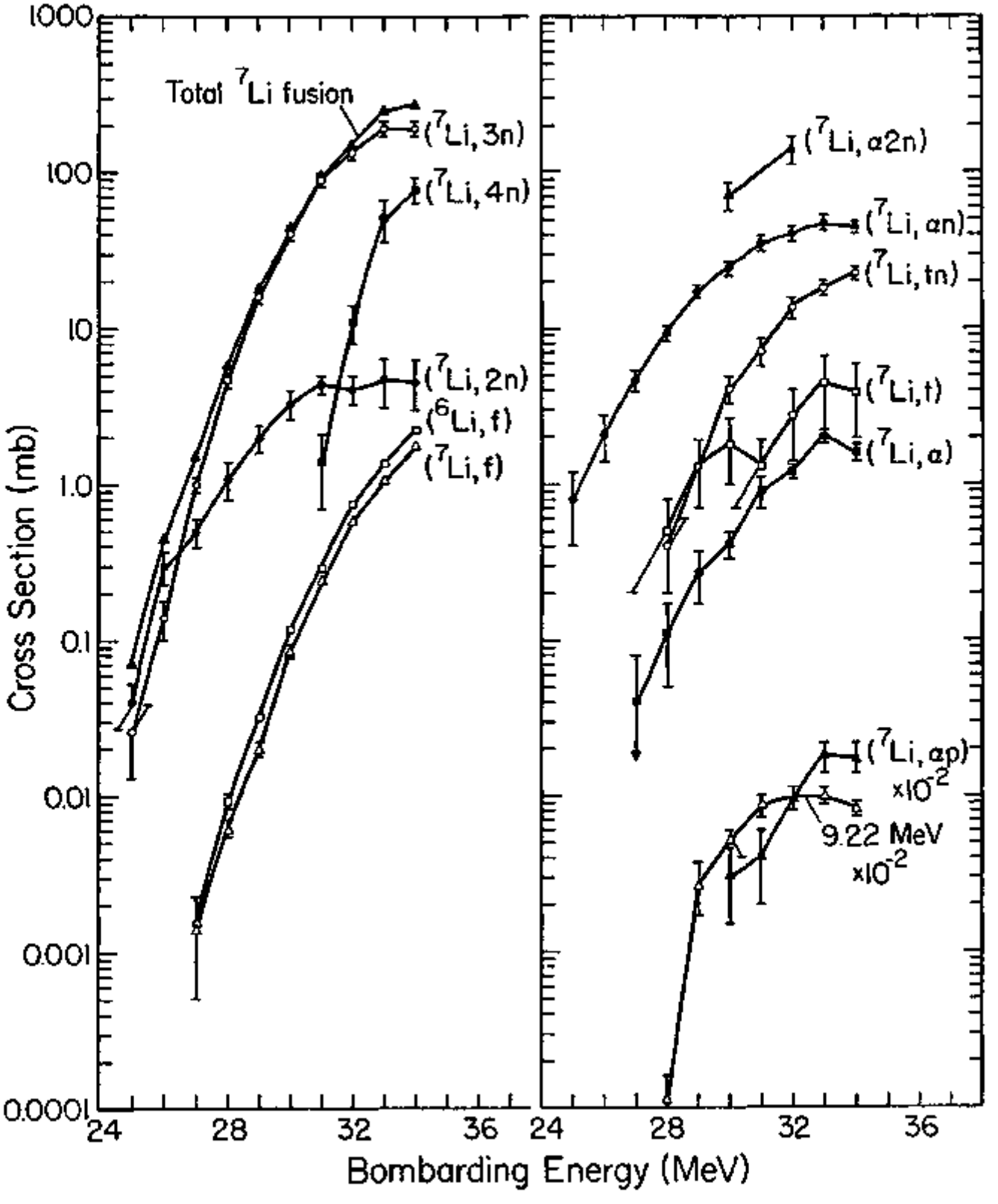
Total ^{7}Li fusion
(^{7}Li, 3n)
(^{7}Li, 4n)
(^{7}Li, 2n)
(^{6}Li, f)
(^{7}Li, f)
(^{7}Li, α2n)
(^{7}Li, αn)
(^{7}Li, tn)
(^{7}Li, t)
(^{7}Li, α)
(^{7}Li, αp)
×10^{-2}
9.22 MeV
×10^{-2}
Cross Section (mb)
1000
100
10
1.0
0.1
0.01
0.001
0.0001
24
28
32
36
Bombarding Energy (MeV)

Figure 19

Table 16. Measured cross sections in millibarns for various transfer reactions.

Laboratory Energy (MeV)	$\sigma(^7Li,\alpha)$	$\sigma(^7Li,\alpha n)$	$\sigma(^7Li,\alpha 2n)$	$\sigma(^7Li,t)$	$\sigma(^7Li,tn)$	$\sigma(^7Li,\alpha p)$	$\sigma(^7Li,9.20MeV)$	$\sigma(^6Li,\alpha)$	$\sigma(^6Li,d)$	$\sigma(^6Li,dn)$
34	1.6±0.2	44±4		3.9±2.0	23±2	1.8±0.4	0.82±0.09			
33	2.0±0.2	47±5		4.4±2.2	18±2	1.8±0.4	0.98±0.10			
32	1.2±0.1	40±4	140±20	2.7±1.3	13±2	1.0±0.2	0.97±0.10			
31	0.9±0.2	35±4		1.3±0.6	7.1±1.4	0.4±0.2	0.86±0.14			
30	0.4±0.08	24±3	71±10	1.8±0.8	4.1±0.8	0.3±0.15	0.49±0.10	0.8±0.2	1.6±0.8	11±2
29	0.27±0.10	17±2		1.3±0.6	1.3±0.6		0.27±0.10			
28	0.11±0.06	9.2±0.9		0.5±0.3	0.4±0.2		0.011±0.005	0.5±0.2	0.25±0.15	1.9±0.4
27	0.04±0.04	4.6±0.7					0.007±0.005			
26		2.1±0.7								
25		0.8±0.4								

the total cross section to Po and At isotopes is 200 mb compared to 150 mb for Rn isotopes. At 30 MeV the transfer cross section (Po + At) has decreased by a factor of 2 to 100 mb but the fusion cross section has decreased by a factor of 3.4 to 44 mb. Thus, at all energies equal to and below 32 MeV the transfer reactions make up the major part of the total reaction cross section.

The results appear consistent with a picture that the total reaction cross section has two major components. The first component is fusion with the subsequent evaporation of several neutrons to form the Rn isotopes. The second component consists of (^{7}Li,α) reactions to highly excited states followed by neutron evaporation to form Po isotopes and (^{7}Li,t) reactions to highly excited states followed by neutron evaporation to form At isotopes. Calculations[10] with a standard equilibrium evaporation code indicate that the contributions to the At and Po yields from evaporation of protons and alpha particles should be very small compared to measured yields.

Average excitation energies associated with the transfer reactions can be estimated from the optimum Q values[11] determined from reaction kinematics. For E_{lab} = 34 MeV, transfers at the optimum Q value lead to initial excitation energies of $\sim$16 MeV and $\sim$10 MeV for the residual nuclei ^{212}Po and ^{213}At formed in the (^{7}Li,α) and (^{7}Li,t) reactions, respectively. This prediction suggests that the most likely residual products should be ^{210}Po from the (^{7}Li,α2n) reaction

and ^{212}At from the (^{7}Li,tn) reaction. This prediction is consistent with the present data although it is still possible that we are missing a fraction of (^{7}Li,α) and (^{7}Li,t) cross sections by not observing the decays of the ^{209}Po and ^{211}At activities which are formed by (^{7}Li,α3n) and (^{7}Li,t2n) reactions, respectively.

The presént results can also be compared to the direct alpha particle and triton measurements from the ^{7}Li + ^{208}Pb reaction at 30 MeV by Häusser, et al.[7]. At 30 MeV we measure total cross sections of 95 mb and 6 mb for populating Po and At isotopes, respectively. This represents a large fraction of the direct alpha particle and triton emission cross sections of ∿150 mb and ∿20 mb respectively, which were determined from the angular distribution measurements of Häusser, et al.[7], and tends to confirm their postulate that the ^{7}Li reactions are dominated by transfer reactions.

1) C.E. Anderson, Second Conference on Reactions between Complex Nuclei, Gatlinburg, 1960, ed. A. Zucker, E.C. Halbert and F.T. Howard (Wiley, New York), p. 67.

2) R. Ollerhead, C. Chasman and D.A. Bromley, Phys. Rev. 134, B374(1964).

3) K. Bethge and K. Meier-Ewert, Phys. Rev. Lett. 18, 1010 (1967).

4) J.L. Quebert and H. Sztark, J. de Phys. 32, 255(1971).

5) D.L. Disdier, A.C. Ball, O. Häusser and R.E. Warner, Phys. Rev. Lett. 27, 1391(1971).

6) K.O. Pfeiffer, E. Speth and K. Bethge, Nucl. Phys. A206, 545(1973).

7) O. Häusser, A.B. McDonald, T.K. Alexander, A.J. Ferguson and R.E. Warner, Phys. Lett. 38B, 75(1972).

8) Alain Fleury, Thesis, University of Bordeaux, 1969 (unpublished) and private communication.

9) H. Freiesleben, H.C. Britt, and J.R. Huizenga in Proceedings of the Third International Atomic Energy Symposium on Physics and Chemistry of Fission, Rochester, 1973 (to be published), paper IAEA/SM-174/56.

10) C.M. Lederer, Table of Isotopes (Wiley, New York, 1967).

11) We are indebted to M. Blann for providing the evaporation code.

12) W. Von Oertzen in Nuclear Spectroscopy, ed. by J. Cerny (Academic Press, New York).

27554

2. Grazing Angles, Reaction Cross Sections and Fission Fragment Symmetry Angles for ^{40}Ar and ^{84}Kr Induced Reactions on Heavy Targets -- J.R. Huizenga and J. Birkelund

In the measurement of two correlated heavy fission fragments for very heavy ion reactions where full momentum transfer is assumed, three different situations arise for different experimental conditions. These situations are (1) the symmetry angle of the two fission fragments (assuming the two detectors are placed at equal angles) is inside the grazing angle (2) the symmetry and grazing angles coincide and (3) the symmetry angle is outside the grazing angle. Using the ^{209}Bi + ^{84}Kr reaction as an example, it is possible to have situation 1, 2 or 3 with bombarding energies of 500, 605 and 714 MeV, respectively. These and similar results are given in tables 17 and 18 for ^{40}Ar and ^{84}Kr induced reactions on selected heavy targets.

The values of θ_c and θ_p listed in tables 17 and 18 are estimated from Fresnel scattering theory (θ_c and θ_p are defined as the angles for which $\sigma_{el}/\sigma_{Ruth} = 1/4$ and has a maximum, respectively). For many heavy ion reactions Frahn[1] has shown that the experimental elastic cross section falls off from its Rutherford value according to the semiclassical expression,

$$\sigma_{el}(\theta)/\sigma_{Ruth}(\theta) = \frac{1}{2}\{[\tfrac{1}{2} - S(y)]^2 + [\tfrac{1}{2} - C(y)]^2\} \qquad (1)$$

where $S(y)$ and $C(y)$ are the Fresnel sine and cosine integrals

Table 17. Theoretical values of θ_c, θ_p, L_{max} and σ_R based on Fresnel scattering for ^{84}Kr induced reactions. The value of the critical radius of $1.32(A_1^{1/3}+A_2^{1/3})$ fm was obtained from elastic scattering data. The symmetric fission correlation angle is the angle on each side of the beam direction where the correlated fragments are expected.

Reaction	Energy MeV(lab)	θ_c* (C. of M.)	θ_p** (C. of M.)	θ_c (lab)	θ_p (lab)	Symm.Fission Corr. Angle (lab)	L_{max}	σ_R
$^{84}Kr+^{165}Ho$	460	103.9	93.0	74.5	65.4	49.4	128	644
	605	59.8	52.4	40.4	35.3	45.5	246	1797
	714	46.2	40.2	31.0	26.8	43.1	305	2336
$^{84}Kr+^{197}Au$	605	67.9	60.3	49.1	43.3	49.2	248	1631
	714	51.9	45.7	37.0	32.4	46.8	316	2247
$^{84}Kr+^{209}Bi$	460	136.9	125.3	115.7	102.2	54.1	79	214
	500	105.6	95.4	82.1	72.8	52.9	146	664
	540	88.3	79.3	66.6	59.1	52.0	191	978
	605	70.5	62.8	52.0	46.0	50.5	248	1572
	714	53.5	47.3	38.8	34.2	47.9	320	2219
$^{84}Kr+^{238}U$	500	118.3	108.0	97.8	87.3	55.6	127	462
	540	96.7	87.6	76.7	68.4	54.7	183	898
	605	76.3	68.5	56.6	52.3	53.0	247	1456
	714	57.1	50.8	43.1	38.2	50.7	328	2171

*θ_c is the angle at which $\sigma_{el}/\sigma_{Ruth} = 1/4$.

**θ_p is the angle at which $\sigma_{el}/\sigma_{Ruth}$ has its maximum value.

Table 18. Theoretical values of θ_c, θ_p, L_{max} and σ_R based on Fresnel scattering for ^{40}Ar induced reactions. The value of the critical radius was assumed to be 1.45 $(A_1^{1/3}+A_2^{1/3})$ fm. The symmetric fission correlation angle is the angle on each side of the beam direction where the correlated fragments are expected.

Reaction	Energy MeV(lab)	θ_c* (C. of M.)	θ_p** (C. of M.)	θ_c (lab)	θ_p (lab)	Symm.Fission Corr. Angle (lab)	L_{max}	σ_R
$^{40}Ar+^{165}Ho$	226	71.8	60.2	59.7	49.5	61.9	110	1391
	288	48.2	39.7	39.3	32.2	58.7	158	2227
	300	45.4	37.2	37.0	30.2	58.4	166	2349
$^{40}Ar+^{197}Au$	288	55.9	46.9	47.3	39.5	63.2	157	2065
	300	52.4	43.8	44.2	36.8	62.8	166	2210
$^{40}Ar+^{209}Bi$	250	74.8	63.4	64.8	54.4	66.0	123	1436
	288	58.4	49.3	50.0	41.9	64.4	157	2015
	300	54.7	46.0	46.7	39.0	63.9	166	2167
$^{40}Ar+^{232}Th$	288	62.7	53.3	54.6	46.1	66.3	156	1932
	300	58.6	49.7	50.9	42.9	65.9	166	2096
	388	39.8	33.2	34.2	28.5	63.0	226	2999
$^{40}Ar+^{238}U$	250	83.3	71.9	74.0	63.2	68.0	117	1251
	260	77.1	66.3	68.1	58.1	67.6	128	1441
	288	64.1	54.6	56.0	47.5	66.5	155	1898
	300	59.8	50.8	52.1	44.1	66.1	165	2068
	416	36.8	30.6	31.7	26.3	62.4	243	3203

* θ_c is the angle at which $\sigma_{el}/\sigma_{Ruth} = 1/4$.

** θ_p is the angle at which $\sigma_{el}/\sigma_{Ruth}$ has its maximum value.

and

$$y = (2\eta/\pi)^{1/2} \text{ cosec } (\frac{\theta_c}{2}) \sin (\frac{\theta-\theta_c}{2}). \quad (2)$$

The quantity η is the Coulomb parameter

$$\eta = Z_1 Z_2 e^2/\hbar v \quad (3)$$

where $Z_1 e$ and $Z_2 e$ are the charges of the two nuclei and v is their relative velocity for large separations. For $\theta = \theta_c$, the ratio $\sigma_{el}(\theta)/\sigma_{Ruth}(\theta) = 1/4$ and the angle θ_c is related to ℓ_{max} by

$$\ell_{max} = \eta \cot (\frac{\theta_c}{2}) \quad (4)$$

The following conditions are necessary for this semiclassical model to be valid, namely that

$$\ell_{max} >> 1 \text{ and } \ell_{max} \sin \theta_c \gtrsim 1. \quad (5)$$

The elastic scattering for several very heavy ion reactions have been analyzed with the above theory[2-6]. The nuclear radius, $R = r_o(A_1^{1/3} + A_2^{1/3})$, obtained from each analysis with the relation,

$$\sin (\frac{\theta_c}{2}) = \eta/(kR - \eta) \quad (6)$$

gives an $r_o = 1.32$ fm for ^{84}Kr projectiles. The value of r_o derived for statically deformed targets by this technique is slightly smaller. However, correcting θ_c for the deformation effects[3,5] gives an effective value of $r_o = 1.32$ fm for a corresponding spherical nucleus.

For the results of Table 17 we have assumed for the ^{84}Kr reactions that $r_o = 1.32$ and have calculated θ_c with eq. 6.

The value of θ_p is given by

$$\sin\left(\frac{\theta_c-\theta_p}{2}\right) = (3\pi/4\eta)^{1/2} \sin\left(\frac{\theta_c}{2}\right) \qquad (7)$$

where $\sin\left(\frac{\theta_c-\theta_p}{2}\right) \approx \frac{\theta_c-\theta_p}{2}$ for the angles of interest (where $\left(\frac{\theta_c-\theta_p}{2}\right)$ is expressed in radians). The value of ℓ_{max} is calculated with eq. 4 and the reaction cross section is calculated with the sharp cutoff approximation

$$\sigma_R = \pi\lambda\!\!\!^{-2} (\ell_{max} + 1)^2 \qquad (8)$$

The results for ^{40}Ar induced reactions presented in Table 18 are calculated in the same way except r_o has been assumed to be 1.45 fm. This value of r_o may be slightly too large for ^{40}Ar. However, if r_o is reduced to 1.32 fm, for example, the value of θ_c (C. of mass) for 388 MeV ^{40}Ar bombardment of ^{232}Th is increased by 5.7° and the value of σ_R is 2236 mbs. (probably too small a reaction cross section on the basis of experimental results).

The grazing angle is expected in the neighborhood of θ_p. This is, however, only an estimate for very heavy ion reactions in that it is known that the angle difference, $\theta_c-\theta_p$, is larger than the predictions from Fresnel scattering theory. In fact a parameter Δ has been defined by the equation[5]

$$\Delta = \left(\frac{4\eta}{3\pi}\right)^{1/2} \frac{\sin\left[\frac{(\theta_c-\theta_p)}{2}\right]}{\sin\left(\frac{\theta_c}{2}\right)} \qquad (9)$$

where Δ gives a measure of the extent to which the cross section has a Fresnel shape. For ^{84}Kr induced reactions on heavy deformed targets Δ has been measured to have values as large as 3.

1) W.E. Frahn, Phys. Rev. Lett. 26, 358(1971).

2) P. Colombani, et al., Phys. Letts. 42B, 197(1972).

3) P. Colombani, University of Paris, Orsay, Thesis (1974).

4) D.M. Brink and N. Rowley, Nucl. Phys. A219, 79(1974).

5) N. Rowley, Nucl. Phys. A219, 93(1974).

6) H. Freiesleben, J.R. Huizenga, J.P. Unik, V.E. Viola and K. Wolf, Unpublished data (1974).

3. Comparison of Experimental Values of the Critical Angular Momentum for ^{40}Ar and ^{84}Kr Induced Reactions with the Predictions of the Wilczynski and Bass Models -- J.R. Huizenga

In Table 19 the experimental fusion cross sections and values of the critical angular momentum for several ^{40}Ar and ^{84}Kr induced reactions on heavy targets are compared with the results predicted from the models of Wilczynski[1] and Bass[2]. These two models have several features in common.

The important criterion in the Wilczynski model is whether a particular angular momentum value has a minimum in the potential energy. All ℓ values which have potential wells are assumed to lead to fusion. Those values of ℓ for which $dV/dr \leq 0$ for all values of r do not fuse. Hence, the critical angular momentum of a colliding system is calculated from the condition of force equilibrium

$$\frac{2\pi(\gamma_1+\gamma_2)R_1R_2}{R_1+R_2} = \frac{Z_1Z_2e^2}{(R_1+R_2)^2} + \frac{\ell_c(\ell_c+1)\hbar^2}{\mu(R_1+R_2)^3} \qquad (1)$$

where R_1 and R_2 are the radii for which the nuclear force has its maximum value. The surface tension coefficients, γ_1 and γ_2, are evaluated on the basis of the liquid drop model.

The sharp cutoff model of Wilczynski contains two important assumptions, (1) that the energy in relative radial motion is dissipated inside the potential barrier. Hence, coupling of the energy in relative radial motion to the other degrees of freedom of the nucleus is assumed inside the

Table 19 Comparison of calculated and experimental values of the critical angular momenta for heavy ion reactions

Target	E_{bomb} MeV(lab)	$E^{B*}_{barrier}$ MeV(lab)	ℓ^{B*}_{crit}	σ^{B}_{fusion}	ℓ^{W**}_{crit}	σ^{W}_{fusion}	σ^{exp}_{fusion}	ℓ^{exp}_{crit}	exp ref.
				^{40}Ar Projectile					
^{165}Ho	226	178.4	79.3	723	87.4	830	860±90	86±5	1
	288		115.2	1189	87.4	688			
	300		121.0	1258	87.4	661	1430±140	129±7	1
^{209}Bi	250	206.4	81.8	640	87.6	732	1110±200	108±10	1
	288		108.8	976	87.6	636			
	300		116.0	1064	87.6	610			
^{232}Th	288	217.2	105.5	889	88.1	622			
	300		113.5	987	88.1	598	1000	114	2
	388		147.4	1282	88.1	462	600	101	2
^{238}U	250	221.0	71.8	475	88.0	633	766±150	91±9	1
	260		81.5	587	88.0	683	1268***	120	3
	288		104.0	858	88.0	616			
	300		112.2	957	88.0	592	1220±120	127±7	1,4
							1551***	143	3
	416		148	1196	88.0	427	1441***	162	5
				^{84}Kr Projectile					
^{165}Ho	460	419	92	332	72	201	200	71	4
	605		152	689	72	157			
	714		152	605	72	133			
^{209}Bi	460	471	0	0	8	2.8			
	500		86	230	8	2.5	<40	<37	4
	540		131	493	8	2.4			
	605		134	455	8	2.1			
	714		134	392	8	1.8			
^{238}U	500	497	36	39	0	0			
	540		112	339	0	0	<10	<18	<4
	605		122	360	0	0			
	714		122	305	0	0			

*Calculated with parameters of Bass, Phys. Letts. 47B, 139 (1973); ℓ^{B}_{crit} is calculated with the classical estimate of the conversion of orbital angular momentum into internal angular momentum of the fragments by surface interactions.

**Calculated with the parameters of Wilczynski, Nucl. Phys. A216, 386 (1973).

***Calculated from σ(full momentum)/σ_R ratios and theoretical estimates of σ_R.

[1]Hanappe et al., IAEA/SM-174/42 (1973).

[2]Artukh et al., Nucl. Phys. A215, 91 (1973); reports transfer σ's of 1100 mbs (297 MeV) and 2400 mbs (388 MeV). These values are subtracted from theoretical σ_R.

[3]S.A. Karamyan et al., Sov. J. Nucl. Phys. 9, 414 (1969).

[4]M. Lefort et al., Nucl. Phys. A216, 166 (1973)

[5]T. Sikkeland, Phys. Letts. 27B, 277 (1968).

potential barrier so that the projectile has no probability to return back over the barrier. On the other hand, it is assumed that no energy in the relative radial motion is lost prior to the time that the projectile has reached the barrier. (2) The angular momentum remains in relative motion until the barrier is crossed.

This simple theory is qualitatively in agreement with some trends in experimental data. For example, the prediction of ℓ_c for 500 MeV ^{84}Kr on ^{209}Bi is in much better agreement with experiment than a much more sophisticated theory with friction[3]. However, one characteristic of the Wilczynski model is that ℓ_c is independent of bombarding energy. This is in contradiction to experimental results (see Table 19). It must be recognized that ℓ_c is independent of bombarding energy only for energies above some saturation energy which corresponds to the barrier for ℓ_c. Wilczynski gives no recipe for calculating the radial dependence of the nuclear potential energy and, hence, the barrier as a function of ℓ. We assume for the entries in Table 19 that the energies listed for each reaction are above the saturation energy in each case.

In the model of Bass the radial dependence of the potential energy is given by

$$V_\ell(r) = \frac{Z_1 Z_2 e^2}{r} + \frac{\hbar^2 f^2 \ell_c(\ell_c+1)}{2\mu r^2} - \frac{d a_s A_1^{1/3} A_2^{1/3}}{R_{12}} e^{-\frac{r-R_{12}}{d}} \qquad (2)$$

where $d = 1.35$ fm, $a_s = 17.0$ MeV and $R_{12} = 1.07(A_1^{1/3}+A_2^{1/3})$. The critical value of the angular momentum, ℓ_c, is given by

the condition that

$$\frac{dV_{\ell_c}}{dr}\ (r = R_{12}) \simeq 0 \qquad (3)$$

The application of eq. 3 gives the result

$$x + 2y\ f^2\ \ell_c(\ell_c + 1) = 1 \qquad (4)$$

where

$$x = \frac{Z_1 Z_2 e^2}{R_{12} a_s A_1^{1/3} A_2^{1/3}} \quad \text{and} \quad y = \frac{\hbar^2}{2\mu R_{12}^2 a_s A_1^{1/3} A_2^{1/3}}.$$

Again it is implicitly assumed in this model that each ℓ wave which has a maximum outside a particular radius (in this case R_{12}) leads to fusion. However, in the Bass model the above assumption (2) is relaxed. The factor f in eq. 2 is given the value of 5/7 in the calculation of ℓ_c corresponding to the classical estimate of the conversion of angular momentum in the relative motion into internal angular momentum of the fragments. Hence, there is less centrifugal force to separate the nuclei after reaction and the fusion cross section is enhanced.

Above the saturation energy, this model also predicts an energy independent value of ℓ_c. However, the radial dependence of the nuclear potential is specified in this model and it is possible to calculate the saturation energy and the energy dependence of ℓ_c below the saturation energy. The energy dependent experimental fusion cross sections for

^{40}Ar bombardments of ^{165}Ho and ^{238}U are qualitatively in agreement with this model. However, the total potential energy (see the barrier energies used in different models shown in Fig. 21) in the Bass model is much larger than the potential energies used in the present models with friction[3,4]. The larger barriers in the Bass model qualitatively play the role of reducing the fusion cross sections in much the same way as the friction does in the models with lower barriers.

1) J. Wilczynski, Nucl. Phys. A216, 386(1973).

2) R. Bass, Phy. Lett. 47B, 139(1973).

3) D.H.E. Gross and H. Kalinowski, Phys. Letts. 48B, 302 (1974).

4) D. Sperber, M. Sobel and J. Bondorf, private communication (1974).

4. Interaction Potentials for Heavy Ion Reactions --

J.R. Huizenga and H. Freiesleben*

The interaction potential between a heavy ion projectile and target nucleus is calculated in this section by folding the nuclear density distribution of one nucleus with the real part of the single-nucleon optical potential of the other nucleus. For the case where the nuclear density distribution and the single-nucleon optical potential each have Saxon-Woods shapes, the calculation of the interaction potential is greatly simplified. If exchange effects are neglected the long-range part of the nucleus-nucleus potential is given by[1,2)]

$$V_{Nucl} = \frac{2\pi}{r} \int\int \rho_1(r_1)\ V_2(r_2)\ r_1 r_2 dr_1 dr_2 \qquad (1)$$

where the Saxon-Woods forms of the functions $\rho_1(r)$ and $V_2(r)$ are

$$\rho_1(r) = \rho_o\{1+\exp(\frac{r-R_1}{T})\}^{-1} \text{ and } V_2(r) = V_o\{1+\exp(\frac{r-R_2}{T})\}^{-1}$$

and nucleus 1 is taken as the projectile and nucleus 2 the target. In most of the calculations reported here we have used the constants suggested by Brink and Rowley[2)]; $\rho_o = 0.212(1+2.66A^{-2/3})^{-1}\text{fm}^{-3}$, $R_1 = 1.04A_1^{1/3}$, $T = 0.59$, $V_o = -50$ MeV and $R_2 = 1.19A_2^{1/3}$. These constants are nearly the same as those of Broglia and Winther[1)].

The radius parameter r_2 of 1.19 fm has been derived by Brink and Rowley by adjusting the interaction potential in order to fit elastic scattering data. The adjustment procedure is as follows. The experimental value of ℓ_{max} is determined

---

*Fachbereich Physik, Universität Marburg, Germany.

from the 1/4 point recipe discussed in section D2 (see eq. 4). Then the radial parameter r_2 used in the computation of the nuclear potential is varied until the calculated value of ℓ_{max} agrees with the experimental value of ℓ_{max}. In the calculation of ℓ_{max} it is assumed that the potential for ℓ_{max} has a maximum at the barrier distance, $R_B(\ell=\ell_{max})$, designated as the distance D, namely

$$\frac{\delta}{\delta r}[V_c(r) + V_{\ell_{max}}(r) + V_{Nucl}(r)]_{r=D} = 0 \qquad (2)$$

(This assumption requires that there is a value of r for which $V'_N(D) = V'_c(D) + V'_{\ell_{max}}(D)$, and will be questioned in section D5 for ^{40}Ar and ^{84}Kr induced reactions on very heavy targets). In addition, the maximum in the potential for ℓ_{max} is equal to the bombarding energy in the center-of-mass,

$$E_{CM} = V_c(D) + V_{\ell_{max}}(D) + V_{Nucl}(D) \qquad (3)$$

By combining eq. 2 and 3 it is possible to solve for D,

$$D = [\,2E_{CM} - V_c(D) - 2V_{Nucl}(D)]/V'_{Nucl}(D) \qquad (4)$$

and from eq. 3

$$\ell_{max} = \left(\frac{2\mu}{\hbar^2}\right)^{1/2} D[E_{CM} - V_c(D) - V_{Nucl}(D)]^{1/2} \qquad (5)$$

The radius parameter r_2 was adjusted in the calculation of $V_{Nucl}(r)$ so that the value of ℓ_{max} calculated by eq. 5 agreed with the experimental value of ℓ_{max}.

Possibly an easier way to visualize the adjustment in r_2 is slightly different from the above procedure described

by Brink and Rowley[2]. With the experimental value of ℓ_{max} the quantity $d(V_C+V_{\ell_{max}})/dr$ is calculated as a function of r. Then with a particular value of r_2, the value of dV_{Nucl}/dr is calculated as a function of r. The value of r for which these two derivatives are equal is D. This value of D is now used to check the equality of eq. 3. If the right hand side of eq. 3 is different from E_{CM}, a new value of r_2 is used in the computation of the nuclear potential and $dV_{Nucl}/dr(r)$. With this new value of D, eq. 3 is again checked. This procedure is repeated until eq. 3 is satisfied.

The nuclear potential calculated by this folding procedure for the $^{209}Bi + ^{84}Kr$ reaction is illustrated in Fig. 20 for two sets of parameters (curve b, Brink and Rowley[2]; curve c, Gross and Kalinowski[3]). In Fig. 20, two other nuclear potentials are plotted also, curve (a) is the nuclear potential of Bass[4] (see section D3) and curve (d) is a Saxon-Woods nuclear potential of Sperber, et al.[5] calculated with V_o = -175 MeV, r_o = 1.25 fm and d = 0.9 fm. In Fig. 21 are displayed the corresponding barriers for ℓ = 0. One sees an enormous variation of 65 MeV in the two extreme barriers.

In Table 20 we list several heavy ion reaction barriers (ℓ=0 and $\ell=\ell_{max}$), radial positions of each of the barriers and the contributions of V_{Nucl} at each of the respective barrier distances as calculated by folding the nuclear density distribution of one nucleus with the real part of the single-nucleon optical potential of the other nucleus.

Fig. 20: Radial dependence of four nuclear potentials for the reaction, $^{209}Bi + ^{84}Kr$. The different curves are identified in the figure. Curves (b) and (c) are calculated with the folding procedure discussed in the text.

$^{209}Bi + ^{84}Kr$

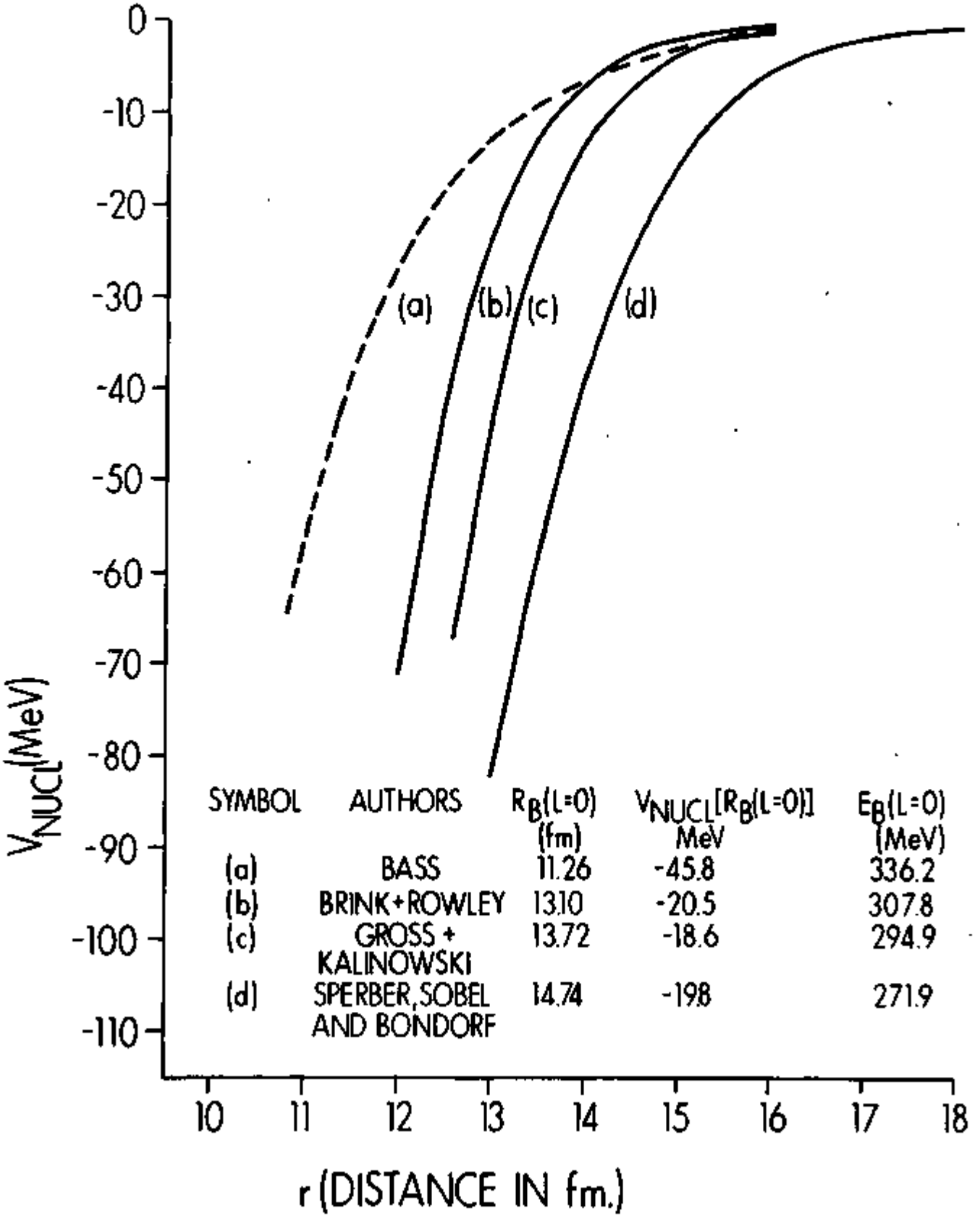

SYMBOL	AUTHORS	$R_B(L=0)$ (fm)	$V_{NUCL}[R_B(L=0)]$ MeV	$E_B(L=0)$ (MeV)
(a)	BASS	11.26	-45.8	336.2
(b)	BRINK+ROWLEY	13.10	-20.5	307.8
(c)	GROSS + KALINOWSKI	13.72	-18.6	294.9
(d)	SPERBER, SOBEL AND BONDORF	14.74	-19.8	271.9

Figure 20

Fig. 21: Barriers (ℓ=0) for four different nuclear potentials for the reaction, $^{209}Bi + ^{84}Kr$. The different curves are identified in the figure. The dashed line is the Coulomb potential, $V_c(r)$.

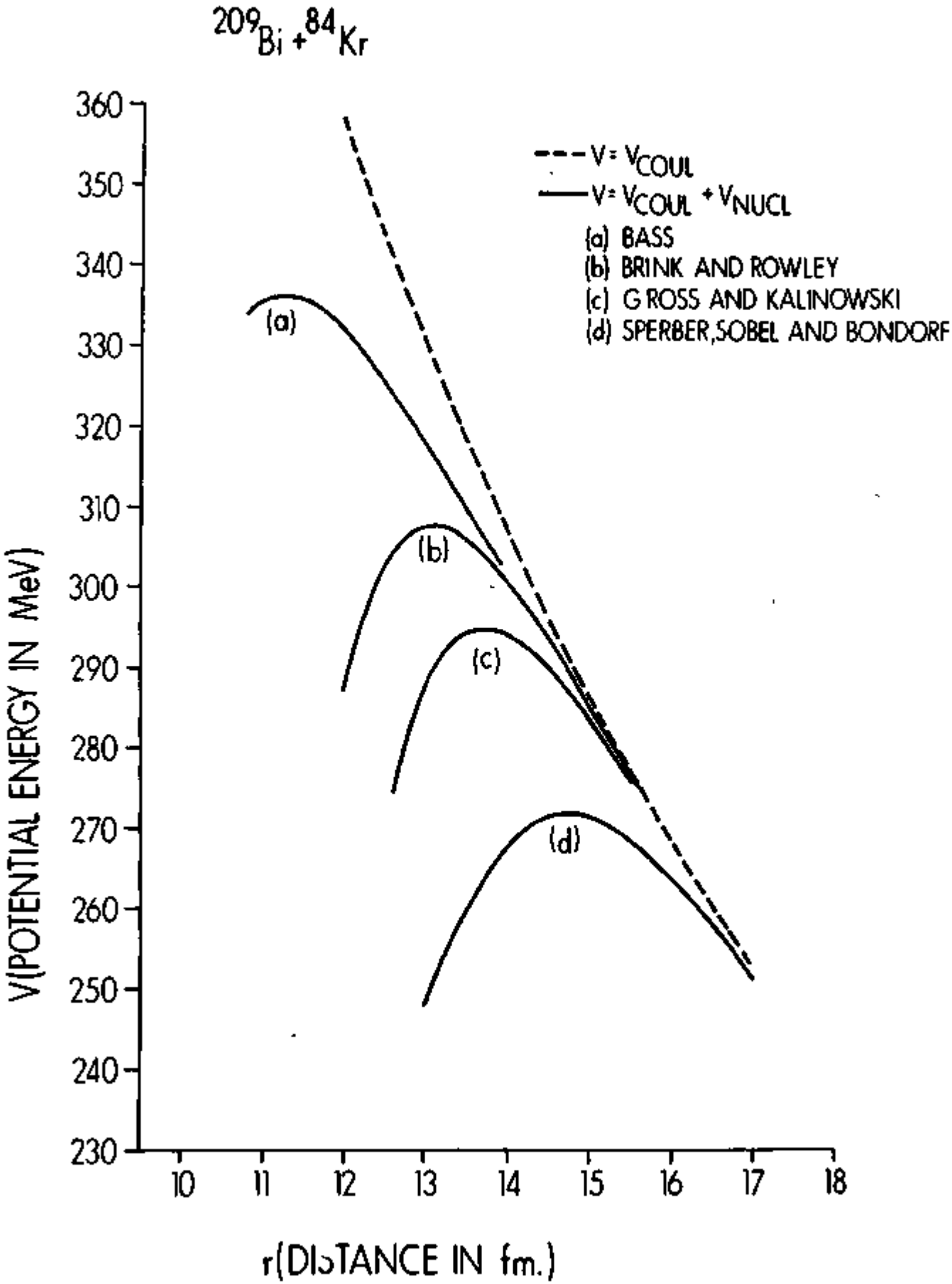
$^{209}Bi + ^{84}Kr$
V = V_{COUL}
V = V_{COUL} + V_{NUCL}
(a) BASS
(b) BRINK AND ROWLEY
(c) GROSS AND KALINOWSKI
(d) SPERBER, SOBEL AND BONDORF
V(POTENTIAL ENERGY IN MeV)
r(DISTANCE IN fm.)
360
350
340
330
320
310
300
290
280
270
260
250
240
230
10
11
12
13
14
15
16
17
18

Figure 21

Table 20. Heavy ion reaction barriers, radial positions of each of the barriers, and the contributions of V_{Nucl} at each of the respective barrier distances calculated by folding the nucleon-nucleon potential with the nuclear matter distribution[a]. The radial parameter r_{o1} = 1.04 fm[a] for all entries except the 5th. For the 5th entry r_{o1} = 1.075 fm[b]. Also included are values of L_{max} for a specific energy and the corresponding values of the radial position of L_{max} and the nuclear contribution at the barrier distance for L_{max}.

Reaction	E_{lab} (MeV)	r_2 (fm)	R_1+R_2 (fm)	$R_B(\ell=0)$ (fm)	$V_{Nucl}[R_B(\ell=0)]$ (MeV)	$E_B(\ell=0)$ (MeV)	ℓ_{max} (in units of $\hbar$)	$R_B(\ell=\ell_{max})$ (fm)	$V_{Nucl}[R_B(\ell=\ell_{max})]$ (MeV)
$^{165}Ho + ^{84}Kr$	605	1.19	11.079	12.662	-17.69	256.5	238.9	11.843	-45.96
$^{186}W + ^{84}Kr$	500	1.19	11.345	12.884	-18.94	278.7	170.4	12.484	-30.50
$^{197}Au + ^{84}Kr$	605	1.19	11.477	12.975	-20.04	295.4	239.5	12.298	-44.08
$^{209}Bi + ^{84}Kr$	605	1.19	11.615	13.100	-20.50	307.8	239.6	12.454	-43.52
$^{209}Bi + ^{84}Kr$	605	1.25	12.125	13.716	-18.63	294.9	263.4	13.027	-41.98
$^{238}U + ^{84}Kr$	605	1.19	11.928	13.362	-22.14	334.6	238.5	12.809	-42.18
$^{238}U + ^{84}Kr$	605	1.10	11.370	12.681	-24.96	351.0	209.5	12.200	-43.43
$^{209}Bi + ^{40}Ar$	288	1.19	10.617	12.438	-11.18	161.7	136.0	11.725	-26.23
$^{238}U + ^{40}Ar$	288	1.19	10.931	12.711	-11.91	175.6	132.9	12.102	-24.71

[a] D.M. Brink and N. Rowley, Nucl. Phys. A219, 79(1974).

[b] D.H.E. Gross and H. Kalinowski, Phys. Letts. 48B, 302(1974).

In the calculations of the fusion cross sections by the various models it is important to have a reasonably accurate knowledge of the radial dependence of the nuclear potential in order to calculate $V_\ell(r)$. Models[3,5] which attempt to derive the fusion cross section with the inclusion of friction also have as a necessary condition for fusion of a particular ℓ wave that it have a potential maximum and, hence a potential well. The potential well in the frictional model is, however, not a sufficient condition for fusion in that if there is not loss of radial kinetic energy in the well the projectile will decay back over the barrier. The number of ℓ waves with potential wells and the magnitude of the barrier for each ℓ wave enter directly into calculating the fusion cross section with the models with friction. For the same fusion cross section, a model with a smaller barrier requires larger friction and vice versa. In the limit of no friction (Bass model), the barrier must be still larger in the direction of the barriers shown in Fig. 21 where barrier (a) is used in a model with no friction and barriers (c) and (d) are used in models which include friction.

1) R.A. Broglia and A. Winther, Physics Reports 4C, 153(1972).

2) D.M. Brink and N. Rowley, Nucl. Phys. A219, 79(1974).

3) D.H.E. Gross and H. Kalinowski, Phys. Letts. 48B, 302(1974).

4) R. Bass, Phys. Letts. 47B, 139(1973).

5) D. Sperber, M. Sobel and J. Bondorf, private communication (1974).

5. Comments on the Validity of the Interaction Potential for Very Heavy Ion Reactions -- J.R. Huizenga and H. Freiesleben*

The interaction potential between two nuclei calculated by folding the nuclear density distribution of one nucleus with the real part of the single-nucleon optical potential of the other nucleus is expected to be reasonably accurate when the densities of the two interacting nuclei do not overlap too much. The important question remains as to what interaction distances such a potential can be used. Brink and Rowley[1] use such a potential for ^{84}Kr induced reactions on very heavy targets at interaction distances where V_{Nucl} has values less than -30 MeV and V'_{Nucl} has values larger than 40 MeV/fm. Gross and Kalinowski[2] indicate confidence in the validity of the nuclear potential for radial distances greater than $1.2(A_1^{1/3}+A_2^{1/3})$. For the ^{209}Bi + ^{84}Kr reaction, this corresponds to a minimum distance of 12.58 fm. From Fig. 20 (curve c) one sees that the nuclear potential at this distance is -68 MeV and the corresponding value of V'_{Nucl} is 71 MeV/fm. This is an extremely large value of V'_{Nucl} and will cause all the ℓ waves for the ^{209}Bi + ^{84}Kr reaction at a bombarding energy of 605 MeV to have maxima and associated potential wells.

In the following paragraphs we discuss the validity of such large values of V'_{Nucl}. As a basis for our remarks we compare the nuclear potential derived by the folding method

---

*Fachbereich Physik, Universität Marburg, Marburg, Germany.

with a nuclear potential having a Saxon-Woods form,

$$V_{Nucl}(r) = \frac{V_o}{1 + \exp[(r-R)/d]} \quad . \tag{1}$$

The derivative of eq. 1 with respect to r is

$$\frac{dV_{Nucl}}{dr}(r) = - \frac{V_o}{d} \frac{\exp[(r-R)/d]}{\{1 + \exp[(r-R)/d]\}^2} \quad . \tag{2}$$

The rate of change of a Saxon-Woods nuclear potential with radial distance has a maximum at r = R, where this maximum is given by,

$$(\frac{dV_{Nucl}}{dr})_{max} = - \frac{V_o}{4d} \quad . \tag{3}$$

It is possible to estimate dV_{Nucl}/dr at r = R (where $R = R_1+R_2$) for two touching spherical nuclei from the liquid drop model[3)]

$$\frac{dV_{Nucl}}{dr} (r=R) = \frac{2\pi(\gamma_1+\gamma_2)R_1R_2}{R_1 + R_2} \tag{4}$$

where γ_1 and γ_2 are the surface tension coefficients[4)] of nuclei 1 and 2, respectively, in units of MeV/fm^2,

$$\gamma = 0.9517[1 - 1.7826(\frac{N-Z}{A})^2] \quad . \tag{5}$$

If one equates the maximum value of the derivative of the nuclear potential in the Saxon-Woods model given by eq. 3 with the force of the touching nuclei in the liquid drop model of eq. 4, one obtains,

$$- \frac{V_o}{4d} = \frac{2\pi(\gamma_1+\gamma_2)r_o A_1^{1/3}A_2^{1/3}}{A_1^{1/3} + A_2^{1/3}} \quad . \tag{6}$$

With a value of $r_o = 1.17$ fm*, one has for the $^{209}Bi + ^{84}Kr$ reaction a limiting value of V'_{Nucl} of 33.3 MeV/fm and

$$\frac{V_o}{d} = - 133.2 \text{ MeV/fm} . \qquad (7)$$

For the $^{238}U + ^{40}Ar$ reaction one obtains a limiting value of V'_{Nucl} of 29.15 MeV/fm and

$$\frac{V_o}{d} = - 116.6 \text{ MeV/fm} . \qquad (8)$$

An estimate of V_o is made also on the basis of the assumption that the two nuclei fuse into a single nucleus. In this approximation V_o for a particular reaction is given by

$$V_o = a_s[(A_1 + A_2)^{2/3} - A_1^{2/3} - A_2^{2/3}] \qquad (9)$$

where a_s is a surface tension constant with a value of about 17 MeV. For the $^{209}Bi + ^{84}Kr$ and $^{238}U + ^{40}Ar$ reactions, V_o in this approximation is -175 MeV and -128 MeV, respectively. These potentials are deeper (1.5 to 1.7 times deeper if d = 0.75 fm) than those of eqs. 7 and 8, however, these potentials are expected to be limiting values. Hence, the estimates of V_o from eqs. 7 and 8 appear to be reasonable first guesses.

The radial dependences of the nuclear potentials for the above two reactions for a Saxon-Woods potential are displayed in Fig. 22. In each case the diffuseness parameter d was set

---

*In order to be consistent with the values of γ determined from the Lysekil constants[4] a radius parameter of 1.2249 fm should be used in eq. 6. This increases V'_{Nucl} by 5%.

Fig. 22: Radial dependence of the nuclear potential for two different models. The solid lines are calculated with a Saxon-Woods potential with the parameters r_o = 1.17 fm, d = 0.75 fm and V_o/d as given by eqs. 7 and 8 (see text). The solid dots are the Brink-Rowley potential calculated by folding the nuclear density distribution of one nucleus with the real part of the single-nucleon optical potential of the other.

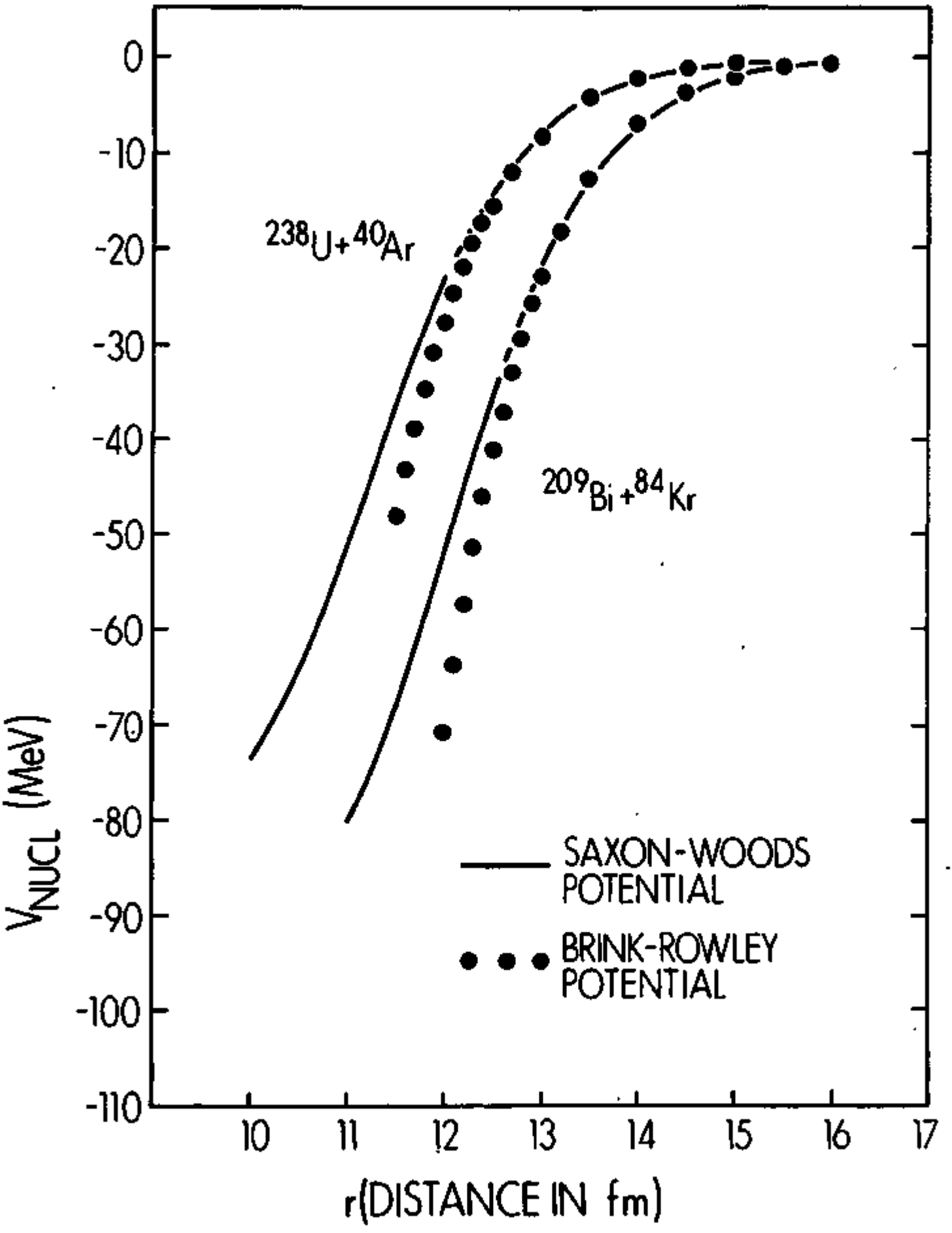
0
-10
-20
-30
-40
-50
-60
-70
-80
-90
-100
-110
V_{NUCL} (MeV)
$^{238}U+^{40}Ar$
$^{209}Bi+^{84}Kr$
SAXON-WOODS POTENTIAL
BRINK-ROWLEY POTENTIAL
10
11
12
13
14
15
16
17
r(DISTANCE IN fm)

Figure 22

equal to 0.75 fm and V_o was calculated from eqs. 7 and 8. The values of the nuclear potential calculated from the Brink-Rowley prescription are included in Fig. 22 also. It can be seen that the nuclear potentials of Fig. 22 are in very close agreement with the Brink-Rowley potential for the larger radial distances where the densities of the two interacting nuclei are not strongly overlapping. The nuclear potential of Broglia and Winther is in qualitative agreement with the potentials of Fig. 22 for the very largest values of r.

The radial dependence of the quantity $V_c + V_{Nucl}$ is plotted in Fig. 23 for the $^{209}Bi + ^{84}Kr$ and $^{238}U + ^{40}Ar$ reactions. The barrier height, $E_B(\ell=0)$, for the $^{209}Bi + ^{84}Kr$ reaction is essentially unchanged from that calculated with the Brink-Rowley potential. However, a very important difference in the two potentials for the $^{209}Bi + ^{84}Kr$ reaction is illustrated in Fig. 24. Whereas the Brink-Rowley potential has maxima for all ℓ waves for the $^{209}Bi + ^{84}Kr$ reaction at a bombarding energy of 605 MeV (ℓ=240 is equal to ℓ_{max} and for this ℓ wave $dV_{Nucl}/dr = d(V_c+V_\ell)/dr$ at a radial distance of 12.454 fm), the Saxon-Woods potential has maxima only for approximately 100 ℓ waves. This results from the fact that dV_{Nucl}/dr for the Saxon-Woods potential has a maximum value of dV_{Nucl}/dr of 33.3 MeV/fm ($-V_o/4d$).

The important conclusion to be drawn from Fig. 24 is that the two very similar nuclear potentials of Fig. 22 give

Fig. 23: The barriers, $E_B(\ell=0)$, of two heavy ion reactions calculated with the Saxon-Woods potential and the parameters listed in Fig. 22.

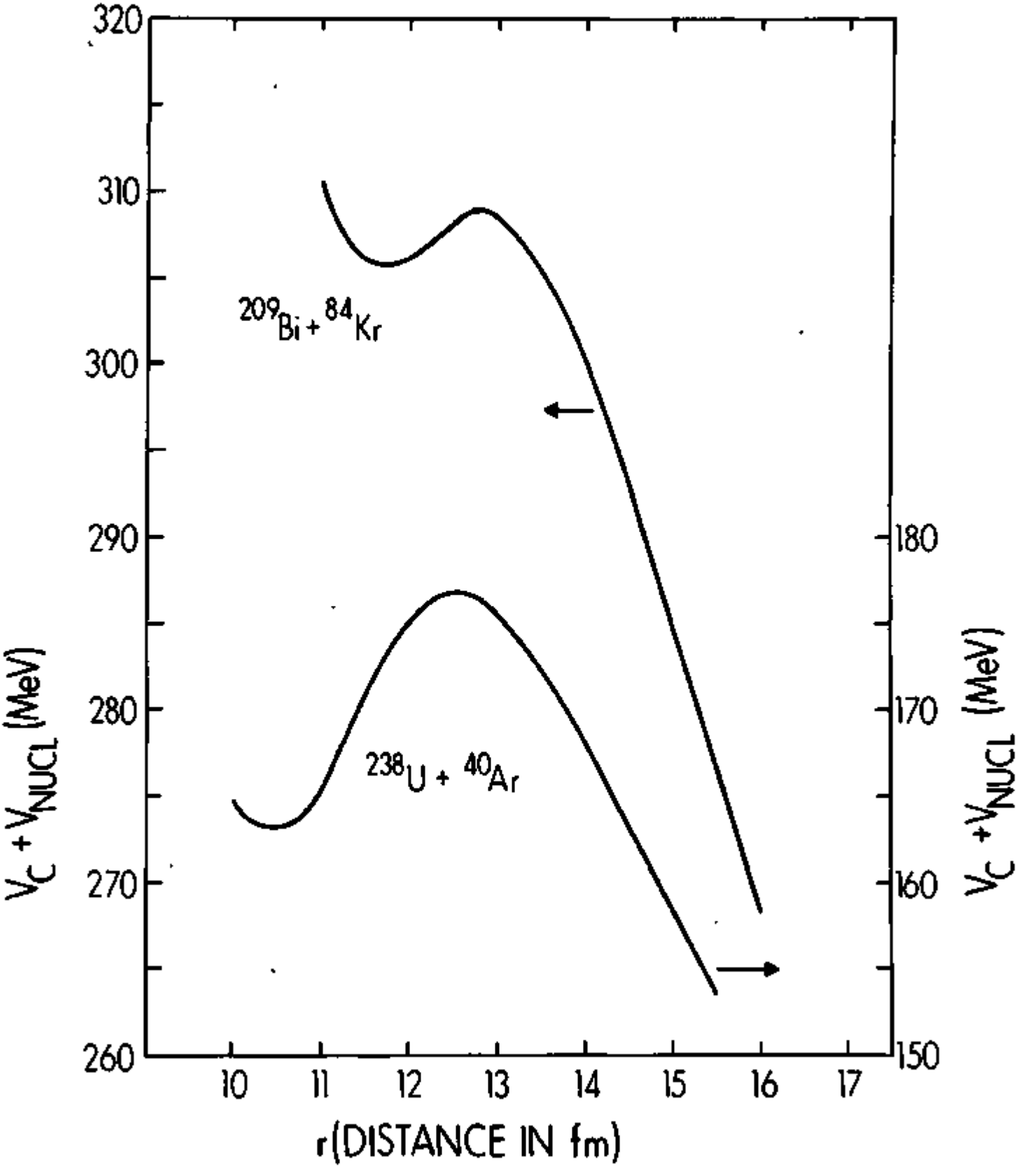
320
310
300
290
280
270
260
180
170
160
150
10
11
12
13
14
15
16
17
$^{209}Bi + ^{84}Kr$
$^{238}U + ^{40}Ar$
$V_C + V_{NUCL}$ (MeV)
$V_C + V_{NUCL}$ (MeV)
r(DISTANCE IN fm)

Figure 23

Fig. 24: Radial dependence of the quantity $d(V_c+V_\ell)/dr$ for the $\ell=0$ and $\ell=240$ waves for the ^{209}Bi + ^{84}Kr reaction. Also shown for the ^{209}Bi + ^{84}Kr reaction are the radial dependences of dV_{Nucl}/dr for two potentials. The solid line results for the Brink-Rowley potential and the dotted line for the Saxon-Woods potential with the parameters of Fig. 22. Crossings of dV_{Nucl}/dr with the curves of $d(V_c+V_\ell)/dr$ for particular ℓ waves correspond to a maximum or minimum in the total potential energy curve. The dotted line crosses the $\ell=0$ curve at r = 12.8 fm(maximum) and 11.7 fm(minimum). See Fig. 23.

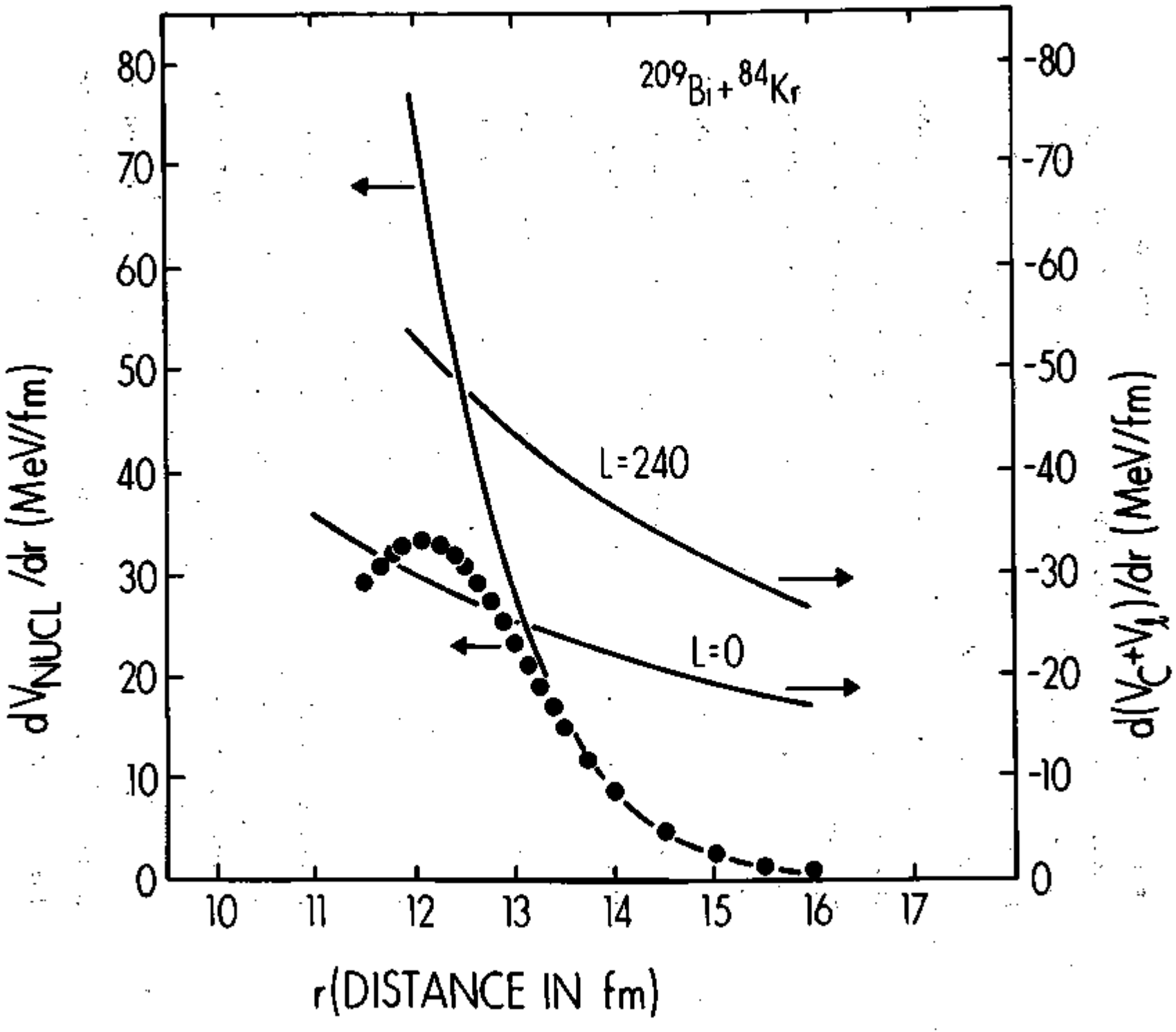
$^{209}Bi + ^{84}Kr$
L=240
L=0
dV_{NUCL}/dr (MeV/fm)
$d(V_C+V_\ell)/dr$ (MeV/fm)
r(DISTANCE IN fm)
0
10
20
30
40
50
60
70
80
-10
-20
-30
-40
-50
-60
-70
-80
10
11
12
13
14
15
16
17

Figure 24

very different results for the number of ℓ waves with potential maxima. The Brink-Rowley procedure described in section D4 of equating the center-of-mass energy to the peak in the total potential for ℓ_{max} is not valid for the Saxon-Woods potential of Fig. 22 for the $^{209}Bi + ^{84}Kr$ reaction since ℓ_{max} has no peak. It should be remarked, however, that the Brink-Rowley procedure starts with the assumption that ℓ_{max} has a potential maximum and then makes adjustments in r_2 and the nuclear potential in order to make the experimental and calculated values of ℓ_{max} agree. If it is the case that a particular reaction has no potential maximum for ℓ_{max}, then the Brink-Rowley procedure forces dV_{Nucl}/dr to be too large in order to produce a maximum in the total potential energy for ℓ_{max}. Hence, this procedure leads to a nuclear potential with too great a slope. (The Brink-Rowley procedure of locating the radial distance of ℓ_{max} by eqs. 2-5 of section D4 is also not valid for models with friction).

In Fig. 25 the radial dependences of $d(V_c+V_\ell)/dr$ for three ℓ waves (0, 100 and 120) are shown for the $^{238}U + ^{40}Ar$ reaction. In the same figure we show the radial dependence of dV_{Nucl}/dr for the Saxon-Woods potential. The balance between dV_c/dr and dV_{Nucl}/dr is not nearly as delicate for the $^{238}U + ^{40}Ar$ reaction as for the $^{209}Bi + ^{84}Kr$ reaction.

It is possible, of course, that even though the derivative of the nuclear potential is grossly overestimated in a particular case, the value of the nuclear potential itself at the

Fig. 25: Radial dependence of the quantity $d(V_c+V_\ell)/dr$ for ℓ=0, 100 and 120 for the $^{238}U + ^{40}Ar$ reaction (solid line curves). Also shown is the radial dependence of dV_{Nucl}/dr (dashed line curve) for the Saxon-Woods potential with the parameters of Fig. 22.

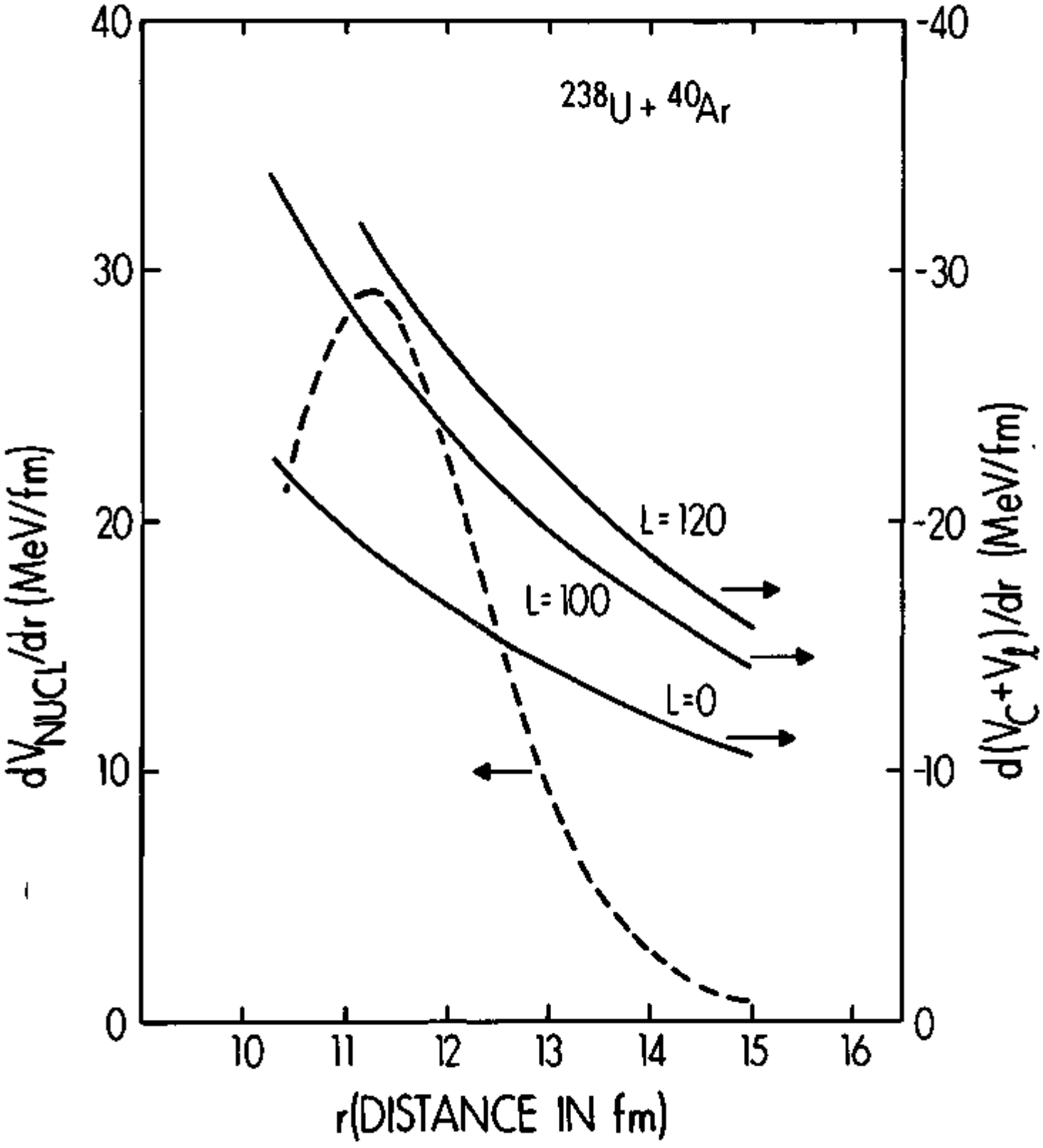
$^{238}U + ^{40}Ar$
L = 120
L = 100
L = 0
dV_{NUCL}/dr (MeV/fm)
$d(V_C+V_\ell)/dr$ (MeV/fm)
r(DISTANCE IN fm)
40
30
20
10
0
-40
-30
-20
-10
0
10
11
12
13
14
15
16

Figure 25

appropiate barrier distance is subject to less uncertainty. This is the case for the $^{209}Bi + ^{84}Kr$ reaction under discussion where the two different nuclear potentials differ by only 6 MeV at r = 12.454 fm (see table 20) where ℓ_{max} has its maximum with the Brink-Rowley potential. The barriers $E_B(\ell=0)$ for the two potentials are nearly the same because they occur at different values of r where the differences in the nuclear and Coulomb potentials cancel each other to first order.

Even though the Brink-Rowley folding potential and the present Saxon-Woods nuclear potential are nearly the same to radial distances near the $\ell=0$ barrier for the $^{209}Bi + ^{84}Kr$ reaction, the two potentials can lead to extremely different fusion cross sections for models (with or without friction) which require a potential well as a necessary condition for fusion. For example, in the Gross-Kalinowski[2] frictional model, 150 ℓ waves lead to fusion for 500 MeV ^{84}Kr on ^{209}Bi. As mentioned previously their nuclear potential calculated by the folding procedure (see curve c, Fig. 20) gives potential wells for all ℓ waves. With the dissipation of energy through friction, it turns out in this model that sufficient energy remains in relative motion so that the system goes over the barriers of ℓ waves up to 150.

The argument against there being such a large number of ℓ waves with maxima for the $^{209}Bi + ^{84}Kr$ reaction comes from a systematic examination of the experimental data. Whereas for all projectiles up to ^{40}Ar the ratio of ℓ_{crit}/ℓ_{max} is in the range 0.75±0.20 for all bombarding energies (see, for

example, the compilation of experimental values of ℓ_{crit} in ref. 2), this ratio is very much smaller for ^{84}Kr reactions. This quantitative difference for ^{84}Kr is not likely to be due to a change in the frictional force but due to the fact that only a relatively few ℓ waves have maxima as discussed above.

It is the purpose of this section to emphasize the importance of having accurate knowledge of the radial dependence of the nuclear potential to radial distances inside the barrier for predicting fusion cross sections of very heavy ion reactions. The folding potentials of Brink-Rowley and Gross-Kalinowski both predict potential wells for many ℓ waves for ^{84}Kr induced reactions on heavy targets. The reason for this result is directly related to the large values of dV_{Nucl}/dr obtained with their potentials at radial distances near the barrier. In fact both folding potentials are used at radial distances where dV_{Nucl}/dr exceeds the maximum calculated on the basis of a simple liquid drop model (eq. 4). With very small changes in the nuclear potential, as illustrated with the present Saxon-Woods potential (see Fig. 22), very marked differences result in the radial dependence of the total potential energy for different ℓ values. It is not the purpose of this note to defend the choice of parameters used in the Saxon-Woods potential but only to point out the serious consequences of slight changes in the nuclear potential for very heavy ion reactions.

The application of a nuclear interaction potential based on a sudden approximation hypothesis to heavy ion reactions

has been discussed recently by Galin, et al.[5]. This method is based on work of Brueckner, et al.[7] and Lombard, et al.[8]. In the sudden approximation limit the structure of each nucleus is conserved during the contact and the nuclear densities overlap in a reversible process without any re-arrangements. Such a nuclear potential has a repulsive core in contrast to the Saxon-Woods potential which saturates to a value of V_o at small distances.

For the low-energy heavy ion reactions under discussion, the relative average velocity of the nuclei in the vicinity of the barrier is only of the order of 1 MeV per nucleon or less. At these small velocities one does not expect the sudden approximation hypothesis to be valid. At velocities of 1 MeV/nucleon, one expects surface waves to be excited in the interacting nuclei and to have an almost continuous exchange of energy between the projectile and target.

Assuming the present frictional models to be valid one will obtain information on the number of ℓ waves with potential wells (and hence information on $V_{Nucl}(r)$) for the $^{209}Bi + ^{84}Kr$ reaction by studying the energy dependence of the fusion cross section. If the fusion cross section does not increase with bombarding energy, for example, one would interpret this result in terms of the present frictional models to mean that there are at most a few ℓ waves with potential minima.

1) D.M. Brink and N. Rowley, Nucl. Phys. A219, 79(1974).

2) D.H.E. Gross and H. Kalinowski, Phys. Lett. 48B, 302(1974).

3) J. Wilczynski, Nucl. Phys. A216, 386(1973).

4) W.D. Myers and W.J. Swiatecki, Arkiv För Fysik, 36, 343(1967).

5) R.A. Broglia and A. Winther, Physics Reports, 4C, 153 (1972).

6) J. Galin, D. Guerreau, M. Lefort and X. Tarrago, Phys. Rev. C9, 1018(1974).

7) K.A. Brueckner, et al., Phys. Rev. 181, 1543(1969).

8) R.J. Lombard, Ann. of Phys., 77, 380(1973); M. Beiner and R.J. Lombard, IPNO/TH 73-39, University of Paris, Orsay Report (1973).

6. Reactions Between Very Heavy Projectiles and Heavy Targets: Experimental Program -- K. Wolf*, J.P. Unik*, V.E. Viola**, H. Freiesleben***, J. Birkelund and J.R. Huizenga

Initial experiments have been performed with very heavy projectiles accelerated in the Berkeley Superhilac as part of our outside users program. In the first series of experiments ^{40}Ar projectiles of 288 MeV were used to bombard ^{209}Bi and ^{238}U targets. In the second series of experiments ^{84}Kr projectiles of 605 MeV were used to bombard ^{165}Ho, ^{197}Au, ^{209}Bi and ^{238}U. Some experiments were performed also with ^{84}Kr projectiles reduced in energy with beryllium foils to approximately 530 MeV.

The energies and angles of two coincident heavy reaction fragments were recorded with a defining angle solid state detector and a large position sensitive solid state detector. The experimental data were recorded on magnetic tape as four separate parameters including 1) the energy of the fragment in the defining detector, 2) the energy of the fragment in the position sensitive detector 3) a quantity related to the position of the fragment in the position sensitive detector and 4) the time spectrum.

One of the primary aims of these correlated fragment experiments is to investigate the reaction mechanism between

---

*Argonne National Laboratory, Argonne, Illinois 60439.
**University of Maryland, College Park, Maryland 20742.
***Fachbereich Physik, Universität Marburg, Marburg, Germany.

very heavy projectiles and heavy targets. It has been reported that complete fusion between 500 MeV ^{84}Kr ions and heavy targets such as ^{209}Bi and ^{238}U is a very improbable process[1]. In fact those authors conclude that most of the reaction products are near the projectile and target masses and that the mechanism is a very inelastic interaction which looks like very asymmetric fission.

The large amount of four parameters data on magnetic tape is currently being analyzed in terms of fusion and various types of inelastic processes for ^{84}Kr induced reactions. Elastic scattering measurements of ^{84}Kr on heavy targets were performed also as a function of angle. In these single spectra we observe a well defined inelastic peak at several angles.

1) M. Lefort, C. Ngô, J. Peter and B. Tamain, Nucl. Phys. A216, 166(1973).

E. Effect of Pressure on Radioactive Decay Constants

The research program designed to characterize the effect of compression on radioactive (electron capture) decay constants has proceeded steadily during the past year. Although much of the progress has been made in experimental areas, several interesting theoretical calculations have been made.

Attempts to calculate the increase in the decay constant of ^{7}BeO with pressure have been made using a number of quantum mechanical models of varying degrees of sophistication. In the simplest possible model, the increase has been estimated using the electron wave functions of the free beryllium atom. In the molecular models, ab initio calculations were used to determine the electron density at the beryllium nucleus $|\Psi(0)|^2$, as a function of interatomic distance by using BeO and BeO_2 as model compounds.

In addition to these atomic and molecular calculations, a prediction of the change in decay rate as a function of volume, $d\ln R/d\ln V$, has been made using a modified solar model.

1. Simple Model Based on the Wave Function of Atomic Be -- W.K. Hensley and J.R. Huizenga

The beryllium atom model has the principal advantages of being: (1) spherically symmetric and (2) inexpensive. In this model which uses the best wave functions that can be obtained within the Hartree-Fock approximation, the fractional

amount of electron density in the outermost portion of the Be atom (a radius of 0.89Å was used) containing 10% of the volume is redistributed inside the new volume after compression to $0.9V_o$ with the original electron density distribution.

This calculation has been described previously[1]; therefore, the details are not included in this report.

1) J.R. Huizenga, AEC Progress Report, COO-3496-29 (1973).

2. Molecular Model I: BeO -- W.K. Hensley and J.R. Huizenga

The most rigorous way of calculating changes in $|\Psi(0)|^2$ in the compressed polycrystalline BeO would be to actually set up a model of the crystal or unit cell, carry out ab initio electronic structure calculations, and then calculate $|\Psi(0)|^2$ for the model at various interatomic distances. The most reasonable model of crystalline BeO is too difficult to calculate because each Be atom is surrounded by four oxygen atoms in a tetrahedral structure. The simplest model to compute would naturally be the BeO molecule. If one calculates $|\Psi(0)|^2$ as a function of the interatomic distance, R, for this model, one may be able to approximate the effect of compression on $|\Psi(0)|^2$ at the Be atom in crystalline BeO.

Attempts to estimate the increase in electron density at the beryllium atom in molecular BeO with compression have been made using two different types of basis sets, Slater type orbitals, STO's, and Gaussian type orbitals, GTO's.

In order to calculate $|\Psi(0)|^2$, the Hartree-Fock molecular orbitals (MO's) of McLean and Yoshimine[1] were used. These orbitals are considered to be very close to the Hartree-Fock limit, namely, the best anyone can do within the Hartree-Fock scheme. The procedure for calculating $|\Psi(0)|^2$ for BeO at the Be nucleus was to evaluate the STO's at r = o for functions originating on the Be atom, and at r = R (R is the interatomic distance) for the functions originating on the

oxygen atom. As one might expect, $|\Psi(0)|^2$ was then evaluated as a function of R and the increase in $|\Psi(0)|^2$ as a function of compression estimated from this curve. The results of these calculations are shown in Fig. 26. As one can see from the lower portion of Fig. 26, $|\Psi(0)|^2$ is a parabolic-like function in the region between 2 and 3 atomic units (a.u.)* with a minimum at about 2.75 a.u. Clearly, the magnitude and sign of the effect of compression on $|\Psi(0)|^2$ are strongly dependent on what value of R is taken as the equilibrium distance, R_0. For example, if one were to use the Be-O bond distance in crystalline BeO (about 3.1 a.u.) as R_0, the calculated effect would, in fact, be negative. Thus, the only R_0 that is valid to use in terms of the model is the one which is determined by the position of the minimum in the total energy curve for the system. The curve for the total energy is shown in the upper portion of Fig. 26, where the minimum in the energy is at approximately 2.44 a.u. When this value of R_0 is used, the value of $\Delta|\Psi(0)|^2$ becomes (34.9195-34.8936)/34.8936 or about 0.075% for a 10% decrease in volume.

Calculations of $|\Psi(0)|^2$ in molecular beryllium oxide have also been made using Gaussian type orbitals, GTO's. The calculations of $|\Psi(0)|^2$ using the GTO's differed from the previous STO calculation (McLean-Yoshimine) in two ways: (1) the atomic basis functions are themselves a linear combination of GTO basis functions and (2) the MO coefficients

---

*1 atomic unit (a.u.) = 0.529167 Å.

Fig. 26: $|\Psi(0)|^2$ and total energy of BeO molecule vs. interatomic distance, R_o, as calculated from the tables of McLean and Yoshimine[1].

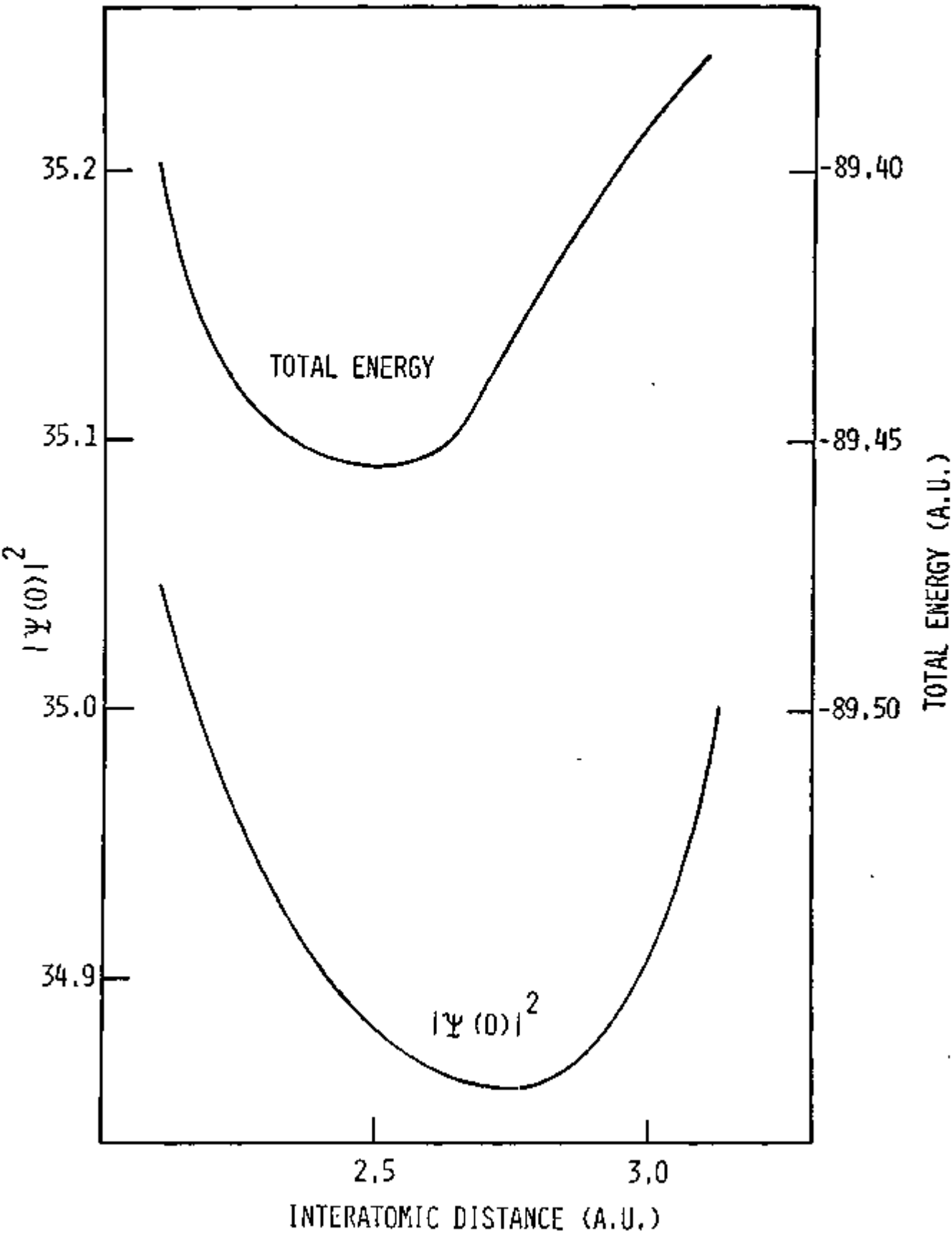
35.2
35.1
35.0
34.9
$|\Psi(0)|^2$
-89.40
-89.45
-89.50
TOTAL ENERGY (A.U.)
TOTAL ENERGY
$|\Psi(0)|^2$
2.5
3.0
INTERATOMIC DISTANCE (A.U.)

Figure 26

were calculated with a Hartree-Fock type molecular orbital program on the University of Rochester's IBM 360-65 computer.

The contraction coefficients and orbital exponents of Huzinaga[2] were used to generate the contracted GTO basis functions used for the MO calculations. The contracted GTO's are formed as a linear combination of GTO's,

$$G_c(\zeta, r) = \sum_i C_i G(\zeta, r),$$

where ζ and r are the orbital exponents and radial parameters, respectively. The C_i's are the contraction coefficients for the i GTO basis functions. The Huzinaga GTO atomic basis set for Be includes 11 s type GTO basis functions divided into four groups of 3, 3, 2 and 3. These 11 functions were contracted to produce the four s type GTO's used in the MO calculations.

In addition to the s type GTO's provided by Huzinaga, the Be basis set was expanded to include one p type GTO function contracted from three p type GTO functions. The p function is of the STO-3G type. That is, a Slater type orbital which is approximated by a linear combination of three Gaussian functions. The method of Hehre, Stewart, and Pople[3] was used to generate the 2p type STO-3G orbital. Although the p orbitals are unoccupied in the ground state of the free atom, they almost certainly contain some of the electron density in the BeO molecule. The Huzinaga GTO basis set for oxygen includes eleven s type GTO basis functions and six p type GTO basis functions. The s type basis functions

are divided into the same size groups as the s type basis functions on the Be atom. The p basis functions are divided into two groups of three so that there are a total of four s and two p type contracted basis functions in the basis set. The shorthand notation that Huzinaga uses to show this type of arrangement is (3, 3, 2, 3; 3, 3).

The Hartree-Fock molecular orbital coefficients were calculated using a modified version of the molecular orbital program, GAUSSIAN-70[4], and the $|\Psi(0)|^2$ values were subsequently calculated as a function of R in the usual manner. The equilibrium distance, R_o, was determined by the position of the minimum of the total energy curve as before; and the increase in electron density after compression to $0.9V_o$ was calculated to be about 0.11%. It was surmised that the relatively small increase in $|\Psi(0)|^2$ in this model is due to electron density being pushed away from the Be atom on the side opposite the oxygen atom when the Be-O bond distance is shortened. In an attempt to reduce this type of loss of electron density at the Be nucleus, calculations were undertaken for the molecule BeO_2.

1) A.D. McLean, M. Yoshimine, Tables of Linear Molecule Wave Functions, a supplement to a paper by the same authors which appears in IBM J. Res. Develop., (Nov. 1967).

2) S. Huzinaga, Approximate Atomic Functions. I, Division of Theoretical Chemistry, Dept. of Chem., University of Alberta, Canada (1971).

3) W.J. Hehre, R.F. Stewart, and J.A. Pople, J. Chem. Phys., 51, 2657(1969).

4) W.J. Hehre, W.A. Lathan, R. Ditchfield, M.D. Newton, and J.A. Pople, submitted to Quantum Chemistry Program Exchange, Indiana University, Bloomington, Indiana.

3. Molecular Model II: BeO_2 -- W.K. Hensley

The values of $|\Psi(0)|^2$ as a function of R have been calculated for the molecule BeO_2. The linear configuration, O-Be-O, was used in order to prevent the loss of electron density discussed for BeO. The atomic basis sets used for the BeO_2 MO calculations were the extended GTO's that had been generated for the BeO MO calculations from the Huzinaga Tables. The increase in $|\Psi(0)|^2$ for a 10% volume reduction is about 0.074%. It is interesting to note that the equilibrium distance, R_0, is closer to the crystalline value of about 3.1 a.u. than the values obtained from both of the BeO calculations.

4. Solar Model Calculation on ^{7}Be -- W.K. Hensley and J.R. Huizenga

A calculation of the change in total electron density at the ^{7}Be nucleus (and thus the electron capture rate) as a function of the most probable electron volume, $d\ell nR/d\ell nV$, has been performed for us by H. Van Horn[1] using a modified solar model. With his model, the electron capture rate has been estimated for electron pressures of 100 and 300 kbars at a temperature of 293°K. Although these results cannot be compared directly to the experimental data due to the fact that different normalization coefficients produce vastly different absolute rates, the theoretical and experimental ratios of $d\ell nR/d\ell nV$ can be compared. The value of the calculated slope from the modified solar model is -0.0410. This value compares very favorably with the experimental data which has a slope of -0.0588.

1) H. Van Horn, Department of Physics and Astronomy, University of Rochester, private communication (1973).

5. Comparison of the Theoretical Models -- W.K. Hensley and J.R. Huizenga

The results of the free atom and molecular orbital calculations are summarized in Table 21. The agreement between the different models used to calculate $|\Psi(0)|^2$, as shown in Table 21, is not very encouraging. The agreement between the theoretical models and the experimental results is even less encouraging. Assuming that the equation of state for BeO as given by Cline and Stephens[1] is correct, the pressure required to compress BeO to 90% of its original volume is roughly 240 kbars. Interpolation of the experimental data above and below 240 kbars leads to the conclusion that the expected experimental value of $(\lambda_c-\lambda)/\lambda$ would be on the order of 0.5%.

The principal reason for the large discrepancies between the experimental and theoretical values of $(\lambda_c-\lambda)/\lambda$ is probably that none of the theoretical models reproduce the symmetry present in crystalline BeO. In the crystalline form, BeO has the wurtzite (ZnS) structure. The wurtzite structure is hexagonal and can be described as a hexagonal close-packed array of cations interpenetrating a hexagonal close-packed array of anions. The two arrays are shifted with respect to each other such that the atoms of each array lie in the center of the tetrahedral interstices of the other[2]. Thus, all the atoms have tetrahedral coordination. Unfortunately due to limitations of the current generation of digital computers

Table 21. Summary of Free Atom and Molecular Orbital Calculations. The last column gives the calculated percentage increase in $|\Psi(0)|^2$, $\Delta|\Psi(0)|^2$, for a 10% reduction in volume.

MODEL	BASIS SET	R_0(a.u.)	$\|\Psi(0)\|^2(R_0)$	$\|\Psi(0)\|^2(r')$	$\Delta\|\Psi(0)\|^2$(%)
Be	*STO	1.68	35.4302	35.569	0.39
BeO	†STO	2.44	34.8936	34.920	0.075
BeO	††GTO	2.5	33.8044	33.842	0.11
BeO_2	††GTO	2.95	34.0875	34.112	0.074

*Composed of six s type STO basis functions.

†Composed of six s, two p, one d, and one f type STO basis function on the O atom.

††Composed of four s and one p type contracted GTO's on the Be atom and four s and two p type contracted GTO's on the O atom(s).

and since the cost of running molecular orbital programs is roughly proportional to the fourth power of the number of atoms in the system, the tetrahedral geometry of crystalline BeO is not possible to handle at the present time.

The agreement between the calculated and experimental results is best for the simple Be atom model and the modified solar model. This is probably due to the spherical symmetry which is inherent in these two models. The BeO and BeO_2 models, which are linear molecules, agree very poorly with the experimental results. The chief problem in the BeO model is that when the Be-O bond distance is reduced, the electron density which should be concentrated on the Be atom due to nearly symmetric compression is repelled away from the Be atom in the direction of the O-Be bond axis. Thus, the calculated effect is only a small fraction of what it would be if the true geometry of the system could be treated theoretically.

In an attempt to partially eliminate the unsymmetrical compression present in the BeO molecular model, the linear BeO_2 calculations were performed. Although the unsymmetric compression was reduced, the effect of the nonstoichiometric ratio of the strongly electron withdrawing oxygen atoms to the Be atoms (Be:O = 1:2, whereas in crystalline BeO, the ratio is 1:1) was greater than the desired effect. As a result, the extra oxygen atom simply withdrew more electron density than was produced by the compression. This result is evident from the data shown in Table 21.

1) C.F. Cline and D.R. Stephens, J. Appl. Phys. 36, 2869(1965).

2) C.F. Cline and J.S. Kahn, J. Electro. Chem. Soc., 110, 777(1963).

6. Experimental Results -- W.K. Hensley, W.A. Bassett* and J.R. Huizenga

a) ^{7}Be

Additional data has been collected on the ^{7}BeO system using a slight variation on the procedure reported here last year. Metallic silver was used as a gasket material (instead of NaCl) in one run in order to try and achieve pressures higher than 270 kbar - this was tried partially because Jayaraman[1)] has claimed to have observed pressures in excess of 300 kbars for a metallic silver system in a press similar to the ones used in this work. Unfortunately, these high pressures were not achieved and for a variety of reasons the silver proved not to be the best gasket material for this type of work.

The result of the run using silver as a gasket material (265 kbar) is shown in Fig. 27 along with the data obtained previously. The relatively large error bar associated with the measurement results from the sample being counted for a period of time which is only about 1/3 as long as for the other measurements. The good agreement between this measurement and the measurements obtained using NaCl as a gasket material seems to validate the assumption that the isotopic dilution of the radioactive sample by the inert carrier is so great that the nature of the gasket material (which also acts as the pressure transmitting medium) has no effect on the experimental results.

---

*Department of Geology, University of Rochester.

Fig. 27: Fractional increase in the total decay constant of ^{7}Be in ^{7}BeO as a function of pressure where λ_C is the decay constant of the compressed sample. The error bars represent one standard deviation. The line is a least-squares fit on our data to the equation $(\lambda_C-\lambda)/\lambda = K_P P$. The data point of Gogarty, et al.[2] is calculated from a least-squares fit to the above equation of some twenty experimental measurements taken near 100 kbars.

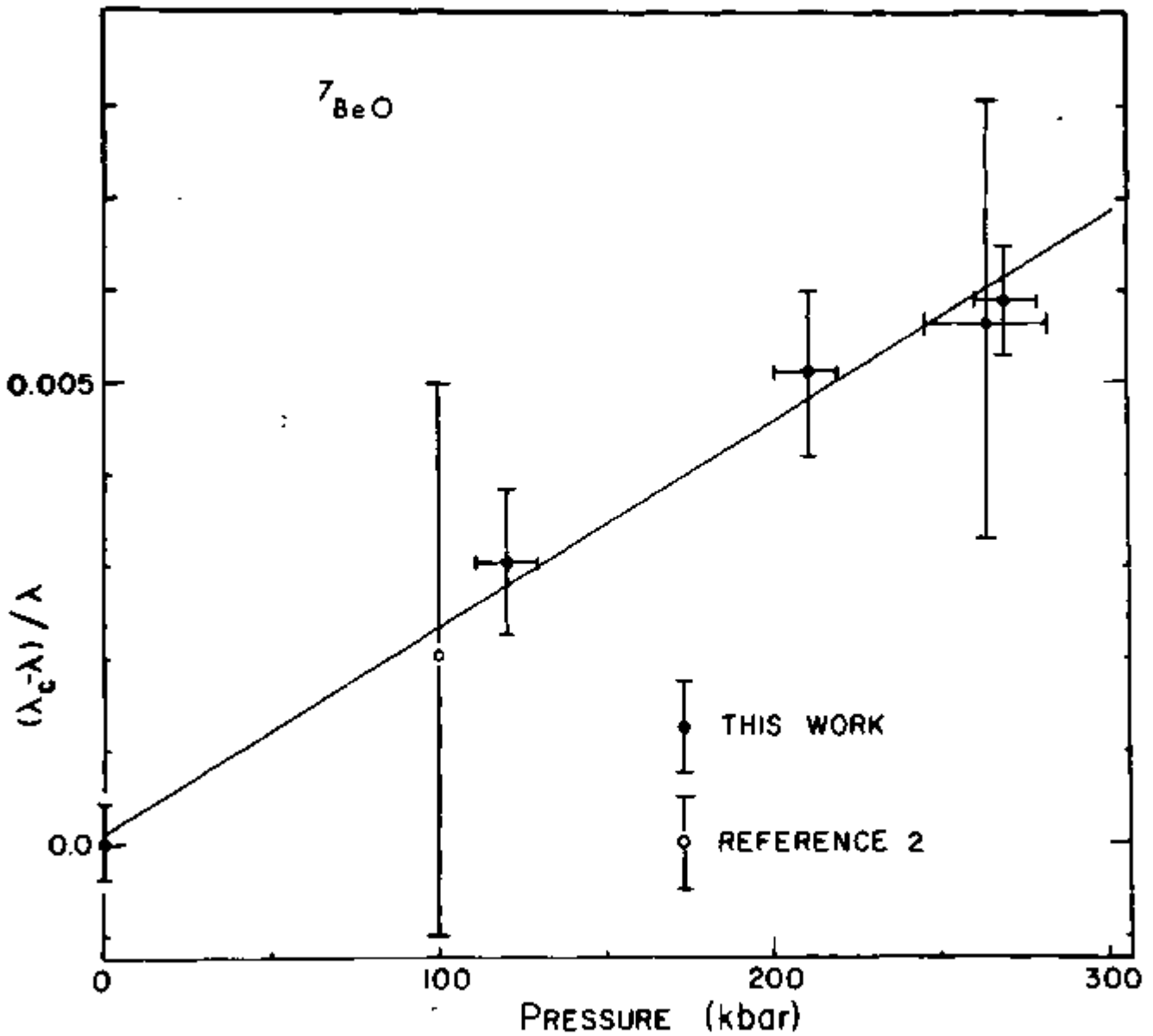
^{7}BeO
0.005
0.0
$(\lambda_c-\lambda)/\lambda$
THIS WORK
REFERENCE 2
0
100
200
300
PRESSURE (kbar)

Figure 27

b) $\underline{^{131}Ba}$

In order to test the hypothesis that a material with a very high compressibility and a large number of electrons may have a measurable pressure dependent electron capture decay rate, the ^{131}Ba system has been studied.

The chemical system chosen (not most judiciously) for the study was the difluoride, $^{131}BaF_2$. Unfortunately BaF_2 undergoes one, and we think two, structure changes in the pressure region between 1 bar and 220 kbars. The first phase change occurs at about 26 kbar where the fluorite (CaF_2) structure is distorted to an orthorhombic α-$PbCl_2$ structure[3]. This phase has been observed up to 150 kbars[4], above which no published data is available. We have performed X-ray diffraction studies on the BaF_2 system in the geology laboratories at the University of Rochester which indicate that around 170 kbar a second high pressure phase transformation takes place. This phase has been observed to be stable up to about 220 kbar. The structure of this new phase has yet to be determined.

The net result of the above is that there are two competing processes taking place when BaF_2 is compressed. The first process is simple compression which will tend to increase the E.C. decay rate as the confining pressure is increased. The second effect, and apparently the larger one, effect is a decrease in E.C. decay rate caused by a phase transformation. In the case of BaF_2, the 1 bar phase

is cubic where the Ba ion has a coordination number of 8. The first phase transition causes the cubic lattice to be distorted to an orthorhombic lattice in which the Ba ion has quasi nine coordination. The increase in coordination number means that the average Ba-F bond distance has increased to accommodate the ninth ion in the coordination sphere. Although the structure of the second high pressure phase is as yet unknown, following a general rule in crystallography, the Ba ion will probably have a higher coordination number than in the α-$PbCl_2$ structure. In any case, the net effect of internal structure transitions and increased confining pressure at 215 kbar is negative. Thus it would appear from our results that at least in the case of BaF_2, when the confining pressure is increased to the point where a structure change takes place, the net electron density at the nucleus decreases because this quantity is much more sensitive to increased bond distances than it is to an increase in coordination number. (See Fig. 28).

1) A. Jayaraman, private communication (1972).

2) W.B. Gogarty, S.S. Kistler, and E.B. Christiansen, Office of Naval Research Technical Report VII (1963)(unpublished).

3) G.A. Samara, Phys. Rev. B2, 4194(1970).

4) D.P. Dandekar and J.C. Jamieson, Trans. Amer. Crystallogr. Assoc. 5, 19(1969).

Fig. 28: Fractional increase in the total decay constant of ^{131}Ba in $^{131}BaF_2$ as a function of pressure where λ_c is the decay constant of the compressed sample. The error bars represent one standard deviation.

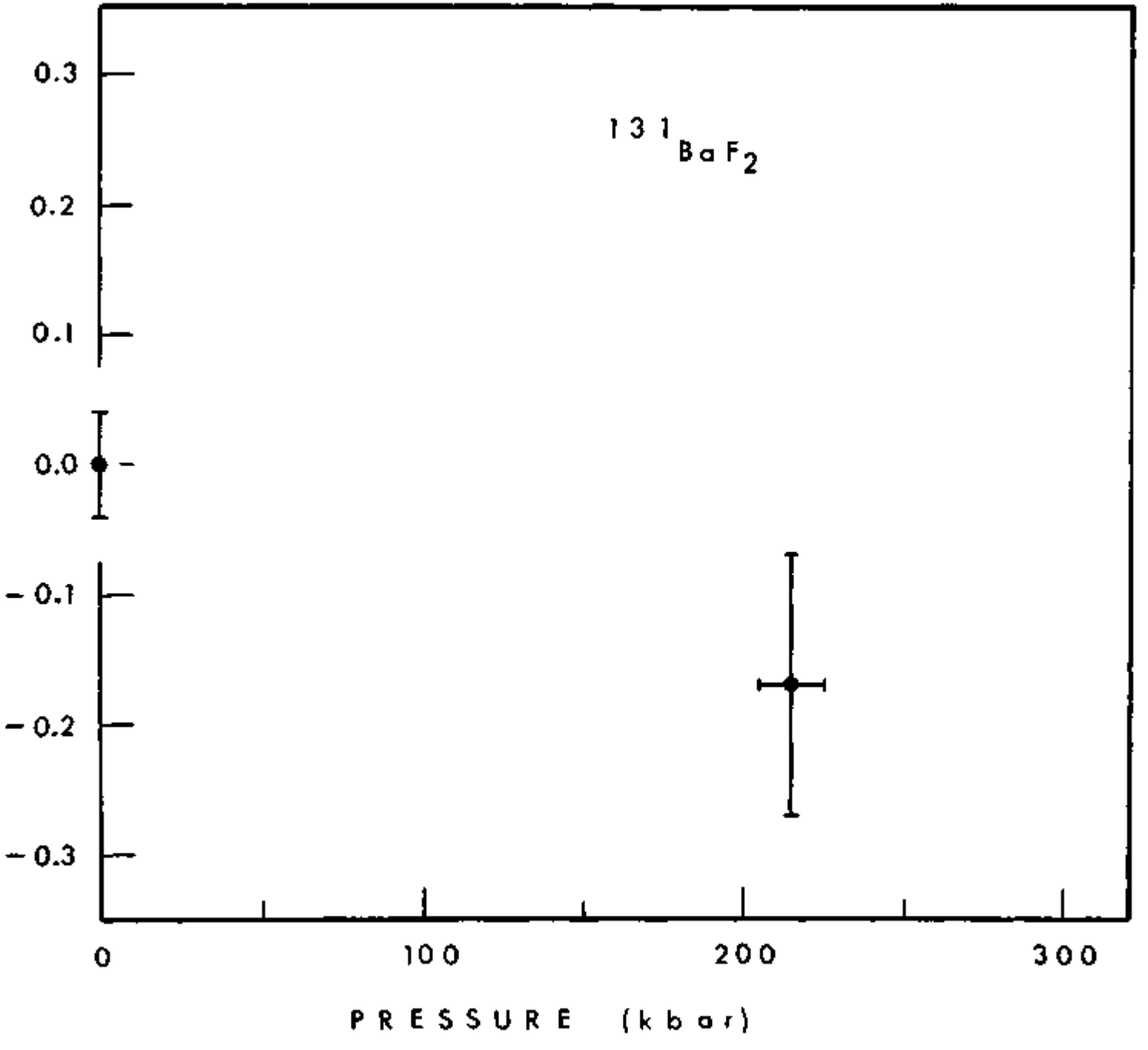
0.3
0.2
0.1
0.0
- 0.1
- 0.2
- 0.3
$^{131}BaF_2$
$(\lambda_C - \lambda)/\lambda$ (%)
0
100
200
300
PRESSURE (kbar)

Figure 28

III. PUBLICATIONS AND ACTIVITIES

1. Book

R. Vandenbosch and J.R. Huizenga, NUCLEAR FISSION, Academic Press, New York (1973).

2. Articles

J.R. Huizenga and H.C. Britt, THRESHOLD PHOTOFISSION: THEORY AND EXPERIMENT, Proceedings of International Conference on Photonuclear Reactions and Applications V2, 833 (1973).

J.R. Huizenga, STUDIES OF NUCLEAR FISSION, LOW-ENERGY NUCLEAR REACTIONS AND TRANSURANIC NUCLEI, AEC Progress Report COO-3496-29 (1973).

J.S. Boyno, J.R. Huizenga, Th. W. Elze and C.E. Bemis, Jr., LEVELS OF ^{234}U AND ^{236}U EXCITED BY THE (d,d') REACTION, Nucl. Phys. A209, 125(1973).

H. Freiesleben, H.C. Britt and J.R. Huizenga, ENERGY DEPENDENCE OF Γ_f/Γ_n FOR THE NUCLEUS ^{216}Rn, Third International Conference on the Physics and Chemistry of Fission, IAEA/SM-174/56(1973).

M. Kildir and J.R. Huizenga, ISOSPIN DEPENDENCE OF THE NUCLEAR LEVEL WIDTH, Phys. Rev. C8, 1965(1973).

A.N. Behkami and J.R. Huizenga, COMPARISON OF EXPERIMENTAL LEVEL DENSITIES AND SPIN CUTOFF FACTORS WITH MICROSCOPIC THEORY FOR NUCLEI NEAR A=60, Nucl. Phys. A217, 78(1973).

C. Kalbach-Cline, RESIDUAL TWO-BODY MATRIX ELEMENTS FOR PRE-EQUILIBRIUM CALCULATIONS, Nucl. Phys. A210, 590(1973).

R.L. Ferguson, F. Plasil, H. Freiesleben, C.E. Bemis, Jr., and H.W. Schmitt, FRAGMENT KINETIC ENERGY IN ^{18}O-INDUCED FISSION OF ^{232}Th AND ^{246}Cm, Phys. Rev. 8C, 1104(1973).

W.K. Hensley, W.A. Bassett and J.R. Huizenga, PRESSURE DEPENDENCE OF THE RADIOACTIVE DECAY CONSTANT OF BERYLLIUM-7, Science, 181, 1164(1973).

H.C. Britt, and J.R. Huizenga, REEVALUATION OF EXPERIMENTAL ESTIMATES OF THE PAIRING GAP AT THE FISSION SADDLE POINT, Phys. Rev., C9, 435(1974).

C. Kalbach-Cline, J.R. Huizenga and H.K. Vonach, ISOSPIN CONSERVATION AND PREEQUILIBRIUM DECAY IN (p,p') REACTIONS ON NEUTRON RICH TIN ISOTOPES, Nucl. Phys., in press.

J.R. Huizenga, A.N. Behkami, J.S. Sventek and R.W. Atcher, COMPARISON OF NEUTRON RESONANCE SPACINGS WITH MICROSCOPIC THEORY FOR SPHERICAL NUCLEI, Nucl. Phys., in press.

J.R. Huizenga, A.N. Behkami, R.W. Atcher, J.S. Sventek, H.C. Britt and H. Freiesleben, COMPARISON OF NEUTRON RESONANCE SPACINGS WITH MICROSCOPIC THEORY FOR NUCLEI WITH STATIC DEFORMATION, Nucl. Phys., in press.

H. Freiesleben and J.R. Huizenga, TOTAL REACTION CROSS SECTIONS OF DEFORMED NUCLEI; A STUDY OF THE $^{233,238}U + \alpha$ SYSTEMS, Nucl. Phys., in press.

H. Freiesleben, H.C. Britt, J. Birkelund and J.R. Huizenga, ^{6}Li, ^{7}Li INDUCED REACTIONS ON ^{209}Bi, Submitted to Phys. Rev.

Th. W. Elze and J.R. Huizenga, LEVELS OF ^{233}Pa EXCITED IN HELIUM-INDUCED SINGLE-PROTON TRANSFER REACTIONS, Submitted to Nucl. Phys.

3. Ph.D. Theses Completed

"Fragment Angular Distributions for Dipole Photofission of ^{233}U, ^{235}U and ^{237}Np: Lithium Ion Induced Fission of ^{232}Th and ^{238}U", by Gary T. Rizzo.

"Isospin Dependence of the Nuclear Level Width from Cross Section Fluctuations", by Mehmet Kildir.

4. Contributed Papers at Professional Meetings

Th. W. Elze and J.R. Huizenga, LEVELS OF ^{233}Pa FROM THE $^{232}Th(He,d)$ AND $^{232}Th(\alpha,t)$ REACTIONS, Proceedings of the International Conference on Nuclear Physics, Munich, Vol. I, 239(1973), North Holland.

C. Kalbach, J.R. Huizenga, S.M. Grimes, J.D. Anderson, C. Wong and J. Daves, COMPARISON OF (p,p') AND (p,n) ENERGY SPECTRA USING THE PREEQUILIBRIUM FORMALISM, Proceedings of the International Conference on Nuclear Physics, Munich, Vol. I, 522(1973), North Holland.

H.C. Britt, H. Freiesleben and J.R. Huizenga, STUDY OF THE $^{7}Li + ^{209}Bi$ REACTION, Bull. Am. Phys. Soc. 18, 1389(1973).

J.R. Huizenga and A.N. Behkami, COMPARISON OF NUCLEAR LEVEL DENSITIES FOR SPHERICAL AND DEFORMED NUCLEI, Bull. Am. Phys. Soc. 18, 1418(1973).

Th. W. Elze and J.R. Huizenga, UNTERSUCHUNG VON ^{233}Pa MITTELS DER ^{232}Th(^{3}He,d) UND ^{232}Th(α,t) REAKTION, Deutsche Physikalische Gesellschaft, Bochum, vom 4 bis 9 März (1974).

H. Freiesleben, J.R. Huizenga, J.R. Birkelund, G.T. Rizzo, C.C. Lu and H.C. Britt, ^{6,7}Li INDUZIERTE SPALTUNG VON ^{209}Bi, ^{232}Th UND ^{238}U, Deutsche Physikalische Gesellschaft, Bochum, vom 4 bis 9 März (1974).

R.C. Thompson, J.R. Huizenga, Th. W. Elze and J.P. Unik, COLLECTIVE STATES IN ^{230}Th, ^{240}Pu AND ^{244}Pu EXCITED BY INELASTIC DEUTERON SCATTERING, Bull. Am. Phys. Soc. 19, 599(1974).

5. Invited Lectures

"Status of Nuclear Fission and Future Experiments", Division of Physical Research, USAEC, May 22, 1973.

"Nuclear Level Densities Revisited: Are the Level Densities Different for Spherical and Deformed Nuclei", Lawrence Berkeley Laboratory, University of California, Berkeley, California, November 19, 1973.

University of Washington, Seattle, Washington, December 4, 1973.

Oregon State University, Corvallis, Oregon, December 5, 1973.

"Comparison of Experimental Nuclear Level Densities with Theory", Lawrence Livermore Laboratory, University of California, Livermore California, December 6, 1973.

"Comparison of Neutron Resonance Spacings with Microscopic Theory for Spherical and Deformed Nuclei", European Conference on Nuclear Physics, Villars, Switzerland, January 24, 1974.

Universität München und Technische Universität München, München, Germany, January 31, 1974.

Institut für Radiumforschung und Kernphysik, Vienna, Austria, March 11, 1974.

Fachbereich Physik, Universität Marburg, Marburg, Germany March 29, 1974.

6. Professional Activities

Member of Advisory Council of Princeton University's Chemistry Department.

Member of Physics Division Review Committee, Argonne National Laboratory.

Member of University of Rochester Senate.

Member of Ad Hoc Panel on Nuclear Data Compilation, NAS-NRC.

Member U. S. Nuclear Data Committee and Neutron Applications subcommittee.

Member NAS-NRC Ad Hoc Panel on Heavy Ion Facilities (Feshbach Panel).

Organizer of the Third International Symposium on the Physics and Chemistry of Fission held at the University of Rochester, Aug. 13-17, 1973.

John Simon Guggenheim Fellowship (1973-74): Time spent at Lawrence Berkeley Laboratory, University of California, Berkeley California; Technical University of Munich, Munich, Germany; and Niels Bohr Institute, University of Copenhagen, Copenhagen, Denmark.

IV. PERSONNEL

Dr. J.R. Huizenga - Professor, Departments of Chemistry and Physics.

Dr. H. Freiesleben* - Postdoctoral Research Associate.

Dr. W.K. Hensley - Postdoctoral Research Associate.

Dr. J. Birkelund** - Postdoctoral Research Associate.

Dr. R.C. Thompson - Postdoctoral Research Associate.

Dr. K. Albrecht*** - Postdoctoral Research Associate.

Dr. A.N. Behkami**** - Visiting Professor on leave from Pahlavi University, Shiraz, Iran.

Dr. Th. W. Elze***** - Visiting Professor on leave from Institut für Kernphysik, Universität Frankfurt, Germany.

Mr. M. Kildir† - Graduate Student, Department of Chemistry.

Mr. R.W. Atcher†† - Graduate Student, Department of Chemistry.

Mr. J.S. Sventek††† - Undergraduate Student, Department of Chemistry.

Mr. P. Richardson††† - Undergraduate Student, Department of Chemistry.

---

*Terminated August 31, 1973.

**Supported jointly by U.S.A.E.C. and fellowship from Western Australia Institute of Technology, Perth, W. Australia.

***Supported by U.S.A.E.C., N.S.F. and Scientific Ministry of West Germany. Terminated August 31, 1973.

****Supported jointly by N.S.F. and U.S.A.E.C. Terminated August 31, 1973.

*****Supported for one month during July-August, 1973.

†Supported in large part during Academic year by a fellowship through the Department of Chemistry. Terminated June 1, 1974.

††Supported during Academic year by teaching assistantship through Department of Chemistry.

†††Supported during June, July and August, 1973.